Tissue Engineering for the Nervous System

A DISSERTATION SUBMITTED TO

THE UNIVERSITY OF OXFORD



FOR THE DEGREE OF

DOCTOR OF PHILOSOPHY

BY

FANGXIN LI

THE QUEEN'S COLLEGE

TRINITY TERM 2018

DEPARTMENT OF MATERIALS

Abstract

Tissue Engineering for the Nervous System

DPhil Thesis
Trinity Term 2018

Fangxin Li
The Queen's College

Tissue engineering for the brain emerged as a promising therapy for traumatic brain injuries (TBIs) after the discovery of neural stem cells (NSCs) in the subventricular zone (SVZ) and the subgranular zone (SGZ). Combining NSCs with novel bioactive scaffolds may encourage and direct tissue regeneration and ultimately repair tissue damaged due to injuries.

In this thesis, a number of collagen-based scaffolds were fabricated into an interlaced network structure. The scaffolds comprised collagen (Coll), hyaluronic acids (HA) and chondroitin sulfates (CS), where the latter two are commonly-found glycosaminoglycans (GAGs) in the brain's extracellular matrix (ECM). Our novel tri-interlaced network scaffold, Coll-CS-HA, is the first to be constructed, characterized and tested on NSCs. The synthesis method successfully incorporated HA and/or CS into the interlaced scaffolds, as demonstrated by FTIR, EDX and histology. Compressive testing and SEM also showed that the interlaced scaffolds had consistent and adequate mechanical properties and pore structure suitable for NSC growth.

Further cell biology studies demonstrated excellent biocompatibility of all scaffolds as evidenced by high cell survival. Interlaced scaffolds encouraged higher cell differentiation, shown by a halved nestin expression, a marker for NSCs, compared to Coll. An increase in MAP2 expression, a marker for mature neurons, by 50-100% in proliferation and differentiation was also observed. Coll-CS scaffolds led to an increase in astrocytic differentiation shown by a doubled GFAP expression, which has been related to glial scar formation.

As a result, Coll-HA and Coll-CS-HA may hold therapeutic potential to become candidates for future TBI treatments as they combined the advantage of adequate mechanical properties similar to that of brains, a high neuronal differentiation of around 40%, and a low astrocytic differentiation of around 20%.

Preface

The work described in this thesis was under taken by the author in the Department of Materials and the Department of Physiology, Anatomy and Genetics, University of Oxford, between October 2014 and July 2018 under the supervision of Prof. Jan T. Czernuszka and Prof. Francis G. Szele. No part of this thesis has been submitted or accepted for any other degree at this university or elsewhere.

Parts of this thesis has been presented at conferences:

F. Li, F. Szele, J. Czernuszka, Interpenetrating polymer network of collagen, chondroitin sulfate and hyaluronic acids - a novel scaffold for tissue engineering for the brain, TERMIS EU 2017 Meeting, June 26-30, Davos, Switzerland

Acknowledgements

I would like to acknowledge the support and guidance I received along my studies, for which I could not have completed my studies without.

My first acknowledgement goes to my head supervisor, Prof. Jan Czernuszka, who has guided me through my research and given me the flexibility to pursue my interests in the four years of study.

I would like to thank Prof. Francis Szele, my co-supervisor, for his generous support to me who had no prior cell biology experience and his guidance for me on adult neurogenesis.

I would also like to thank my Biomaterials group: Xue, Karim, Maryam, Narjes, Yun, Mariam, Rabia, Jim, Sonia, Jerry, Sasza and Mu-Huan, for their help on my research, inspiring discussions and time listening to my complaints.

Also, thanks are due to my group in DPAG, especially Bin, Julie, Martin, Yichen, who taught me how to do cell work and to analyse data. Also I'd like to thank the rest of the group for helping me with ordering mice and items.

Thanks must go to my personal friends, who have enriched my times after work. I'd like to thank them for our times hosting events and helping me become an alcoholic.

Last but not least, my thanks must go to my family, for their financial support and care to my study.

Table of Content

Abstract

Preface

Acknowledgements

Table of content

Chapter 1: Introduction **1**

1.1 Introduction 1

1.2 References 4

Chapter 2: Literature review **6**

2.1 Introduction 6

2.1.1 Tissue engineering 7

2.1.2 Tissue engineering for the central nervous system 8

2.2 Central nervous system 10

2.2.1 Extracellular matrix in the central nervous system 12

2.2.2 Adult neurogenesis in the subventricular zone 14

2.2.3 Migration of neural stem cell progeny 16

2.2.4 Differentiation pathway of neural stem cell progeny 18

2.3 Scaffolds 19

2.3.1 Collagen 22

2.3.2 Hyaluronic acid 23

2.3.3 Chondroitin sulfate 26

2.3.4 Fabricating collagen, hyaluronic acid and chondroitin sulfate scaffolds 28

2.4 Cell-scaffold interactions 31

2.4.1 Cell-scaffold interactions on collagen 32

2.4.2 Cell-scaffold interactions on chondroitin sulfates 34

2.4.3 Cell-scaffold interactions on hyaluronic acids 35

2.5 Conclusions 41

2.6 References 43

Chapter 3: Materials synthesis and characterisation **58**
3.1 Introduction 58
3.2 Materials and methods 59
3.2.1 Synthesis of Coll scaffolds 59
3.2.2 Synthesis of interlaced scaffolds 59
3.2.3 Fourier transformed infrared spectroscopy 65
3.2.4 Histology 66
3.2.5 Energy dispersive X-ray spectroscopy 66
3.2.6 Nuclear magnetic resonance spectroscopy 68
3.2.7 Pore size and morphological analysis 68
3.2.8 Compressive tests 69
3.2.9 Degradation studies 70
3.2.10 Statistics 71
3.3 Results 72
3.3.1 Fourier transformed infrared spectroscopy 72
3.3.1.1 Pure components analysis 72
3.3.1.2 Interlaced scaffolds analysis 74
3.3.1.3 Second derivatives of FTIR spectroscopy 76
3.3.2 Histology 79
3.3.3 Energy dispersive X-ray spectroscopy 81
3.3.4 Nuclear magnetic resonance spectroscopy 83
3.3.5 Scanning electron microscopy 86
3.3.6 Compressive tests 92
3.3.7 Degradation studies 93
3.4 Discussion 95
3.4.1 EDC/NHS crosslinking 95
3.4.2 Fourier transformed infrared spectroscopy 100
3.4.3 Histology 102
3.4.4 Energy dispersive X-ray spectroscopy 104
3.4.5 Nuclear magnetic resonance spectroscopy 106
3.4.6 Pore size and morphological analysis 107

3.4.7 Mechanical properties 109
3.4.8 Degradation studies 113
3.5 Conclusions 116
3.6 References 118
Chapter 4: *In vitro* cell studies **125**
4.1 Introduction 125
4.2 Materials and methods 127
4.2.1 Isolation and culture of SVZ NSCs 127
4.2.2 Coating 128
4.2.3 Culture of NSCs 128
4.2.4 Immunohistochemistry 131
4.2.5 Confocal microscopy 133
4.2.6 Total colony size measurement 134
4.2.7 Morphology studies 134
4.2.8 Migration studies 135
4.2.8.1 Isolation and culture of neuroblast spheroids 136
4.2.8.2 Isolation and culture of SVZ explants 137
4.2.9 Statistics 137
4.3 Results 138
4.3.1 Isolation of SVZ NSCs 138
4.3.2 Tripotent differentiation capability of SVZ NSCs 139
4.3.3 No primary control 142
4.3.4 ReNcell culture 143
4.3.5 Cell death 144
4.3.6 Total colony sizes 146
4.3.7 Morphological analysis 151
4.3.8 Nestin expression 153
4.3.8.1 Nestin and PHi3 co-expressions 155
4.3.9 GFAP expression 158
4.3.10 Dcx and MAP2 expressions 162
4.3.10.1 MAP2 and VGLUT1 co-expressions 170

4.3.11 Migration studies 172
4.3.11.1 Neuroblast spheroids 172
4.3.11.2 Migration on scaffolds 173
4.4 Discussion 175
4.4.1 Cell seeding 176
4.4.2 SVZ NSCs 177
4.4.3 Colony size measurement 178
4.4.4 Morphologies of colonies and individual NSCs 179
4.4.5 Nestin expression on scaffolds 182
4.4.6 Astrocytic differentiation 185
4.4.7 Neuronal differentiation 187
4.4.7.1 Dcx expression 187
4.4.7.2 MAP2 expression 188
4.4.7.3 VGLUT1 expression 191
4.4.8 Migration 193
4.4.9 The optimal candidate scaffolds for tissue engineering for the brain 195
4.5 Conclusions 197
4.6 References 199
Chapter 5: Conclusions **205**
Chapter 6: Future work **207**

Chapter 1 – Introduction

1.1 Introduction

The human body is regulated by extreme complex mechanisms. The most complicated system of all is likely to be the brain, which consists of billions of neurons and glial cells that form an unimaginably complex network that regulates and controls other organs of the body. The brain is also responsible for crucial processes including learning, memory, sensory input integration and homeostasis. This complex organ however, is susceptible to many injuries and diseases, including Parkinson's disease, Alzheimer's disease, motor neuron disease, schizophrenia and stroke.

Traumatic brain injuries (TBI) are characterised by injuries to the brain caused by external forces. Depending on the severity, the injuries can be categorised as mild, moderate or severe. The injuries often lead to loss of tissue that results in impaired neurological functions. TBI is the leading cause of disability among young people. Inadequate treatment of TBI was also shown to increase the risk of hypotension, hyperxaemia and brain swelling. Approximately 2% of the US population is affected by TBI, and it is responsible for 300,000 hospital admissions in the UK. TBI is responsible for approximately 56,000 death in the US, placing it as the 9th leading causes of death [3, 4]. Comparing to death per year by other diseases, including liver cancer (24,000 death), AIDS (15,000 death) and suicide (44,000 death), TBI therefore poses a serious challenge to the medical community [3, 5, 6].

Current treatment options for TBIs however, mainly focus on neuroprotection, i.e. protecting the remaining tissue from secondary injuries, rather than neuroregeneration. The common perception is that the brain lacks the ability to regenerate. The discovery of adult neurogenesis, the process of generating new neurons in the brain after adulthood, in the late 20th century showed the brain's capability of generating new neurons from the subventricular zone (SVZ) lining the lateral ventricles and the subgranular zone (SGZ) in the dentate gyrus of the hippocampus [7]. This discovery sparked interests in utilising the brain's regenerative capability to assist TBI repair.

Tissue engineering aims at regenerating diseased tissue by the combination of cell therapy and biomaterials. The concept of generating new tissues has been long embedded in arts and literature. The regeneration myth of Prometheus may represent some of the earliest recorder imaginations of regenerative medicine. The development of tissue engineering and regenerative medicine in the 1980s provided much hope for the realisation of this fantasy. In 1987, 'tissue engineering' was officially introduced in medicine [8]. To date, it has provided promising perspectives for replacing the conventional stem cell or organ transplant. While the former often faces challenges in cell distribution, survival and differentiation, the latter is limited by long waiting lists and an ever increasing demand for new organs. Tissue engineering therapy therefore solves the above challenges by providing a suitable environment for implanted cells and a customised tissue synthesis for patients.

Several groups have attempted developing a tissue engineered therapy for the treatment of TBIs. However, despite many attempts and positive claims, none have successfully

devised a therapy suitable for clinical trials. In addition, most laboratories have struggled to induce high neuronal differentiation and long term survival of NSCs [9-13].

The aim of this study is thus to develop a bio-scaffold suitable for the treatment of TBI. The thesis incorporates the studies on scaffold synthesis, scaffold characterisation, which consists of Fourier-transformed infrared spectroscopy (FTIR), scanning electron microscopy (SEM), histology, energy dispersive X-ray spectroscopy (EDX) and nuclear magnetic resonance spectroscopy (NMR), and cell biology, which includes proliferation studies, differentiation studies and migration studies. The thesis is arranged in the following format:

Chapter 1: Introduction

Chapter 2: Literature review

Chapter 3: Materials synthesis and characterisation

Chapter 4: *In vitro* cell studies

Chapter 5: Conclusions

Chapter 6: Future work

1.2 References

1. Headway tbia. Brain injury statistics 2015 [cited 2015 25/09]. Available from: https://www.headway.org.uk/brain-injury-statistics.aspx.

2. Foundation BT. TBI Statistics, Facts About TBI in the USA 2015. Available from: https://www.braintrauma.org/tbi-faqs/tbi-statistics/.

3. Statistics NCHS. Deaths and Mortality: Centers for Disease Control and Prevention; 2017 [cited 2018 14/06].

4. Taylor CA, Bell JM, Breiding MJ, Xu L. Traumatic brain injury–related emergency department visits, hospitalizations, and deaths — United States, 2007 and 2013. Surveillance Summaries. 2017;66(9):1-16.

5. Prevention CDC. Liver Cancer: Division of Cancer Prevention and Control, Centers for Disease Control and Prevention; 2017 [cited 2018 14/06].

6. Diagnoses of HIV Infection in the United States and Dependent Areas, 2016: Centers for Disease Control and Prevention; 2016 [cited 2018 14/06].

7. Gross CG. Neurogenesis in the adult brain: death of a dogma. Nature Reviews. 2000;1:67-73.

8. Meyer U. The history of tissue engineering and regenerative medicine in perspective. In: Meyer U, Handschel J, Wiesmann HP, Meyer T, editors. Fundamentals of Tissue Engineering and Regenerative Medicine. XXVI. Springer: Springer; 2009. p. 6-12.

9. Egawa EY, Kato K, Hiraoka M, Nakaji-Hirabayashi T, Iwata H. Enhanced proliferation of neural stem cells in a collagen hydrogel incorporating engineered epidermal growth factor. Biomaterials. 2011;32:4737-43.

10. Koutsopoulos S, Zhang S. Long-term three-dimensional neural tissue cultures in functionalized self-assembling peptide hydrogels, Matrigel and Collagen I. Acta Biomaterialia. 2013;9:5162-9.

11. Elias PZ, Spector M. Implantation of a collagen scaffold seeded with adult rat hippocampal progenitors in a rat model of penetrating brain injury. Journal of Neuroscience Methods. 2012;209:199-211.

12. Chen SS, Revoltella RP, Dapini S, Michelini M, Fitzgerald W, Zimmerberg J, *et al*. Multilineage Differentiation of Rhesus Monkey Embryonic Stem Cells in Three-Dimensional Culture Systems. Stem Cells. 2003;21:281-95.

13. Zhong J, Chan A, Morad L, Kornblum HI, Fan G, Carmichael ST. Hydrogel matrix to support stem cell survival after brain transplantation in stroke. Neurorehabil Neural Repair. 2010;24(7):636-44.

Chapter 2 – Literature Review

2.1 Introduction

Organ transplant operations are highly successful in treating organ failures, with over 4000 surgeries in the UK and 28,000 in the US performed annually [1, 2]. However, problems associated with organ transplants are also prominent. For example, the waiting list for organs in the US has expanded six-fold over the past 20 years to over 120,000, while the number of donors remains generally flat [2]. Also, immunorejection by the host limits organ transplantation success rates. Even successful patients need to rely on expensive immunosuppression drugs for their entire lives. For example, a kidney transplant would cost, on average, $10,000 to $14,000 per year even after the surgery [3]. In addition to the price tag, the drugs can also lead to immunodeficiency [4] and diseases such as hypertension and hyperlipidemia [5, 6].

Since the acceleration of stem cell studies in the 1990s, our understanding of their biology and ability to manipulate these cells has grown rapidly. Stem cell therapies have been extensively researched and are now being translated into treatments of diseases [7]. Scaffolds, either with or without stem cells, have now become promising candidates for solving the issues of organ transplantation. Instead of using a donated organ, one can extract cells from patients and grow them on the scaffolds *in vitro*. The cells impregnated scaffolds are then transplanted into the patient, allowing regeneration of new organs *in vivo* [8].

2.1.1 Tissue engineering

Tissue engineering is an interdisciplinary field that combines expertise in engineering, biology, clinical medicine and materials science [9]. In the past century, biomaterials and implants have been passive in their *in vivo* functions and rarely react positively to biological activities after implantation, examples include total hip replacements and artificial heart valves. The tissue engineering approach however, is now active in developing ways of engaging and responding to biological signals and activities, and therefore can restore functions that traditional biological implants cannot restore [10].

Novel biomaterials will ideally be able to facilitate cell proliferation, migration, attachment and differentiation in order to grow functional tissue. The biomaterial needs to meet a number of essential mechanical, biological and commercial requirements. The most important requirements are:

1. Biocompatibility: to avoid inducing toxicity, immunorejection and formation of scar tissue around the biomaterial, a phenomenon named fibrous encapsulation [10, 11].
2. Bioreplacable and biodegradable: the material will encourage growth of extracellular matrix (ECM) *in vivo*, and eventually be replaced by the newly formed ECM. Optimally, the degradation rate of the implant would match the growth of ECM *in vivo*. In addition, the degraded materials need to be non-toxic to patients [12].
3. Supportive of cell growth: to be able to support cell migration, proliferation and differentiation within the scaffold. The mechanical properties of the scaffold also

need to match those of the host tissue. In the case of the brain, the scaffold will need to have low stiffness yet be strong enough to support cells [9].

2.1.2 Tissue engineering for the central nervous system

The central nervous system (CNS) includes the brain and the spinal cord. It is a vulnerable system and is subject to various kinds of injuries. The recovery of these injuries are often difficult due to the inability of mature neurons to regenerate. The tissue engineering approach may provide a promising solution to these injuries, including TBI and stroke.

The injury caused by TBI is divided in two stages. In stage 1, the injury, namely the primary damage or mechanical damage, is due to the impact to the brain; and in stage 2, the secondary damage, or delayed non-mechanical damage, is caused by the subsequent pathological processes, such as cerebral ischemia and intracranial hypertension [13].

As a result, patients suffering from TBI will often experience loss of functions such as impaired memory, executive dysfunction, motor, cognitive and other functional impairments. In addition, TBI increases the chance of patients developing neurodegenerative diseases including Alzheimer's disease (AD), motor neuron disease (MND) and Parkinson's disease (PD). In severe cases, TBI and stroke can easily lead to death [14, 15]. Currently, approximately 2% of the US population are affected by disability resulting from TBI, and there are over 300,000 admissions annually in the UK for acquired brain injuries [16, 17]. However, despite the progress in clinical medicine, the current clinical therapy focuses more on neuroprotection, i.e. protecting the brain from

secondary injury, rather than neuroregeneration. Hence, there are no clinical therapies that leads to full recovery from the injury [18]. Although some treatments, such as methylprednisolone and cell therapy showed some effects on improvement, they both failed to induce complete recovery [19].

Implantation of stem cells is considered by many a promising treatment for TBI. However, they cannot overcome problems of uncontrollable cell distribution and low cell viability after implantation [20]. The combination of the stem cell therapy with a biocompatible scaffold therefore is used in the hope of circumventing these issues. The scaffolds can be either implanted with or without the cells. Guan *et al*. compared direct injection of mesenchymal stem cells (MSCs) and implantation of MSCs with a collagen (Coll) scaffold over a 28 day period, and noticed a significant improvement on cell viability and differentiation on the Coll scaffold [20]. Similarly, implantation studies of Coll-GAG also showed an enhanced functional recovery and reduction of the injured area [21]. Having said that, these studies were still far from inducing full recovery and thus were not considered clinically feasible yet. Unlike the peripheral nervous system (PNS), which already has several nerve guidance conduits approved by the US Food and Drug Administration (FDA), the CNS is far more complicated and is also inferior in its neuroregeneration abilities [22].

2.2 Central Nervous System

The human nervous system is divided into two major systems: the central nervous system (CNS) and peripheral nervous system (PNS). The CNS is composed of the brain and the spinal cord, while the PNS consists of the neural systems outside of the skull and spinal cord [23].

Approximately 75-90% of the brain volume is composed by neurons and glial cells. The human brain consists of hundreds of billions of neurons and glial cells [24], which are arranged in extremely complex networks. Neurons are responsible for transmission of information within the CNS. They consist of a cell body with dendrites and axons [25]. Depending on the neurotransmitters, neurons can be broadly categorised as glutamatergic or GABAergic. Upon triggering action potentials, glutamatergic neurons release glutamate, an excitatory neurotransmitter, whereas GABAergic neurons release gamma-aminobutyric acid (GABA) that is an inhibitory neurotransmitter. Thus, glutamatergic neurons are perceived as excitatory neurons and GABAergic neurons are perceived as inhibitory neurons in the CNS. The former usually wire up distant parts of the brain with distinct functions whereas the latter make local connections. The regeneration of functional glutamatergic neurons is thus considered important for functional recovery in neurodegenerative diseases [26, 27]. Interestingly, glutamate was found to be upregulated after a TBI, while GABA was found to be downregulated, indicating brain's natural response to increase excitation levels after injuries [28], providing a potential target for the tissue engineering therapy.

Astrocytes and oligodendrocytes are the two main types of glial cells in the CNS, although astrocytes are more prevalent [29]. Astrocytes are characterised by a small cell body of approximately 10 μm in diameter and extended star-shaped processes that can extend up to 150 μm [29]. They are involved in a number of neural activities in the CNS, including neurogenesis, synapse formation and function, blood-brain barrier maintenance and ion homeostasis [30-32]. Normal astrocytes in the parenchyma are quiescent and have exited the cell cycle. Upon diseases or injuries however, they are activated, a phenomenon named reactive astrocytosis in the vicinity of the injury, where some astrocytes become mitotic and most astrocytes express high levels of an intermediate filament protein called glial fibrillary acidic protein (GFAP) [33]. It is evident that reactive astrocytes are responsible for forming the glial scar after brain injury, which inhibits neurite outgrowth and thus recovery [34]. However, astrocytes are highly plastic and can promote growth of neurite under some circumstances [35].

Oligodendrocyte are the other type of the main glial cells in the CNS. Compared to astrocytes, oligodendrocytes have shorter yet more branched radial arms [25]. They are involved in myelination [36], where they produce myelin sheaths that wrap around axons, ensuring rapid transmission of action potential [37]. They also support neurons by producing neurotrophic factors [38]. Oligodendrocytes are also suspected to play a role in neurodegenerative diseases, including AD and definitely multiple sclerosis, since their dysfunction was shown in diseased patients [37].

2.2.1 Extracellular matrix in the central nervous system

The CNS is composed of neurons, glial cells, blood vessels and approximately 10-20% extracellular matrix (ECM) by volume. ECM is present in all human tissues as an important structural support network and anchorage points for cells [39]. In the human brain, the ECM plays a vital role in maintaining the blood-brain barrier (BBB), regulating homeostatic functions [40] and affecting cell behaviours, including cell migration [41], endothelial cell activation after acute brain injuries [40], and astrocyte responses to external stimuli [42].

The ECM is composed of a number of molecules: glycosaminoglycans (GAGs), such as hyaluronan and chondroitin sulfate proteoglycans (CSPG), fibrous proteins, such as Coll and elastin, adhesive glycoproteins, such as fibronectin, laminin and tenascin, and also a range of different growth factors and other molecules. Structurally in human brain ECM, the link proteins bind hyaluronan and tenascin interacts with CSPG [43-47]. The ECM is secreted extracellularly by neurons and glial cells and forms a dense network around the cells [48]. However, the exact ratios of these components in different subregions of the brain still remains unknown [49].

The ECM in the CNS is organised into three compartments: basement membrane (BM), a densely packed perineuronal nets (PNNs) and looser neural interstitial matrix. The PNNs and neural interstitial matrix can be found both *in vitro* and *in vivo*. Depending on the type of neurons, PNNs can be also substantially different [50]. The compartments differ in both location and composition, as illustrated in figure 2.1. The BM has a very thin sheet-like structure which supports the BBB and separates blood vessels endothelial cells from the

neural cells [51, 52]. The ECM of the BM contains type IV Coll, laminin, heparin sulfate proteoglycan and fibronectin. The PNNs, on the other hand, consist of different molecules: hyaluronan, CSPG and tenascin R [48, 53, 54]. Within the CNS, PNNs surround neural cell bodies and axons, but are absent at synaptic contacts. PNNs were discovered to take part in ion homeostasis around highly active neurons, neuroprotection, and also possibly in memory and learning [48].

The neural interstitial matrix occupies the space between neurons and glial cells, and consists of a mixture of components found in the BM and PNN. It consists of a network of hyaluronan, CSPG, tenascin R and a small amount of laminin and type IV Coll [39]. Since hyaluronan and CSPG occupies most of the PNN and neural interstitial matrix, it makes sense to consider these two materials as the major constituents for the scaffolds.

Although CSPG and hyaluronan are commonly found in the brain's ECM, their molecular weight, for example, differ considerably. Versican, a family of CSPGs in the brain, has the longest central domain of roughly 1,700 amino acid residues, while brevican, another CSPG, has only 300. The differences in length affects their attachment sites and thus determine their attachment to growth factors, tenascin R, and/or hyaluronan [55].

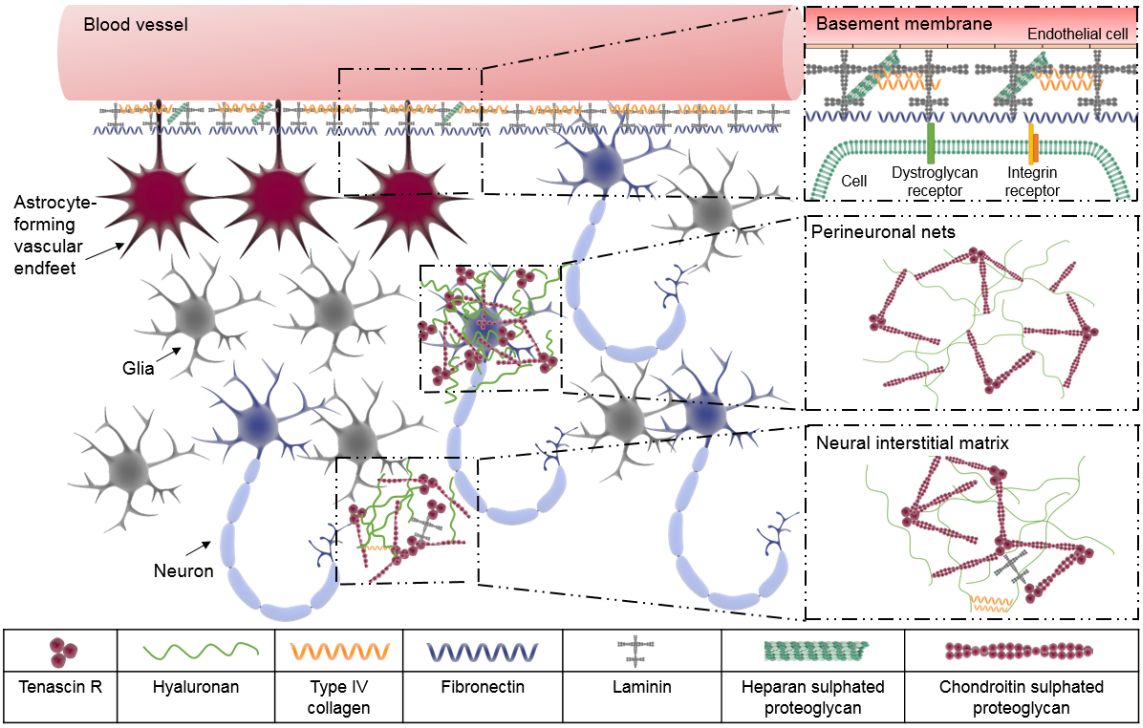


Figure 2.1 – A schematic illustration of the three major components of the ECM in the brain. Adapted from [39]

2.2.2 Adult neurogenesis in the subventricular zone

Neurogenesis, the process of generating new neurons from progenitor cells within the CNS, was thought, for several hundred years, to only occur during embryonic stages in mammals [56-58]. In the early 20th century, there were scattered research reports mitosis in the walls of lateral ventricle [59]. In the 1960's, Altman used tritiated thymidine to claim neurogenesis in rats after birth, from the age of 20 days to one year, although the developmental neurobiology community did not accept his findings and assumed he was detecting gliogenesis [60, 61]. In the 1990's bromodeoxyuridine, immunohistochemistry,

confocal microscopy, cell culture and related modern techniques confirmed Altman's findings and created the new field of adult neurogenesis [62, 63]. Several studies revealed neurogenesis in the subventricular zone (SVZ) and the subgranular zone (SGZ) in the dentate gyrus of the hippocampus [57]. Since then, adult neurogenesis in healthy brains has been claimed in other brain areas such as the cerebral cortex, but these have largely been disproven. The one notable exception is the hypothalamus, a region at the base of the forebrain packed with small clusters of neurons that regulate a diversity of functions such as feeding, sleeping, and stress. Low-grade neurogenesis has now been confirmed in this fascinating part of the brain [64, 65].

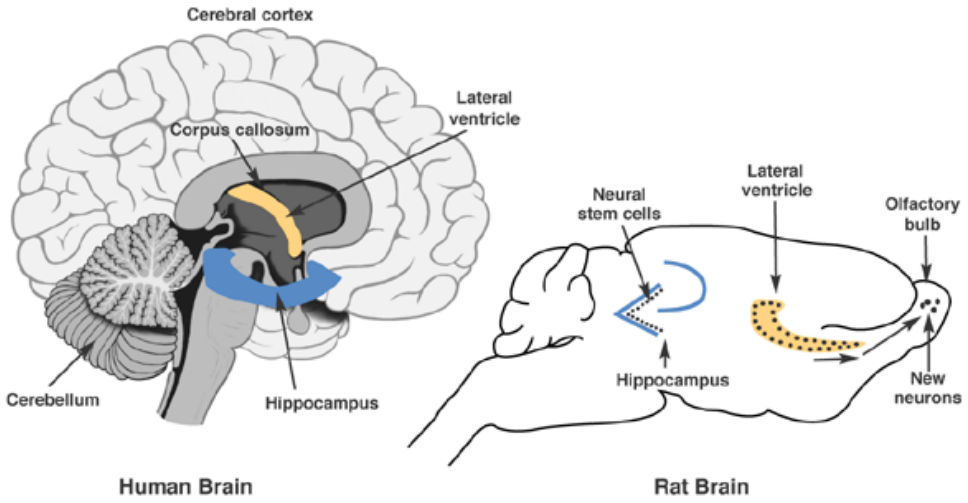


Figure 2.2 – Sites of adult neurogenesis, including the SVZ of the lateral ventricle and the SGZ of the hippocampus, observed in the human and rat brains. Adapted from [66]

Today, adult neurogenesis in the SVZ and the SGZ stem cell niches is widely accepted to take place in many species, including rodents and primates. Neuroblasts generated from the SVZ migrate through the rostral migratory stream (RMS) to the olfactory bulb, where

they differentiate into mature neurons and modulate our sense of smell. Neuroblasts born from the SGZ however differentiate and synapse within the local circuitry of the hippocampus [67].

Functionally, adult neurogenesis is enhanced by behaviours including environmental enrichment and running in rodents [68, 69]. It can also be limited by factors such as stress and drugs, or enhanced by stroke, seizures and brain tumours as observed in animal models [70, 71]. Adult neurogenesis in the SVZ is also enhanced after controlled cortical impact, proliferation increases and neuroblasts migrate from the SVZ to the injured cortex [72].

The newborn neurons from the SVZ and the dentate gyrus are fully functional. The review by Braun *et al*. suggests that these neurons can contribute to olfactory- and hippocampus-dependent learning and memory, respectively. Various aspects of memory have been implicated in adult neurogenesis including spatial and object recognition [73], pattern separation [74], fear conditioning and synaptic plasticity [75]. Patients with low newborn neurons in the hippocampus would also suffer from hippocampus-dependent behaviour deficits [76].

Due to the possibility that the human brain could repair itself, the discovery of adult neurogenesis has raised hope that endogenous stem cells and neurogenesis have therapeutic potential for brain injuries and even neurodegenerative diseases such as Alzheimer's disease and Huntington's disease [77]. A number of interesting studies have tested this using NSCs from the SVZ, and these studies will be discussed later in the review.

2.2.3 Migration of neural stem cell progeny

After being generated in the SVZ, neuroblasts migrate anteriorly through a path named the rostral migratory stream (RMS) to the olfactory bulb, where they differentiate into interneurons. The pathway is illustrated in figure 2.3.

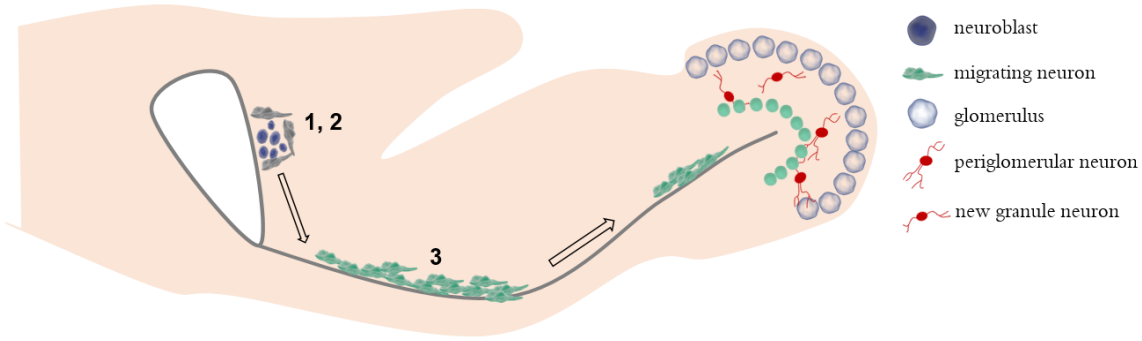


Figure 2.3 – Migration of neural stem cells from the subventricular zone to olfactory bulb. Adapted from [78]

The generation of interneurons and their migration towards the olfactory bulb consists of several key stages. Firstly, quiescent NSCs from the lateral ventricle become activated and proliferate, thereby generating transit amplifying progenitor cells (TAPs). Secondly, TAPs go through 3-4 rounds of division and ultimately give rise to young neurons called neuroblasts. In the third stage, these immature neurons migrate through the RMS, occasionally stopping to divide thereby further expanding their numbers. The detachment of the immature neurons from the RMS is signalled by the diffusible molecule reelin and initiated by tenascin R, which also directs neuroblast migration to their target areas [78]. When they reach the olfactory bulb, the neuroblasts differentiate into a variety of granule

layer or periglomerular neurons. The time course from NSCs to differentiated neurons in the olfactory bulb takes approximately 2-4 weeks in rodents [78].

2.2.4 Differentiation pathway of neural stem cell progeny

It is clear that in the SVZ and SGZ, stem cells can generate neurons, astrocytes and oligodendrocytes. However, whether individual stem cells can give rise to all three lineages has been difficult to prove. There is some evidence for a small number of these "tripotential" stem cells in the dentate gyrus [79], but in the SVZ it has not been proven. *In vitro*, NSCs are grown as neurospheres (figure 2.4) in the presence of growth factors (epidermal growth factors and fibroblast growth factor 2) and are able to self-renew and differentiate into neurons, astrocytes or oligodendrocytes. SVZ NSCs can be grown at clonal dilution or as individual cells which are tri- or bi-potential [80]. At higher density culture, NSCs adhere into clusters and thus statements about individual potency can no longer be made. Neurospheres are frequently referred to as neural stem/progenitor cells (NSPGs) as the colonies contain a mixed population of neural stem cells, neural progenitor cells and glial progenitor cells. The mixture is illustrated in figure 2.4B.

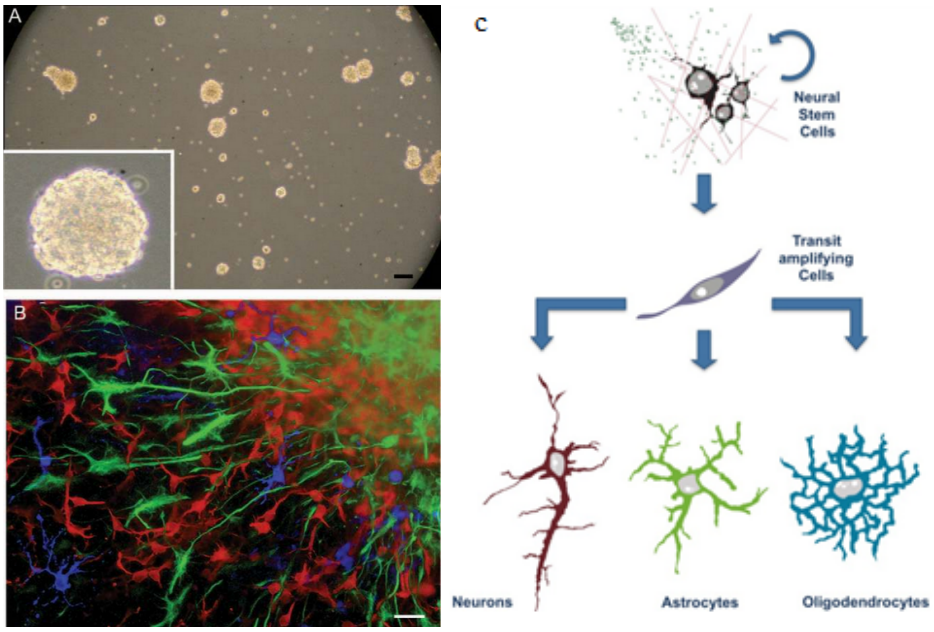


Figure 2.4 – A) Neurospheres from adult mouse subventricular zone after 5 days culture *in vitro* (scale bar = 50 μm), B) Differentiation of neurospheres after withdrawal of growth factors to neurons (red, β-tubulin III), astrocytes (green, GFAP) and oligodendrocytes (blue, O4) (scale bar = 25 μm). C) The differentiation pathway of neural stem cells. Adapted from [80, 81]

2.3 Scaffolds

Scaffolds for tissue engineering are usually constructed as highly porous structures to imitate the natural ECM. Porous structures provide anchor points for cell attachment, allow diffusion of nutrients and waste [9], and guide cell migration. It is known that cell survival, growth and activity are guided by not only biological factors, including

signalling molecules and surface chemistry, but also by the physical topography, which plays a vital role [23]. For example, patterned substrates are able to guide cell alignment [82], morphogenesis, differentiation [83] and migration [84].

Traditionally, cell and tissue culture are performed in 2D environments such as multi well-plates or petri dishes. In the brain however, neurons reside in a complex 3D network of ECM. The topography of stem cell niches around the SVZ can significantly affects the differentiation of NSCs. Cells residing in ECM are able to remodel themselves and their environment by degrading and secreting ECM. Thus the 2D environments in which tissue are cultured lack the complexity and topography compared to the natural ECM. Therefore 3D scaffolds is very likely essential for tissue engineering studies [12].

Scaffolds can be classified into natural scaffolds, which are those based on natural substances, and synthetic scaffolds, which are frequently man-made polymer-based materials. Common synthetic biomaterials include polylactic acid (PLA), polyglycolic acid (PGA) and polycaprolactone (PCL) [85]. Synthetic biomaterials avoid the batch-to-batch variance observed on natural biomaterials [86] and often cost less as the synthetic process is usually less complicated than natural biomaterial extraction [87]. Synthetic materials however, fail to match cell viability and proliferation rates that are observed on natural materials [88], and may also result in toxic by-products after degradation [89].

Natural biomaterials can be classified into two major categories: protein-based biomaterials, including Coll, CSPG, fibronectin and silk, and polysaccharide-based, including hyaluronan and chitosan [90]. Naturally-derived biomaterials have superior biocompatibility compared to synthetic biomaterials as their products are often non-toxic,

and their degradation rate can be altered based on processing formulation or molecular weight [89]. In addition, the helical structure of some macromolecules such as Coll is crucial for morphogenesis [91]. However, they may also cause an immunogenic response in the host tissue [92], and are often difficult to process due to their high water solubility [93]. Table 2.1 below summarises the major advantages and disadvantages of synthetic and natural biomaterials. Despite the advantages of synthetic biomaterials, their inferior biocompatibility is a key weakness. Thus we believe that natural biomaterials hold a better chance of becoming the most suitable scaffold materials for tissue engineering.

Table 2.1 – Advantages and disadvantages of synthetic v. natural biomaterials

Biomaterial	Advantages	Disadvantages
Natural	Better biocompatibility [89, 94]	Generally weak mechanical properties
	Better bioactivity, e.g. morphogenesis [91]	May cause immunogenic response [92]
		Batch-to-batch variance [86]
	Better controlled degradation rate [89]	More difficult to process [93]
	Non-toxic products	
Synthetic	Controllable shape, architecture and chemistry [93]	Inferior biocompatibility [88]
		May release toxic or acidic products after degradation [89]
	Controllable mechanical properties	
	Low immunogenicity [95]	
	Less batch-to-batch variance [86]	

2.3.1 Collagen

Coll is the most abundant protein within the human body, constituting one-third of total protein and 75% of the total weight of dry skin. To date, 28 types of Coll have been discovered [96]. Although not widely expressed in the CNS, it is found in most other organs, including tendon, cartilage, bone, teeth and blood vessels [97]. It is the most important constituent of the ECM in terms of structural support in organs other than the CNS [98]. In addition, Coll is involved in a number of other essential biological activities such as scaffolding, morphogenesis and injury repair. As a naturally derived polymer, Coll has excellent biocompatibility, and therefore has been employed in tissue engineering of a range of organs, including heart valves [99], lungs [100], and bone [101].

Coll is a fibrous protein consists of a triple helix structure of two identical repeating polypeptide chains (α1-chains) and one different α2-chain. All chains have the same molecular structure -(glycine-X-Y)$_n$-, where X and Y are typically proline and hydroxyproline. Glycine is the smallest amino acid, allowing the chains to form a triple helix structure. The extensive H bonds within the triple helix structure give rise to the high tensile strength of Coll, and the triple helix structure of Coll, where every X and Y position is exposed to solvents, makes Coll easy to bind to other molecules [102-104].

Due to its easy fabrication process, abundance in the human body and good structural properties, Coll has been widely used in tissue engineering, including the brain. It has also been widely functionalised or used to incorporate other molecules to enhance bioactivity and cell adhesion by providing anchorage points [105-107]. Although commonly thought of as a structural protein, Coll has been recently studied for other biological functions in

the nervous system. Studies have shown that Coll can be expressed by neurons and to assist multiple aspects of neural development including cell proliferation, attachment, migration, differentiation and attachment and axonal outgrowth [22, 108].

Moreover, it is worth noting that type I Coll is also a major component for a number of commercialised nerve conduits for the PNS, including Neuragen®, Neuroflex™, NeuroMatrix™, NeuraWrap™ and NeuroMend™ [22].

2.3.2 Hyaluronic acid

Hyaluronic acid (HA), or hyaluronan, is a ubiquitous high molecular weight glycosaminoglycan (GAG) that is found in virtually all ECM. It is a repeating polymer that contains $_{D}$-glucuronic acids and n-acetyl-$_{D}$-glucosamine as illustrated by figure 2.5 [107]. HA, along with chondroitin sulfate proteoglycan (CSPG), is the most commonly found ECM component in the human brain.

Within the CNS, HA is predominately expressed by astrocytes and sometimes by other glial cells and neurons [109]. Within the white matter, HA is localised around myelinated fibres, where HA is secreted in between myelin and astrocyte processes. In grey matter, HA tends to localise around neurons.

HA is responsible for a number of important biological activities. For example, HA maintains the ECM surrounding cells, creates free-space for cells upon hydration, and importantly, activates cell receptors for growth, migration and differentiation. Increased HA content and crosslinking density were shown to reduce cell migration and proliferation,

while higher RGD content promotes earlier cell differentiation and more abundant migration [110].

In developing rodents, HA is expressed at high levels in the CNS ECM. In adults however, the expression is largely reduced. Recent studies showed that in adult rats, HA still remained at high levels in the SVZ, where NSCs regenerate and proliferate, and in the RMS, where NSCs migrate towards the olfactory bulb. In addition, HA was shown to accumulate around the lesion area after photothrombotic stroke, where migration of neurons were observed [111]. Although the authors did not specify the functions of HA, the coincidence that HA is expressed in the same area of NSCs proliferation and migration suggests that it may play a crucial role in NSC migration and proliferation. The hypothesis is further supported by the studies of Baier *et al*., who discovered that HA forms fibre-like structures along the migratory pathways in the developing cerebellum [112].

In the nervous system, HA functions along with a number of HA-binding proteoglycans, also known as hyalectans or lecticans. Lecticans consist of four major proteoglycans: aggrecan (CSPG1), neurocan (CSPG3) and brevican (CSPG7) and versican (CSPG2) [9]. It is hypothesised that HA binds to neuronal cell bodies, and HA and the hyalectans are suspected to regulate glial cell and neuron migration, inhibit scar formation, neurite outgrowth, synaptic modulation and axon pathfinding [9, 105, 113, 114]. In contrast, there were also studies which showed that HA inhibited neurite outgrowth *in vitro* [115, 116].

HA binds to a number of transmembrane receptors, including CD44, receptor for hyaluronic acid-mediated motility (RHAMM), layilin, LYVE-1 and toll-like receptor 2 and 4, which all bind and signal to different molecular weights of HA [109]. Many of

these receptors are able to assist cell migration *in vivo*. For example, developing neurons were observed to express RHAMM and oligodendroglial cells were observed to express both RHAMM and CD44 [112]. CD44 was shown to lead astrocyte migration [117] and RHAMM was shown to be expressed by migrating SVZ and cranial neural crest cells, indicating potential roles in migration [111, 118].

Furthermore, CD44 was shown to take part in neuronal differentiation. Removal of CD44 in mice led to a delayed neuronal differentiation and an enhanced astrocytic differentiation [119]. In addition, an increase in CD44 was found to activate Wnt-induced activation, thereby directly influence on Wnt/β-catenin signalling, which is an important cascade in neuronal differentiation [120].

The surfaces of both HA and CSPG are highly negatively charged, with one to three charges per disaccharide unit on average [121], hence they attract cations and positively charged proteins. Consequently, brain tissue can expand up to 10 times in volume upon hydration [9]. Although having the same molecular structure, fragmented HA (lower molecular weight) and the native polymer form of HA (higher molecular weight) behave differently in terms of their biological functions. Fragmented HA was found to induce inflammatory responses by binding to a number of immune cells, whereas higher molecular weight HA is able to support cell survival [107] and migration and transcriptional activation via HA-CD44 binding [117].

HA functions have been studied in the regeneration of bone [122], cartilage [123] and spinal cord [124]. HA is often synthesised in the laboratory in the form of hydrogels, where cells are encapsulated prior to gelation. The hydrogels are injectable, thus reducing

the need to conduct open surgeries [107]. Studies of injectable crosslinked HA showed that the intrathecal injection of the gel into the spinal cord did not cause functional or tissue damage [124].

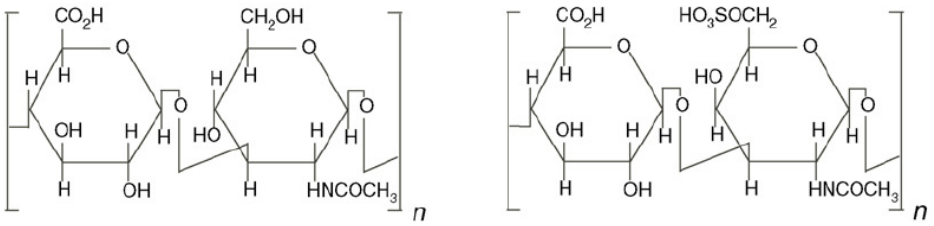


Figure 2.5 – Molecular structure of hyaluronan (left) and chondroitin-6-sulfate (right) [109]

2.3.3 Chondroitin sulfate

As illustrated in figure 2.1, chondroitin sulfate proteoglycans (CSPG), along with hyaluronan, are the major components in the PNNs and the neural interstitial matrix. Within the brain ECM, CSPGs are secreted by all cell types and are responsible for providing guidance cues for growth of neuronal boundaries in the developing CNS [125]. CSPGs contain a core protein chain with side chains of covalently bonded chondroitin sulfate glycosaminoglycans (CS-GAGs). The GAG chains are polysaccharides consisting of linear repeating CS disaccharide molecules. Depending on the core protein, CSPG can be subdivided into different forms, including aggrecan (CSPG 1), brevican (CSPG 7), versican (CSPG 2), NG2 (CSPG 4), neurocan (CSPG 3), and phosphacan, etc.. All types of CSPGs are generally extracellular although NG2 is also found in the cell membrane

[52]. It is generally accepted that only the GAGs are the major functional component of CSPGs since the core protein contributes little to its biological activities.

As discussed in the previous section, the surface of CSPG is also highly negatively charged. This property makes it able to bind to positively charged ions and molecules, including glutamate, a charged neurotransmitter [126]. CSPG is also able to bind to a number of proteins in the brain's ECM and adhesion molecules, and thus has various functions [127]. The proteins include laminin, neural cell adhesive molecule (NCAM) and neural glial cell adhesive molecule (NgCAM). NCAM and NgCAM are the most important neural cell adhesion molecules for cell adhesion, migration and axonal development. NCAM and its post-tranlational glycosylation via polysialic acids is especially important for SVZ neuroblast migration [128, 129]. Studies have shown that through interaction with these molecules, neurocan was able to inhibit cell adhesion and neurite outgrowth [130, 131].

CS can take various forms depending on the position of the sulfate groups. The most common ones are chondroitin-4-sulfate (C4S) and chondroitin-6-sulfate (C6S), although the latter is more common than C4S in developing brains [132]. The structure of CS contains repeating units of $_{D}$-glucuronic acids and n-acetyl-galactosamine, as illustrated in figure 2.5 [109].

CS has been widely employed in tissue engineering for many organs, including skin [133], cartilage [134], bone [135] and less commonly in CNS [49].

After human brain injuries, CSPG is significantly upregulated. In spinal cord injuries, CSPG is secreted by astrocytes and subsequently forms a major component in the glial scar, which hinders penetration of neurite outgrowth, and thus neuroregeneration [136]. Studies on astrocyte cultures *in vitro* also showed that epidermal growth factor (EGF) stimulates the synthesis of neurocan and phosphacan, which are part of the CSPG family.

The lack of neuroregeneration after CNS injuries is attributed to both the inability of neurons to grow, and the inhibitory molecules that seal the injury sites. CSPG is thought to be as one of the major ECM molecules that inhibits axonal regeneration. This phenomenon is confirmed by several studies which showed that CSPG induced growth cone collapse. Removal of CSPG by chondroitinase ABC, an enzyme that digests the CS-GAG side chains of CSPG by eliminative degradation of the polysaccharides of disaccharides within the CS molecules, also seemed to remove most of the glial scar and enhance axonal spouting [43, 125].

On the other hand, studies on contactin-1, a cell-surface receptor for CS, was shown to promote neurite outgrowth on neuroblastoma [137]. Hence although the inhibitory ability of CS is confirmed by numerous studies, the exact mechanism of each receptor needs to be investigated in much more detail to elucidate the context-dependent specific functions of CS in the CNS.

2.3.4 Fabricating collagen, hyaluronic acid and chondroitin sulfate scaffolds

The fabrication process for a Coll scaffold is frequently a freeze-drying process [135-138]. Coll slurries are first mixed with diluted hydrochloric acid or ethanoic acid solution, frozen at various temperatures and subsequently freeze-dried. The frozen water produces an interconnected porous structure, and sublimates during the freeze-drying process. In tissue engineering for the CNS, 1.0wt% Coll was determined by Elias to be optimal, as the scaffold has the closest stiffness to the brain's [141]. In a human brain, stiffness can be affected by a variety of factors, including region, age and disease. However, the stiffness of healthy patients' brains is normally 2-3 kPa [142, 143]. Coll, along with HA, are also often synthesised as a hydrogel, where cells are encapsulated before [144] or after gelation [145-147]. Furthermore, Coll is often tailored to incorporate other biomaterials, including CS [49], HA, chitosan, polyethylene glycol (PEG) and alginate [9] for the CNS.

Due to the weak physico-mechanical properties of CS, it is rarely used alone (Czernuszka lab, unpublished data). Some other materials used with CS for the CNS include multi-wall carbon nanotubes (MWCNTs) [148], Coll [21] and HA [149]. Coll-CS scaffolds are commonly synthesised by mixing Coll and CS in a single solution, where the solution is then frozen and freeze-dried. To avoid CS from dissolving away, the composite scaffolds are often crosslinked. Common crosslinking approaches include 1-ethyl- 3-(3-dimethyl aminopropyl) carbodiimide hydrochloride (EDC) and N-hydroxysuccinimide (NHS) crosslinking [49] and dehydrothermal (DHT) crosslinking [150].

Another approach to produce composite scaffolds of Coll-CS or Coll-HA is named interpenetrating polymer network (IPN), which consists of two or more networks formed

independently. Depending on the preparation process, an IPN can be classified as a simultaneous IPN, where both networks form simultaneously, or a sequential IPN, where one network forms prior to the other [151]. IPNs have been successfully used in biomedical and pharmaceutical applications due to their distinct ability to maintain the original properties of both polymers and lead to improved properties from the composite [152]. In addition, IPN structure offers greater choice of components and crosslinking densities, since the basic networks can be either physically entangled or chemically crosslinked [153].

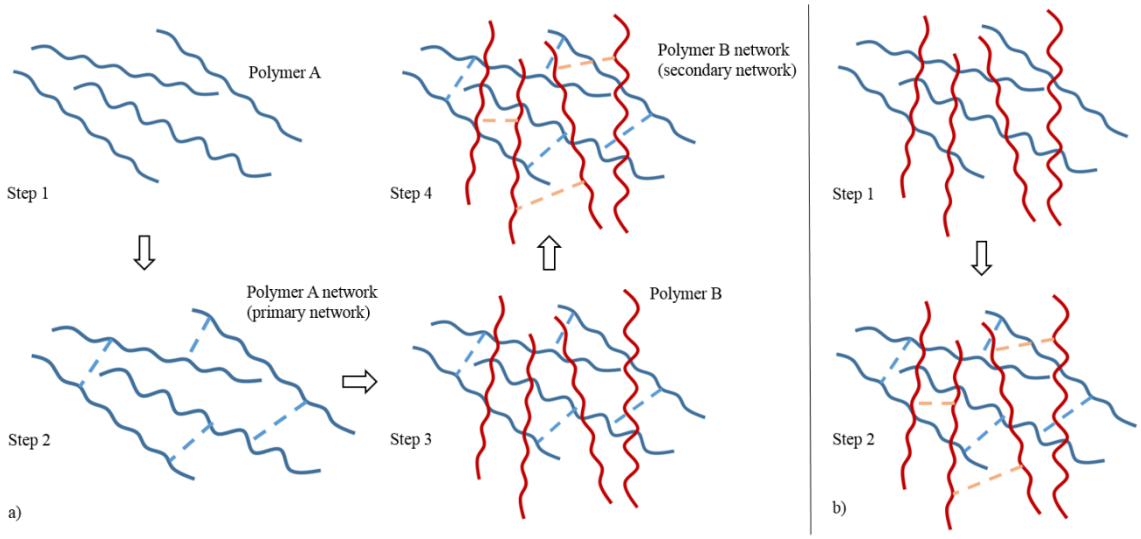


Figure 2.6 – Illustration of the sequential pathway and the simultaneous pathway of synthesising an IPN from polymer A and B. A) In a sequential IPN, polymer A forms a network (primary network) prior to polymer B (secondary network), B) whereas in a simultaneous IPN, both networks forms at the same time in the presence of crosslinkers [152]

The definition of an IPN prohibits the formation of chemical bonding between the primary and secondary networks, and limits the interactions to physical entanglements only. However, current technologies limit the detection of all chemical bonding in a macroscopic sample. Techniques including atomic force microscopy (AFM) can only scan a small area. Thus, it is difficult for researchers to completely eliminate any chemical bonding that may occur in IPN synthesis, which often includes the use of crosslinkers to form the network. The common practices to avoid chemical crosslinking include dialysis to remove crosslinkers, react for an excess amount of time to degrade crosslinkers, and use an excess amount of crosslinkers to react most of the available crosslinking sites on one network. Although these approaches are effective, these cannot ensure that not a single chemical crosslinking has taken place.

2.4 Cell-scaffold interactions

Despite the complexity of the CNS and the short history of the field, there have been various reports of tissue engineering for the CNS using natural scaffolds seeded with cells in the past few years. Although not extensively studied, the current results, which will be discussed here, clearly show that tissue engineering therapy for CNS diseases is not beyond reach.

Studies have shown that neural activities within the brain are highly dependent on interaction with the ECM. The microenvironment can strongly affect cell viability,

differentiation, migration and proliferation [154]. The biological scaffolds therefore must imitate the natural ECM as much as possible, ideally in a way to enhance the endogenous regenerative abilities of the brain. The cellular responses, both *in vivo* and *in vitro*, to engineered matrices is summarised in this section.

2.4.1 Cell-scaffold interactions on collagen

As the most commonly used natural biomaterial, Coll has been shown to encourage neurite outgrowth, proliferation, migration and differentiation in culture. Although not extensively expressed in the CNS, Coll has been used as scaffolds for neurons due to its proven bioactivity with other tissues [155-158].

The mechanical properties of scaffolds can affect cell migration *in vitro*. Mori *et al*. studied the discrepancies of migration behaviour of neurons and glial cells differentiated from NSPCs on a Coll gel. Neuronal migration was independent of scaffolds stiffness, whereas glial cells migrated more on stiffer scaffolds. After brain injuries, glial cells proliferate near the injury site and form a glial scar. This scar is detrimental to brain recovery since it blocks the growth of neurite axons. Implanting a soft scaffold after brain injury may prevent astrocytosis *in vivo*, which could potentially alleviate the formation of glial scar and support neuroregeneration [159]. The same results is also observed on polyacrylamide gel scaffolds [160].

3D Coll scaffolds seeded with motor neurons from the spinal cord of postnatal day 7 Sprague-Dawley rats were analysed by Allodi *et al*. Neurite outgrowth was observed 4

days after culture and glial cells had migrated outwards to support the neurites [161]. Egawa *et al*. also observed proliferation of NSCs on Coll gel bound with epidermal growth factor (EGF) by using the MTT assay, a colorimetric assay that measures cell metabolism. According to their studies, Coll could prevent glial cell invasion *in vivo*, thereby preventing cell death after implantation of NSCs. In addition, NSCs cultured on EGF-incorporated Coll gels tend to differentiate more in a 3D environment than on flat scaffolds. This was speculated to be due to the tendency of NSCs to form neurospheres in 3D, which inhibited the diffusion of growth factors to their centre [162].

3D culture of embryonic stem cells (ESCs) on both type I Coll gel and sponge showed most of the cells were able to penetrate into both of them. Those differentiated into neuronal lineages were shown to express nestin, a NSC marker, Ki-67, a proliferation marker, and class III β-tubulin, a neuronal marker [163].

However, the resulting suggesting that Coll would facilitate NSC growth, in many cases, were very likely to due to growth factors. Long-term studies of culturing SVZ NSCs on type I Coll showed a continuous drop of viability, reaching 25% at the end of three months. The results suggest that Coll by itself might not be effective enough for long term NSC survival. In addition, NSCs cultured on Coll also showed low cell differentiation and migration [164].

Despite the concern from long-term studies, *in vivo* studies of implanting Coll scaffolds showed promising results. Chen *et al*. compared the survival of human amnion-derived multipotent progenitor (AMP) cells injected *in vivo*, with or without a Coll type I scaffold. AMP cells with the scaffold significantly reduced axonal degeneration in the corpus

callosum and thalamus, and enhanced motor functions, as shown by a higher falling latency on the rotarod test [165]. Functional recovery stimulated by a Coll matrix is further supported by Yu *et al*., who noticed a functional recovery as indicated by the formation of synapses after 30 days of implanting pure Coll type I scaffold into cerebral ischemic injury of adult Wistar rats [166].

To further prove the effectiveness of Coll as an implant for CNS repair, Elias *et al*. studied the cellular reaction of implanting a pure Coll scaffold to a penetrating brain injury site on adult Sprague-Dowley rats. The scaffold was seeded with neural progenitor cells (NPCs) from the adult rat hippocampus. After four weeks, proliferating cells were observed to migrate several hundreds of micrometers into the lesion site. However, a large portion of the implanted progenitor cells remained undifferentiated [167]. This results confirmed with Koutsopoulos and Zhang's results mentioned earlier that Coll does not promote significant differentiation [164].

In addition, the Coll scaffold was not observed to have an effect on the surrounding glial scar detected by an intense GFAP staining, and astrocytes from the glial scar did not migrate into the scaffold. These results suggest that Coll may not play an active role in interacting with the glial scar in the CNS [167].

Although various studies reported that type I Coll scaffolds may promote proliferation and differentiation, many of these studies are based on the use of growth factors. Coll by itself does not seem to be enough to support NSC differentiation and survival.

2.4.2 Cell-scaffold interactions on chondroitin sulfate

Although a vital component of the CNS ECM, CS as scaffolds for CNS tissue engineering has been barely studied. This could be due to its ability to inhibit neurite outgrowth and its high solubility in water, rendering the experiments difficult. *In vitro* studies on CSPG indicated it inhibits neurite outgrowth, even in culture. Chicken dorsal root ganglia (DRG) neurons cultured on laminin plates were allowed to spread over the dish. However neurite either stopped abruptly or turned away from the CS-rich region [168].

However, a study on a CS hydrogel showed somewhat contradictory results. Conovaloff *et al*. compared the effect of CS and HA hydrogels on DRG. The cultures lasted for three days, however they noticed faster neurite outgrowth and significantly higher neurite growth rates on CS [169]. This result seems to contradict to the above observation. However this may be due to a different environment in the gel, compared to a flat dish, and CS's surface receptors, e.g.contactin-1, which may improve neuronal growth.

Huang *et al*. implanted an unseeded acellular Coll-CS scaffold into a surgical TBI. Results revealed increased numbers of migratory doublecortin positive (Dcx+) cells in the implant and increased proliferation compared to the injured sites without the scaffold. In addition, they also observed an increased brain-derived neurotrophic factor (BDNF) expression, a regulator of adult synapses in the CNS, and glia-derived neurotrophic factor (GDNF), a neurotrophic factor for neurite outgrowth, recruited by the scaffold [21]. Hence, it is difficult at this point to generate a conclusive statement on the effectiveness of CS as a potential scaffold for CNS tissue engineering. Even if CS inhibits neurite outgrowth in culture, there are possibilities of utilising it as a guide for NSCs migration.

2.4.3 Cell-scaffold interactions on hyaluronic acid

Compared to CS, HA was shown to induce more positive cellular responses, including differentiation and cell survival. Lam *et al* studied the effect of implanting a pure HA gel with NPCs from induced pluripotent stem cells (iPSC/NPC), and compared that to the direct transplantation of the cells into a murine model of stroke. As a result, they noticed that HA did not enhance cell viability significantly, but enhanced differentiation of NPC into neuroblasts over one week, as observed by an approximately 30% increase in normalised Dcx+ area fraction [110].

Another study on an injectable HA hydrogel investigated the survival of transplanted mouse C17.2 cell line, human NPCs and human glial-restricted precursors, and significant improvement (1.2 to 1.5 fold) in cell viability was observed in all cell types [107].

Several more studies have investigated the survival of NSCs within HA hydrogels. In the first study, Zhong *et al*. compared the survival of NPCs derived from embryonic cortex cultures with and without a hyaluronan-heparin-Coll hydrogel. The study lasted for two weeks and they noticed that 8% of the cells survived on the hydrogel, compared to 4% without the hydrogel. Contrary to some other studies, however, they failed to notice differences in cell differentiation and cell migration caused by the hydrogel scaffold, including Dcx+ cells [114].

In addition, Placone *et al*. studied HA as a scaffold for astrocytes. As a result, addition of HA into Coll was able to increase total processes length, degree of branching and size of the cells, although no branching was observed on HA scaffold without Coll [29].

Furthermore, differentiation of neural progenitor cells (NPCs) was investigated on high molecular weight HA hydrogels with different stiffnesses. The stiffness was controlled by varying photocrosslinkable methacrylate groups on HA. As a result, Seidlits *et al*. noticed a very low NPC viability on the stiffest hydrogel and remarkable differences in the differentiation behaviour of NPCs. After 21 days of culture in a HA hydrogel, NPCs on softer gel with similar stiffness to neonatal brains differentiated mostly to ß-III tubulin positive cells (neurons), whereas on stiffer gels with similar stiffness to adult brain, NPCs tend to differentiated into GFAP+ cells [33].

This result, along with the experiment by Mori *et al*. [159] and [160] on Coll and polyacrylamide gel respectively, suggests that implanting a stiffer scaffold into a brain lesion may lead to formation of a glial scar (more GFAP+ cells), while implanting a soft scaffold may result in functional improvement (more ß-III tubulin+ cells).

To conclude, Coll-HA scaffolds seem to be a more promising scaffold compared to Coll-CS scaffolds. The reasons are:

1. HA is suggested by many to enhance cell viability, as compared to other scaffolds,
2. *In vivo* properties of CS indicates that it may prohibit neurite outgrowth, and
3. *In vivo* studies of HA implants indicate a higher neuronal differentiation.

As discussed, it is difficult to draw a conclusive statement on the effect of HA, CS or Coll as scaffolds for CNS tissue engineering yet, since contradictory cellular responses are common. However, it is evident that these scaffolds alone are insufficient for the total recovery because they lack either mechanical properties or biological properties. Hence,

an IPN that combine these materials together may be a reasonable choice, as it combines the advantages of these materials in a more efficient way.

Table 2.2 below summarises the *in vivo* functions of these biomaterials hypothesised and their cellular response observed in culture.

Table 2.2 – Effect of different scaffolds on types of CNS cells

Biomaterial	Functions in CNS	Cellular response
Coll	- Assist differentiation, migration, proliferation and cell attachment - Regulation of axonal outgrowth [22, 108]	- Enhances motor neuron migration [161] - Enhances NSC survival [162] and glial cell migration [161] - Promotes NPC migration *in vivo* [167] - Reduce NSC viability, discourage differentiation and migration in long term [164]
CS	- Forms glial scar upon injury - Inhibits neurite outgrowth - Induced neurite growth cone collapse	- Enhances Dcx+ migration in a Coll-GAG scaffold [21] - Enhances DRG neurite outgrowth and growth rate compared to HA [169]
HA	- May promote NSC migration and differentiation [110-112, 117] - Attract cations and positively-charged proteins [9]	- Enhances NPC differentiation [110] - Enhances NSC, mouse C17.2 cells, human neural progenitor cells and human glial-restricted precursors survival [107, 114]

Table 2.3 below summarises the detailed cellular behaviours in different culture experiments mentioned in the section.

Table 2.3 – Cellular behaviours on Coll, CS and HA scaffolds (continued from page 40)

Differentiation	Migration	Neurite outgrowth	Cell viability	Others
Neuronal and glial lineages differentiated better in 3D			40% of seeding density	
50% cells expressed Nestin, a marker for undifferentiated NSCs	Most ESCs penetrated into the gel, forming dense clusters as well as tubular or spherical glandular-like structures			
Limited differentiation observed	Low cell migration		25% NSCs alive after 3 months	
No differentiation observed	AMP cells migrated from striatum to SVZ and corpus	Significantly reduced neurite degeneration		Functional recovery on a rotarod
In vivo: no neurons, no Dcx+ cells in or around the scaffold; *in vitro*: few astrocytes, no neurons	Migration several hundred micrometers into the lesion site		Low surviving cells	No effect on the glial scar
				New synapses formed between NSCs
1-4% tubulin III+ neuron	Migration of neuron is independent of stiffness, while migration of glial cells is			
		Neurite either stopped or turned away from the CS		
		DRGs on CS had longer neurites than those on HA. Significantly higher growth		
a 7-fold increase in Dcx+/ NeuN+ cells on D21	Migration of immature migratory neurons observed	Enhanced concentration of GDNF, a neurotrophic factor for neurite outgrowth		Enhanced GDNF and BDNF expression
NPCs differentiating to neuroblasts			No significant enhancement	
	Cells migrated out from scaffold without restriction		1.2 - 1.5 fold increase in all cell types	
No difference in cell differentiation	No difference in cell migration		8% survived, compared to 4% without hydrogel	
NPCs on softer gel were mostly ß-III tubulin+, whereas on stiffer gels, NPCs tend to differentiated into astrocytes			Low NPCs viability on the stiffest hydrogel	

Materials	Cell type	Cell density	Days in culture	Proliferation
Coll gel [162]	NSCs fetuses embryonic D17 Sprague Dawley rats	2.0 x 10^6 cells/mL	7D *in vitro*	Coll cannot provide enough proliferation for NSCs without EGF
Coll sponge [163]	Undifferentiated R366.4 rhesus monkey ES cells	n/a	24D *in vitro*	Many proliferation cells observed by Ki-67
Coll gel [164]	Adult NSCs isolated from the SVZ of an 8 week old CD-1 albino mouse	5 x 10^5 cells/mL	5 months *in vitro*	
Coll sponge [165]	human amnion-derived multipotent progenitor (AMP) cells	2× 10^6 AMP cells in 150 μL Coll	14D *in vivo*	
Coll sponge [167]	Adult hippocampal NPCs	4 x 10^6 per scaffold 4 mm diameter 3 mm thickness	4 weeks *in vivo* (1 week post-PBI)	
Coll sponge [166]	NSCs from 14-day-old embryos Wistar rats	1 x 10^5 cells/mL in vitro, 15,000 cells *in vivo*	6D *in vitro*, 30D *in vivo*	
Coll gel [159]	Cerebral cortex of E14 ICR mice	n/a	7D *in vitro*	
CSPG [168]	Chick E9 DRG	n/a	1D *in vitro*	
CS hydrogel [169]	Chick DRG from fertilised white leghorn eggs	n/a	3D *in vitro*	
1% Coll/0.02% CS [21]		Acellular	28D *in vivo*	Many proliferation cells observed near the cavity
HA gel + RGD [110]	hiPS-NPC	1 x 10^5 cells injected	7D after stroke *in vivo*	HA significantly promoted cell proliferation by 3 fold
HA:gelatin:PEGDA = 2:2:1 [107]	C17.2 NSCs	5 x 10^5 C17.2 cells, in 50 μL of hydrogel	14D *in vivo*	
HA-heparin- Coll hydrogel [114]	NPCs derived from embryonic cortex	1 x 10^4 cells/mL	14D *in vivo* (7D post-stroke)	
Methacrylic anhydride modified HA hydrogel [33]	NPCs from ventral midbrains of E13.5 mice and spinal cord astrocytes	5 mL containing 4 x 10^4 cells	21D *in vitro*	

2.5 Conclusions

Tissue engineering for the CNS is emerging as a promising solution for brain injuries, where scaffolds combined with NSCs may facilitate the regeneration of brain tissue. Adult neurogenesis found in the SVZ of the lateral ventricle and SGZ in the hippocampus has provided much hope for a clinically feasible therapy for diseases such as TBI and stroke. In addition, ES and iPSC derived progenitor cells have been combined with engineered matrices in culture and brain implants. In this review, the ECM of the brain, the adult neurogenesis process, and the three commonly used natural biomaterials: Coll, CS and HA for the tissue engineering for the CNS were reviewed. The fabrication processes for these materials into scaffolds were also examined. As a result, we believe that the use of Coll and HA as a scaffold may be a potential therapy and would push the field closer to a clinically feasible cure.

Studies have shown promising results, as these scaffolds were able to encourage cell migration, proliferation, survival, differentiation and neurite outgrowth. In culture, Coll was shown to promote cell migration and HA was shown to promote mostly differentiation. Migration studies on HA scaffolds were not extensively studied, although HA is suspected to be heavily involved in neural cell migration in the brain. Despite the fact that HA and CS are the main components of the brain's ECM, Coll and HA are considered more promising candidates for ideal scaffolds, as CS inhibits neurite outgrowth after brain lesions by forming scar. However, this property may be eventually utilised in a way to control the migration of NSCs, which can be used to enhance the efficiency of

the tissue engineering therapy. Furthermore, Coll on its own may not be enough as many reports that it lacks the ability to promote differentiation.

Although studies on these materials often show promising results, there lacks a systematic and direct comparison between these materials and their corresponding cellular responses. More detailed research into the exact mechanisms of these materials is needed before we draw conclusions about their functions, both *in vivo* and *in vitro*. For future clinical applications, long-term studies are also essential, since they are vital for later clinical studies and are suggested to have a different cellular response compared to short-term studies.

2.6 References

1. Donation O. UK Statistics for Organ Donation and Transplantation: National Health Service; 2014 [cited 2015 10/04/2015]. Available from: http://www.organdonation.nhs.uk/statistics/.

2. OrganDonor. Organ Procurement and Transplantation Network: U.S. Department of Health & Human Services; 2015 [updated 10 Jul 2015; cited 2015 20 Jul]. Available from: http://optn.transplant.hrsa.gov/.

3. Gordon EJ, Prohaska TR, Sehgal AR. The financial impact of immunosuppressant expenses on new kidney transplant recipients. Clinical transplantation. 2008;22(6):738-48.

4. Foundation NK. Immunosuppressants: National Kidney Foundation; 2015 [cited 2015 20 Jul]. Available from: https://www.kidney.org/atoz/content/immuno.

5. Chmiel B, Karkoszka H, Cierpka L, Wiecek A. Rheological properties of red blood cells in kidney transplant recipients: the role of lipid profile and type of immunosuppresion. Transplantation Proceedings. 2005;37(4):1885-8.

6. Enuganti VKR. P24.14 Severe intracranial hypertension in children on immunosuppresants. European Journal of Paediatric Neurology. 2011;15, Supplement 1:S129-S30.

7. Caplan AI. Review: Mesenchymal stem cells: cell-based reconstructive therapy in orthopedics. Tissue Engineering. 2005;11(7-8):1198-211.

8. Saltzman WM. Tissue engineering: Principles for the design of replacement organs and tissues. New York: Oxford University Publisher; 2004.

9. Hopkins AM, DeSimone E, Chwalek K, Kaplan DL. 3D *in vitro* modeling of the central nervous system. Progress in Neurobiology. 2015;125:1-25.

10. Anderson JM. Biological responses to materials. Annual Review of Materials Research. 2001;31:81-110.

11. Takahashi H, Wang Y, Grainger DW. Device-based local delivery of siRNA against mammalian target of rapamycin (mTOR) in a murine subcutaneous implant model to inhibit fibrous encapsulation. Journal of Controlled Release. 2010;147(3):400-7.

12. Lee J, Cuddihy MJ, Kotov NA. Three-dimensional cell culture matrices: state of the art. Tissue Engineering: Part B. 2008;14(1):61-86.

13. Werner C, Engelhard K. Pathophysiology of traumatic brain injury. British Journal of Anaesthesia. 2007;99(1):4-9.

14. Jaracz K, Grabowska-Fudala B, Górna K, Kozubski W. Consequences of stroke in the light of objective and subjective indices: A review of recent literature. Neurologia I Neurochirurgia Polska. 2014;48:280-6.

15. Ling H, Hardy J, Zetterberg H. Neurological consequences of traumatic brain injuries in sports. Molecular and Cellular Neuroscience. 2015;66:114-22.

16. Headway tbia. Brain injury statistics 2015 [cited 2015 25/09]. Available from: https://www.headway.org.uk/brain-injury-statistics.aspx.

17. Foundation BT. TBI Statistics, Facts About TBI in the USA 2015. Available from: https://www.braintrauma.org/tbi-faqs/tbi-statistics/.

18. Martínez-Ramos C, Gómez-Pinedo U, Esparza MaAG, Soria JM, Barcia JA, Pradas MM. Neural tissue regeneration in experimental brain injury model with channeled scaffolds of acrylate copolymers. Neuroscience Letters. 2015;598:96-101.

19. Wang X, He J, Wang Y, Cui F-Z. Hyaluronic acid-based scaffold for central neural tissue engineering. Interface Focus. 2012;2:278-91.

20. Guan J, Zhu Z, Zhao RC, Xiao Z, Wu C, Han Q, *et al*. Transplantation of human mesenchymal stem cells loaded on collagen scaffolds for the treatment of traumatic brain injury in rats. Biomaterials. 2013;34:5937-46.

21. Huang K-F, Hsu W-C, Chiu W-T, Wang J-y. Functional improvement and neurogenesis after collagen-GAG matrix implantation into surgical brain trauma. Biomaterials. 2012;33:2067-75.

22. Trends in the design of nerve guidance channels in peripheral nerve tissue engineering [Internet]. Progress in Neurobiology. 2015 [cited 27 Jul 2015].

23. Clements IP, Munson JM, Bellamkonda RV. Neuronal Tissue Engineering. In: Ratner BD, Hoffman AS, Schoen FJ, Lemons JE, editors. Biomaterials Science: An Introduction to Materials in Medicine. 3rd ed: Academic Press; 2012. p. 1291-306.

24. Herculano-Houzel S. The human brain in numbers: a linearly scaled-up primate brain. Frontiers in Human Neuroscience. 2009;3.

25. Levitan IB, Kaczmarek LK. The Neuron: Cell and Molecular Biology. 3 ed. New York: Oxford University Press; 2002.

26. Zhou H-X, Li X-Y, Li F-Y, Liu C, Liang Z-P, Liu S, *et al*. Targeting RPTPσ with lentiviral shRNA promotes neurites outgrowth of cortical neurons and improves

functional recovery in a rat spinal cord contusion model. Brain Research. 2014;1586:46-63.

27. Cao S-Y, Hu Y, Chen C, Yuan F, Xu M, Li Q, *et al*. Enhanced derivation of human pluripotent stem cell-derived cortical glutamatergic neurons by a small molecule. Scientific Reports. 2017;7(1):3282.

28. Guerriero RM, Giza CC, Rotenberg A. Glutamate and GABA imbalance following traumatic brain injury. Current neurology and neuroscience reports. 2015;15(5):27-.

29. Placone AL, McGuiggan PM, Bergles DE, Guerrero-Cazares H, Quinones-Hinojosa A, Searson PC. Human astrocytes develop physiological morphology and remain quiescent in a novel 3D matrix. Biomaterials. 2015;42:134-43.

30. Oberheim NA, Wang X, Goldman S, Nedergaard M. Astrocytic complexity distinguishes the human brain. Trends in Neurosciences. 2006;29(10):547-53.

31. Volterra A, Meldolesi J. Astrocytes, from brain glue to communication elements: the revolution continues. Nat Rev Neurosci. 2005;6(8):626-40.

32. Song H, Stevens CF, Gage FH. Astroglia induce neurogenesis from adult neural stem cells. Nature. 2002;417(6884):39-44.

33. Seidlits SK, Khaing ZZ, Petersen RR, Nickels JD, Vanscoy JE, Shear JB, *et al*. The effects of hyaluronic acid hydrogels with tunable mechanical properties on neural progenitor cell differentiation. Biomaterials. 2010;31:3930-40.

34. Silver J, Miller JH. Regeneration beyond the glial scar. Nat Rev Neurosci. 2004;5(2):146-56.

35. Fawcett JW, Asher RA. The glial scar and central nervous system repair. Brain Research Bulletin. 1999;49(6):377-91.

36. Cameron-Curry P, Le Douarin NM. Oligodendrocyte precursors originate from both the dorsal and the ventral parts of the spinal cord. Neuron. 1995;15(6):1299-310.

37. Liu Y, Zhou J. Oligodendrocytes in neurodegenerative diseases. Frontiers in Biology. 2013;8(2):127-33.

38. Peferoen L, Kipp M, Valk Pvd, Noort JMv, Amor S. Oligodendrocyte-microglia cross-talk in the central nervous system. Immunology. 2013;141:302-13.

39. Lau LW, Cua R, Keough MB, Haylock-Jacobs S, Yong VW. Pathophysiology of the brain extracellular matrix: a new target for remyelination. Nature Review. 2013;14:722-9.

40. Summers L, Kangwantas K, Rodriguez-Grande B, Denes A, Penny J, Kielty C, *et al*. Activation of brain endothelial cells by interleukin-1 is regulated by the extracellular matrix after acute brain injury. Molecular and Cellular Neuroscience. 2013;57:93-103.

41. Henriksson HB, Papadimitriou N, Tschernitz S, Svala E, Skioldebrand E, Windahl S, *et al*. Indications of that migration of stem cells is influenced by the extra cellular matrix architecture in the mammalian intervertebral disk region. Tissue and Cell.

42. Johnson KM, Milner R, Crocker SJ. Extracellular matrix composition determines astrocyte responses to mechanical and inflammatory stimuli. Neuroscience Letters. 2015;600:104-9.

43. Galtrey CM, Fawcett JW. The role of chondroitin sulfate proteoglycans in regeneration and plasticity in the central nervous system. Brain Research Reviews. 2007;54:1-18.

44. Iozzo, RV. Proteoglycans: Structure, Biology and Molecular Interactions, 1st ed: CRC Press; 2000. p391-3

45. Dityatev A, Schachner M. Extracellular matrix molecules and synaptic plasticity. Nat Rev Neurosci. 2003;4(6):456-68.

46. Yasuhara O, Akiyama H, McGeer EG, McGeer PL. Immunohistochemical localization of hyaluronic acid in rat and human brain. Brain Research. 1994;635(1–2):269-82.

47. Oohashi T, Edamatsu M, Bekku Y, Carulli D. The hyaluronan and proteoglycan link proteins: Organizers of the brain extracellular matrix and key molecules for neuronal function and plasticity. Experimental Neurology. 2015;274;B: 134-44

48. Bitanihirwe BKY, Woo T-UW. Perineuronal nets and schizophrenia: The importance of neuronal coatings. Neuroscience and Biobehavioral Reviews. 2014;45:85-99.

49. Pietrucha K. Physicochemical properties of 3D collagen-CS scaffolds for potential use in neural tissue engineering. International Journal of Biological Macromolecules. 2015;80:732-9.

50. Bikbaev A. Frischknecht R. Heine M. Brain extracellular matrix retains connectivity in neuronal networks. Scientific Report. 2015;5(14527)

51. Halfter W, Yip J. An organizing function of basement membranes in the developing nervous system. Mechanisms of Development. 2014;133:1-10.

52. Haylock-Jacobs S, Keough MB, Lau L, Yong VW. Chondroitin sulphate proteoglycans: Extracellular matrix proteins that regulate immunity of the central nervous system. Autoimmunity Reviews. 2011;10(766-772).

53. Koppe G, Bruckner G, Hartig W, Delpech B, Bigl V. Characterization of proteoglycan-containing perineuronal nets by enzymatic treatments of rat brain sections. J Mol Hist. 1997;29(1):11-20.

54. Deepa SS, Carulli D, Galtrey C, Rhodes K, Fukuda J, Mikami T, *et al*. Composition of Perineuronal Net Extracellular Matrix in Rat Brain: A DIFFERENT DISACCHARIDE COMPOSITION FOR THE NET-ASSOCIATED PROTEOGLYCANS. Journal of Biological Chemistry. 2006;281(26):17789-800

55. Yamaguchi Y. Lecticans: organizers of the brain extracellular matrix. Cellular and Molecular Life Sciences. 2000;57:276-89

56. Ihrie RA, Alvarez-Buylla A. Lake-Front Property: A Unique Germinal Niche by the Laterla Ventricles of the Adult Brain. Neuron Review. 2011;70:674-86.

57. Gross CG. Neurogenesis in the adult brain: death of a dogma. Nature Reviews. 2000;1:67-73.

58. Kempermann G, Gage FH. New nerve cells for the adult brain. Scientific American. 1999;280:48-53.

59. Allen E. Studies on cell division in the albino rat (Mus norvegicus, var. alba). II. Experiments on technique, with description of a method for demonstrating the cytological details of dividing cells in brain and testis. The Anatomical Record. 1916;10(9):565-89.

60. Altman J. Are new neurons formed in the brains of adult mammals? Science. 1962;135(3509):1127-8.

61. Altman J. Autoradiographic and histological studies of postnatal neurogenesis. IV. Cell proliferation and migration in the anterior forebrain, with special reference to persisting neurogenesis in the olfactory bulb. The Journal of Comparative Neurology. 1969;137(4):433-57.

62. Reynolds BA, Weiss S. Generation of Neurons and Astrocytes from Isolated Cells of the Adult Mammalian Central Nervous System. Science. 1992;255(5052):1707-10.

63. Lois C, Alvarez-Buylla A. Proliferating subventricular zone cells in the adult mammalian forebrain can differentiate into neurons and glia. Proceedings of the National Academy of Sciences. 1993;90(5):2074-7.

64. Kokoeva MV, Yin H, Flier JS. Neurogenesis in the Hypothalamus of Adult Mice: Potential Role in Energy Balance. Science. 2005;310(5748):679-83.

65. Robins SC, Stewart I, McNay DE, Taylor V, Giachino C, Goetz M, *et al*. α-Tanycytes of the adult hypothalamic third ventricle include distinct populations of FGF-responsive neural progenitors. Nat Commun. 2013;4.

66. Crews FT, Nixon K. Alcohol, Neural Stem Cells, and Adult Neurogenesis: National Institute on Alcohol Abuse and Alcholism; 2014 [cited 2015 23/09].

67. Deng W, Aimone JB, H.Gage F. New neurons and new memories: how does adult hippocampal neurogenesis affect learning and memory? Nature Reviews Neuroscience. 2010;11:339-50.

68. van Praag H, Kempermann G, Gage FH. Neural consequences of enviromental enrichment. Nat Rev Neurosci. 2000;1(3):191-8.

69. van Praag H, Kempermann G, Gage FH. Running increases cell proliferation and neurogenesis in the adult mouse dentate gyrus. Nat Neurosci. 1999;2(3):266-70.

70. Young CC, Brooks KJ, Buchan AM, Szele FG. Cellular and Molecular Determinants of Stroke-Induced Changes in Subventricular Zone Cell Migration. Antioxidants & Redox Signaling. 2011;14(10):1877-88.

71. Young CC, van der Harg JM, Lewis NJ, Brooks KJ, Buchan AM, Szele FG. Ependymal Ciliary Dysfunction and Reactive Astrocytosis in a Reorganized Subventricular Zone after Stroke. Cerebral Cortex (New York, NY). 2013;23(3):647-59.

72. Ramaswamy S, Goings GE, Soderstrom KE, Szele FG, Kozlowski DA. Cellular proliferation and migration following a controlled cortical impact in the mouse. Brain Research. 2005;2053:38-53.

73. Jessberger S, Clark RE, Broadbent NJ, Clemenson GD, Consiglio A, Lie DC, *et al*. Dentate gyrus-specific knockdown of adult neurogenesis impairs spatial and object recognition memory in adult rats. Learning & Memory. 2009;16(2):147-54.

74. Clelland CD, Choi M, Romberg C, Clemenson GD, Fragniere A, Tyers P, *et al*. A functional role for adult hippocampal neurogenesis in spatial pattern separation. Science. 2009;325(5937):210-3.

75. Saxe MD, Battaglia F, Wang J-W, Malleret G, David DJ, Monckton JE, *et al*. Ablation of hippocampal neurogenesis impairs contextual fear conditioning and synaptic plasticity in the dentate gyrus. Proceedings of the National Academy of Sciences. 2006;103(46):17501-6.

76. Braun SMG, Jessberger S. Adult neurogenesis: mechanisms and functional significance. Development. 2014;141:1983-6.

77. Taupin P. Adult neurogenesis, neuroinflammation and therapeutic potential of adult neural stem cells. International Journal of Medical Sciences. 2008;5(3):127-32.

78. Ming G-l, Song H. Adult neurogenesis in the mammalian central nervous system. Annual Review of Neuroscience. 2005;28:223-50.

79. Bonaguidi MA, Wheeler MA, Shapiro JS, Stadel RP, Sun GJ, Ming G-l, *et al*. *In vivo* clonal analysis reveals self-renewing and multipotent adult neural stem cell characteristics. Cell. 2011;145(7):1142-55.

80. Casarosa S, Zasso J, Conti L. Systems for ex-vivo Isolation and Culturing of Neural Stem Cells2013 2013-04-24.

81. Deleyrolle LP, Rietze RL, Reynolds BA. The neurosphere assay, a method underscrutiny. Acta Neuropsychiatrica. 2008;20:2-8.

82. Hsiao TW, Tresco PA, Hlady V. Astrocytes alignment and reactivity on collagen hydrogels patterned with ECM proteins. Biomaterials. 2015;39:124-30.

83. McUsic AC, Lamba DA, Reh TA. Guiding the morphogenesis of dissociated newborn mouse retinal cells and hES cell-derived retinal cells by soft lithography-patterned microchannel PLGA scaffolds. Biomaterials. 2012;33:1396-405.

84. Zhang Q, Zhao Y, Yan S, Yang Y, Zhao H, Li M, *et al*. Preparation of uniaxial multichannel silk fibroin scaffolds for guiding primary neurons. Acta Biomaterialia. 2012;8:2628-38.

85. Fallahiarezoudar E, Ahmadipourroudposht M, Idris A, Yusof NM. A review of: Application of synthetic scaffold in tissue engineering heart valves. Materials Science and Engineering C. 2015;48:556-65.

86. Leong W, Wang D-A. Engineering Biomaterials for Anchorage-Dependent and Non-anchorage Dependent Therapeutic Cell Delivery in Translational Medicine. In: Cai W, editor. Engineering in Translational Medicine. 1. London: Springer; 2014.

87. Baldwin AD, Kiick KL. Polysaccharide-Modified Synthetic Polymeric Biomaterials. Biopolymers. 2010;94(1):128-40.

88. Pascual-Gil S, Garbayo E, Díaz-Herráez P, Prosper F, Blanco-Prieto MJ. Heart regeneration after myocardial infarction using synthetic biomaterials. Journal of Controlled Release. 2015;203:23-38.

89. Stoppel WL, Ghezzi CE, McNamara SL, III LDB, Kaplan DL. Clinical applications of naturally derived biopolymer-based scaffolds for regenerative medicine. Annals of Biomedical Engineering. 2015;43(3):657-80.

90. Chen F-M, Liu X. Advancing biomaterials of human origin for tissue engineering. Progress in Polymer Science. 2015;In Press, Corrected Proof.

91. Chung W-J, Oh J-W, Kwak K, Lee BY, Meyer J, Wang E, *et al*. Biomimetic self-templating supramolecular structures. Nature. 2011;478(7369):364-8.

92. Badylak SF, editor. Host Response to Biomaterials: The Impact of Host Response on Biomaterial Selection: Elsevier; 2015.

93. Sionkowska A. Current research on the blends of natural and synthetic polymers as new biomaterials: Review. Progress in Polymer Science. 2011;36:1254-76.

94. Khaing ZZ, Schmidt CE. Advances in natural biomaterials for nerve tissue repair. Neuroscience Letters. 2012;519:103-14.

95. Grzesiak J, Marycz K, Szarek D, Bednarz P, Laska J. Polyurethane/polylactide-based biomaterials combined with rat olfactory bulb-derived glial cells and adipose-derived mesenchymal stromal cells for neural regenerative medicine applications. Materials Science and Engineering C. 2015;52:163-70.

96. Gebauer JM, Kobbe B, Paulsson M, Wagener R. Structure, evolution and expression of collagen XXVIII: Lessons from the zebrafish. Matrix Biology. 2015;In Press, Accepted Manuscript.

97. Bhattacharjee A, Bansal M. Collagen Structure: The Madras Triple Helix and the Current Scenario. IUBMB Life. 2005;57(3):161-72.

98. Shoulders MD, Raines RT. Collagen Structure and Stability. Annual Review of Biochemistry. 2009;78:929-58.

99. Chen Q, Bruyneel A, Carr C, Czernuszka J. Bio-mechanical properties of novel bi-layer collagen-elastin scaffolds for heart valve tissue engineering. Procedia Engineering. 2013;59:247-54.

100. Dunphy SE, Bratt JAJ, Akram KM, Forsyth NR, Haj AJE. Hydrogels for lung tissue engineering: Biomechanical properties of thin collagen–elastin constructs. Journal of the Mechanical Behavior of Biomedical Materials. 2014;38:251-9.

101. Kane RJ, Roeder RK. Hydroxyapatite reinforced collagen scaffolds with improved architecture and mechanical properties. Journal of the Mechanical Behavior of Biomedical Materials. 2012;7:41-9.

102. Kadler KE, Holmes DF, Trotter JA, Chapman JA. Collagen fibril formation. Biochemical Journal. 1996;316:1-11.

103. Bella J, Brodsky B, Berman HM. Hydration structure of a collagen peptide. Structure. 1995;3(9):893-906.

104. Vitagliano L, Nemethy G, Zagari A, Scheraga HA. Structure of the type I collagen molecule based on conformational energy computations: the triple-stranded helix and the N-terminal telopeptide. Journal of Molecular Biology. 1995;247:69-80.

105. Wang T-W, Spector M. Development of hyaluronic acid-based scaffolds for brain tissue engineering. Acta Biomaterialia. 2009;5:2371-84.

106. Harley BAC, Gibson LJ. *In vivo* and *in vitro* applications of collagen-GAG scaffolds. Chemical Engineering Journal. 2008;138:102-21.

107. Liang Y, Walczak P, Bulte JWM. The survival of engrafted neural stem cells within hyaluronic acid hydrogels. Biomaterials. 2013;34:5521-9.

108. Seppänen A. Collagen XVII in the Human Brain: University of Eastern Finland; 2011.

109. Sherman LS, Back SA. A 'GAG' reflex prevents repair of the damaged CNS. Trends Neuroscience. 2008;31(1):44-52.

110. Lam J, Lowry WE, Carmichael ST, Segura T. Hyaluronic acid matrix promotes the differentiation of transplanted cells. Advanced Functional Materials. 2014;24:7053-62.

111. Lindwall C, Olsson M, Osman AM, Kuhn HG, Curtis MA. Selective expression of hyaluronan and receptor for hyaluronan mediated motility (Rhamm) in the adult mouse subventricular zone and rostral migratory stream and in ischemic cortex. Brain Research. 2013;1503:62-77.

112. Baier C, Baader SL, Jankowski J, Gieselmann V, Schilling K, Rauch U, *et al*. Hyaluronan is organized into fiber-like structures along migratory pathways in the developing mouse cerebellum. Matrix Biology. 2007;26:348-58.

113. Sherman LS, Struve JN, Rangwala R, Wallingford NM, Tuohy TMF, IV CK. Hyaluronate-based extracellular matrix: keeping glia in their place. Glia. 2012;38:93-102.

114. Zhong J, Chan A, Morad L, Kornblum HI, Fan G, Carmichael ST. Hydrogel matrix to support stem cell survival after brain transplantation in stroke. Neurorehabil Neural Repair. 2010;24(7):636-44.

115. Verna J-M, Fichard A, Saxod R. Influence of glycosaminoglycans on neurite morphology and outgrowth patterns *in vitro*. International Journal of Developmental Neuroscience. 1989;7(4):389-99.

116. Oohira A, Kushima Y, Yokita Y, Sugiura N, Katsukiyo, Suzuki S, *et al*. Effects of lipid-derivatized glycosaminoglycans (GAGs), a novel probe for functional analyses of GAGs, on cell-tosubstratum adhesion and neurite elongation in primary cultures of

fetal rat hippocampal neurons. Archives of Biochemistry and Biophysics. 2000;378(1):78-83.

117. Bourguignon LYW, Gilad E, Peyrollier K, Brightman A, Swanson RA. Hyaluronan-CD44 interaction stimulates Rac1 signaling and PKNckinase activation leading to cytoskeleton function and cellmigration in astrocytes. Journal of Neurochemistry. 2007;101:1002-17.

118. Casini P, Nardi I, Ori M. RHAMM mRNA expression in proliferating and migrating cells of the developing central nervous system. Gene Expression Patterns. 2010;10:93-7.

119. Su W, Foster SC, Xing R, Feistel K, Olsen RHJ, Acevedo SF, *et al*. CD44 Transmembrane Receptor and Hyaluronan Regulate Adult Hippocampal Neural Stem Cell Quiescence and Differentiation. Journal of Biological Chemistry. 2017;292(11):4434-45.

120. Schmitt M, Metzger M, Gradl D, Davidson G, Orian-Rousseau V. CD44 functions in Wnt signaling by regulating LRP6 localization and activation. Cell Death And Differentiation. 2014;22:677.

121. Hrabětová S, Masri D, Tao L, Xiao F, Nicholson C. Calcium diffusion enhanced after cleavage of negatively charged components of brain extracellular matrix by chondroitinase ABC. The Journal of Physiology. 2009;587(16):4029-49.

122. Cui N, Qian J, Liu T, Zhao N, Wang H. Hyaluronic acid hydrogel scaffolds with a triple degradation behavior for bone tissue engineering. Carbohydrate Polymers. 2015;126:192-8.

123. Palumbo FS, Fiorica C, Stefano MD, Pitarresi G, Gulino A, Agnello S, *et al*. In situ forming hydrogels of hyaluronic acid and inulin derivatives for cartilage regeneration. Carbohydrate Polymers. 2015;122:408-16.

124. Führmann T, Obermeyer J, Tator CH, Shoichet MS. Click-crosslinked injectable hyaluronic acid hydrogel is safe and biocompatible in the intrathecal space for ultimate use in regenerative strategies of the injured spinal cord. Methods. 2015;84:60-9.

125. Dyck SM, Karimi-Abdolrezaee S. Chondroitin sulfate proteoglycans: Key modulators in the developing and pathologic central nervous system. Experimental Neurology. 2015;269:169-87.

126. Berretta S. Extracellular matrix abnormalities in schizophrenia. Neuropharmacology. 2012;62(3):1584-97.

127. Miller GM, Hsieh-Wilson LC. Sugar-dependent modulation of neuronal development, regeneration, and plasticity by chondroitin sulfate proteoglycans. Experimental Neurology. 2015;In Press, Accepted Manuscript.

128. Chazal G, Durbec P, Jankovski A, Rougon G, Cremer H. Consequences of neural cell adhesion molecule deficiency on cell migration in the rostral migratory stream of the mouse. The Journal of Neuroscience. 2000;20(4):1446-57.

129. Cremer H, Lange R, Christoph A, Plomann M, Vopper G, Roes J, *et al*. Inactivation of the N-CAM gene in mice results in size reduction of the olfactory bulb and deficits in spatial learning. Nature. 1994;367(6462):455-9.

130. Friedlander DR, Mflev P, Karthikeyan L, Margolis RK, Margolis RU, Grumet M. The neuronal chondroitin sulfate proteoglycan neurocan binds to the neural cell adhesion molecules ng-cam/l1/nile and n-cam, and inhibits neuronal adhesion and neurite outgrowth. Journal of Cell Biology. 1994;125(3):669-80.

131. Grumet M, Flaccus A, Margolis RU. Functional characterization of chondroitin sulfate proteoglycans of brain: interactions with neurons and neural cell adhesion molecules Journal of Cell Biology. 1993;120(3):815-24.

132. Lin R, Rosahl T, Whiting P, Fawcett J, Kwok J. 6-Sulphated Chondroitins Have a Positive Influence on Axonal Regeneration. PLOS One. 2011;6(7):e21499

133. Yan S, Zhang Q, Wang J, Liu Y, Lu S, Li M, *et al*. Silk fibroin/chondroitin sulfate/hyaluronic acid ternary scaffolds for dermal tissue reconstruction. Acta Biomaterialia. 2013;9(6):6771-82.

134. Kuo C-Y, Chen C-H, Hsiao C-Y, Chen J-P. Incorporation of chitosan in biomimetic gelatin/chondroitin-6-sulfate/hyaluronan cryogel for cartilage tissue engineering. Carbohydrate Polymers. 2015;117:722-30.

135. Schneiders W, Claudia Rentsch, Rehberg S, Rein S, Zwipp H, Rammelt S. Effect of chondroitin sulfate on osteogenetic differentiation of human mesenchymal stem cells. Materials Science and Engineering C. 2012;32:1926-30.

136. Barnabé-Heider F, Göritz C, Sabelström H, Takebayashi H, Pfrieger FW, Meletis K, *et al*. Origin of new glial cells in intact and injured adult spinal cord. Cell Stem Cell. 2010;7(4):470-82.

137. Mikami T, Yasunaga D, Kitagawa H. Contactin-1 Is a Functional receptor for neuroregulatory chondroitin sulfate-E*. Journal of Biological Chemistry. 2008;284:4494-9.

138. Offeddu GS, Ashworth JC, Cameron RE, Oyen ML. Multi-scale mechanical response of freeze-dried collagen scaffolds for tissue engineering applications. Journal of the Mechanical Behavior of Biomedical Materials. 2015;42:19-25.

139. Schoof H, Apel J, Heschel I, Rau G. Control of pore structure and size in freeze-dried collagen sponges. Journal of Biomedical Materials Research. 2001;58(4):352-7.

140. Davidenko N, Campbell JJ, Thian ES, Watson CJ, Cameron RE. Collagen–hyaluronic acid scaffolds for adipose tissue engineering. Acta Biomaterialia. 2010;6(10):3957-68.

141. Elias PZ, Spector M. Viscoelastic characterization of rat cerebral cortex and type I collagen scaffolds for central nervous system tissue engineering. Journal of the Mechanical Behavior of Biomedical Materials. 2012;12:63-73.

142. Murphy MC, Jones DT, Jack CR Jr, Glaser KJ, Senjem ML, Manduca A *et al*. Regional brain stiffness changes across the Alzheimer's disease spectrum. NeuroImage Clinical. 2006;10:283-90

143. Cha S. Experimental measurement of stiffness with magnetic resonance elastography for in vivo healthy human brains. The Ohio State University. 2014

144. Simon DD, Horgan CO, Humphrey JD. Mechanical restrictions on biological responses by adherent cells within collagen gels. Journal of the Mechanical Behavior of Biomedical Materials. 2012;14:216-26.

145. Uchihashi K, Aoki S, Matsunobu A, Toda S. Osteoblast migration into type I collagen gel and differentiation to osteocyte-like cells within a self-produced mineralized matrix: A novel system for analyzing differentiation from osteoblast to osteocyte. Bone. 2013;52(1):102-10.

146. Xu K, Lee F, Gao S, Tan M-H, Kurisawa M. Hyaluronidase-incorporated hyaluronic acid–tyramine hydrogels for the sustained release of trastuzumab. Journal of Controlled Release. 2015;216:47-55.

147. Sakai S, Ueda K, Taya M. Peritoneal adhesion prevention by a biodegradable hyaluronic acid-based hydrogel formed in situ through a cascade enzyme reaction initiated by contact with body fluid on tissue surfaces. Acta Biomaterialia. 2015;24:152-8.

148. Serrano MC, Nardecchia S, García-Rama C, Ferrer ML, Collazos-Castro JE, del Monte F, *et al*. Chondroitin sulphate-based 3D scaffolds containing MWCNTs for nervous tissue repair. Biomaterials. 2014;35(5):1543-51.

149. Ni Y, Tang Z, Cao W, Lin H, Fan Y, Guo L, *et al*. Tough and elastic hydrogel of hyaluronic acid and chondroitin sulfate as potential cell scaffold materials. International Journal of Biological Macromolecules. 2015;74:367-75.

150. Tierney CM, Haugh MG, Liedl J, Mulcahy F, Hayes B, O'Brien FJ. The effects of collagen concentration and crosslink density on the biological, structural and mechanical properties of collagen-GAG scaffolds for bone tissue engineering. Journal of the Mechanical Behavior of Biomedical Materials. 2009;2(2):202-9.

151. Dragan ES. Design and applications of interpenetrating polymer network hydrogels. A review. Chemical Engineering Journal. 2014;243:572-90.

152. Matricardi P, Di Meo C, Coviello T, Hennink WE, Alhaique F. Interpenetrating Polymer Networks polysaccharide hydrogels for drug delivery and tissue engineering. Advanced Drug Delivery Reviews. 2013;65(9):1172-87.

153. Nazir R. Collagen–hyaluronic acid based interpenetrating polymer networks as tissue engineered heart valve. Materials Science and Technology. 2015:1743284715Y.0000000097.

154. Baiguera S, Gaudio CD, Lucatelli E, Kuevda E, Boieri M, Mazzanti B, *et al*. Electrospun gelatin scaffolds incorporating rat decellularized brain extracellular matrix for neural tissue engineering. Biomaterials. 2014;35:1205-14.

155. Puetzer JL, Bonassar LJ. High density type I collagen gels for tissue engineering of whole menisci. Acta Biomaterialia. 2013;9(8):7787-95.

156. Liu Y, Ren L, Wang Y. Crosslinked collagen–gelatin–hyaluronic acid biomimetic film for cornea tissue engineering applications. Materials Science and Engineering: C. 2013;33(1):196-201.

157. Meimandi-Parizi A, Oryan A, Moshiri A, Silver IA. Novel application of a tissue-engineered collagen-based three-dimensional bio-implant in a large tendon defect model: A broad-based study with high value in translational medicine. Tissue and Cell. 2013;45(4):282-94.

158. Liu Y, Bharadwaj S, Lee SJ, Atala A, Zhang Y. Optimization of a natural collagen scaffold to aid cell–matrix penetration for urologic tissue engineering. Biomaterials. 2009;30(23–24):3865-73.

159. Mori H, Ayumi Takahashi, Horimoto A, Hara M. Migration of glial cells differentiated from neurosphere-forming neural stem/progenitor cells depends on the stiffness of the chemically cross-linked collagen gel substrate. Neuroscience Letters. 2013;555:1-6.

160. Georges PC, Miller WJ, Meaney DF, Sawyer ES, Janmey PA. Matrices with compliance comparable to that of brain tissue select neuronal over glial growth in mixed cortical cultures. Biophysical Journal. 2006;90:3012-8.

161. Allodi I, Guzmán-Lenis M-S, Hernàndez J, Navarro X, Udina E. *In vitro* comparison of motor and sensory neuron outgrowth in a 3D collagen matrix. Journal of Neuroscience Methods. 2011;198:53-61.

162. Egawa EY, Kato K, Hiraoka M, Nakaji-Hirabayashi T, Iwata H. Enhanced proliferation of neural stem cells in a collagen hydrogel incorporating engineered epidermal growth factor. Biomaterials. 2011;32:4737-43.

163. Chen SS, Revoltella RP, Dapini S, Michelini M, Fitzgerald W, Zimmerberg J, *et al*. Multilineage differentiation of rhesus monkey embryonic stem cells in three-dimensional culture systems. Stem Cells. 2003;21:281-95.

164. Koutsopoulos S, Zhang S. Long-term three-dimensional neural tissue cultures in functionalized self-assembling peptide hydrogels, Matrigel and Collagen I. Acta Biomaterialia. 2013;9:5162-9.

165. Chen Z, Lu XCM, Shear DA, Dave JR, Davis AR, Evangelista CA, *et al*. Synergism of human amnion-derived multipotent progenitor (AMP) cells and a collagen scaffold in promoting brain wound recovery: Pre-clinical studies in an experimental model of penetrating ballistic-like brain injury. Brain Research. 2011;1368:71-81.

166. Yu H, Cao B, Feng M, Zhou Q, Sun X, Wu S, *et al*. Combinated transplantation of neural stem cells and collagen type i promote functional recovery after cerebral ischemia in rats. The Anatomical Record: Advances in Integrative Anatomy and Evolutionary Biology. 2010;293(5):911-7.

167. Elias PZ, Spector M. Implantation of a collagen scaffold seeded with adult rat hippocampal progenitors in a rat model of penetrating brain injury. Journal of Neuroscience Methods. 2012;209:199-211.

168. Snow DM, Lemmon V, Carrino DA, Caplan AI, Silver J. Sulfated proteoglycans in astroglial barriers inhibit neurite outgrowth *in vitro*. Experimental Neurology. 1990;109:111-30.

169. Aaron C, Alyssa P. Characterization of a chondroitin sulfate hydrogel for nerve root regeneration. Journal of Neural Engineering. 2011;8(5):056003.

Chapter 3 – Materials Synthesis and Characterisation

3.1 Introduction

The purpose of this chapter is to study the composition, the morphology, and the mechanical properties of Coll and interlaced Coll-GAG scaffolds. It is well established that the composition, morphology, and mechanical properties of scaffolds are all able to direct cell behaviours [1-4]. In order to study scaffold composition, NMR, histology, FTIR and EDX were used to characterise Coll, HA and CS within the interlaced scaffolds. SEM was used to image the scaffolds and measure their average pore sizes, and compression testing studied the mechanical properties. The objectives of these studies were to establish that 1) interlaced scaffolds synthesis has been successful in incorporating HA and/or CS onto Coll, and 2) all interlaced scaffolds have similar morphologies and mechanical properties to 1.0wt% Coll, which was previously determined to have the most suitable mechanical properties and an acceptable pore size for NSC growth [5-7].

There are several previous studies on using Coll-based scaffolds for TBI treatment [5, 8, 9]. However, there lacks a direct comparison of the effects of HA and CS on brain tissue engineering. The combined effects of these two important molecules have not been studied either. In this study, we fabricated three interlaced Coll-GAG scaffolds: Coll-CS, Coll-HA and Coll-CS-HA, and a pure Coll scaffold, to study their physical and biological properties for potential use in tissue engineering for the brain.

This chapter provides a basic physical understanding of the scaffolds prior to cell culture, which will be discussed in chapter 4. The experimental methods will be described in section 3.2, results will be described in section 3.3, and discussed in section 3.4.

3.2 Materials and Methods

3.2.1 Synthesis of Coll scaffolds

Coll scaffolds were prepared from type I Coll from bovine achilles tendon (Sigma Aldrich, C9879) via a freeze-drying method. 0.5g, 1.0g, 0.75g or 1.5g of Coll slurries were mixed with 100 mL water in an ice bath to form 0.5wt%, 0.75wt%, 1.0wt% and 1.5wt% Coll suspensions respectively. The pH was adjusted to 3.2-3.5 by dropwise addition of ethanoic acid. The mixture was blended by a household blender (Breville, IHB086), followed by 5 minutes' centrifugation at 2,500 rpm (relative centrifugal force = 1,015g) to remove trapped air bubbles (Thermo, IEC CL10). The mixture was then refrigerated at 4°C overnight for the solution to diffuse and become homogeneous again, followed by casting in cylindrical PTFE moulds (8 mm diameter, 15 mm height) and frozen in a -80°C freezer (Sanyo, Ultra Low Freezer) for at least 4 hours. Subsequently, the mixture was freeze-dried in a Christ Alpha I-5 freeze-dryer for 24 hours. As a result, the ice crystals sublimed and left the Coll as a foam-like porous structure.

3.2.2 Synthesis of interlaced scaffolds

As discussed in chapter 2, CS and HA are the main components that construct the perineuronal nets and interstitial matrix in our brain's ECM [10]. Since the purpose of our scaffold is to mimic the physiological environment of neural cells, we have chosen these two GAGs as our main components in the interlaced scaffolds. We have also synthesised

a novel interlaced network composing all three materials: Coll-CS-HA. The Coll-CS-HA scaffold would hopefully resemble the highest similarity to the natural ECM of brains, and thus create the most optimal environment for cells. Therefore, we hypothesise that the Coll-CS-HA would be an optimal scaffold for the treatment of TBI.

Our main synthesis method for Coll-GAGs scaffolds was to sequentially construct interlaced networks comprising independent Coll and GAG networks. This was achieved by firstly constructing a primary network of Coll, followed by immersing it in a solution containing HA, CS, or HA-CS with rapid stirring. This method was successful in producing secondary networks of GAGs that had penetrated into Coll and becoming an interlaced network.

Another approach by simply mixing Coll and CS into a composite scaffold was attempted. To construct the composite scaffolds, 0.75g Coll was immersed in ice-cold 100 mL distilled water, whose pH was previously adjusted to 3.2-3.5 by dropwise addition of ethanoic acid. The solution was subsequently blended with the same household blender and centrifuged to remove air bubbles, followed by addition of 0.25g of chondroitin sulfate sodium salt from shark cartilage (Sigma Aldrich, 9082-07-9) to the Coll suspension. Addition of CS would create phase separation of Coll to the solution. The solution was homogenised by dropwise addition of 70wt% NaOH, before frozen at -80°C and freeze-dried.

In our interlaced scaffolds, Coll was chosen to be the primary network, and HA, CS or HA-CS was chosen to be the secondary network. For Coll-HA, the scaffold was formed via an EDC/NHS crosslinking approach. 0.75wt% Coll was used based on several factors:

1) a strong structural integrity and 2) a similar pore size to a 1.0wt% Coll. Freeze dried 0.75wt% Coll scaffolds were stirred in absolute ethanol for 30 minutes. This step dehydrated the scaffolds and rendered them less susceptible to shrinkage during crosslinking. An HA crosslinking solution containing 0.25wt% sodium hyaluronate (Mw = 1.5-2.2 MDa, ACROS Organics, 9067-32-7), 60 mM N-Ethyl-N′-(3-dimethylaminopropyl)carbodiimide hydrochloride (EDC) (Sigma Aldrich, 25952-53-8), 30mM N-hydroxysuccinimide (NHS) (Sigma Aldrich, 6066-82-9), 30 molar excess (of HA) adipic acid dehydrate (ADH) (Sigma Aldrich, 1071-93-8), and 50 mM 2-morpholinoethane sulfonic acid (MES) hydrate (Sigma Aldrich, 1266615-59-1) was allowed to react for 4 hours on a stirrer at room temperature, and subsequently stored in a 4°C fridge for a minimum of 12 hours before adding Coll. During which the EDC would lose its activity due to hydrolysis so that crosslinking of Coll could be avoided. The crosslinking concentrations of EDC, NHS and ADH were chosen as they exceeded the concentration required for 100% crosslinking to take place based on literature and previous work from the group [11]. ADH functionalised HA by addition of NH_2 bonds onto HA molecules, which were then crosslinked to their carboxylic groups to form a secondary network. To add HA network onto Coll, 0.75wt% scaffolds were immersed in the crosslinking solution for 4 hours, washed once in 0.1M Na_2HPO_4 solution for one hour, twice in distilled water for one hour, frozen at -80°C and then freeze-dried for 24 hours.

Coll-CS scaffolds were synthesised via a similar approach. 0.75wt% Coll scaffolds were mixed with absolute ethanol for 30 minutes to dehydrate, then immersed in a CS secondary network solution consisting of 0.25wt% CS, 60 mM EDC, 30 mM NHS, 30

molar excess (of CS) ADH, and 50 mM MES hydrate for 4 hours on a stirrer at room temperature. The crosslinking solution has been previously reacting for 4 hours to form the secondary network and stored in a 4°C fridge for a minimum of 12 hours. The scaffolds were then washed and freeze-dried via the same way as Coll-HA.

Coll-CS-HA scaffolds were synthesised by adding ethanol-dehydrated 0.75wt% Coll scaffolds to a HA-CS crosslinking solution containing 0.25wt% HA, 0.25wt% CS, 60 mM EDC, 30 mM NHS, 50 mM MES, 30 molar excess (of CS and HA) ADH, and ADH for 4 hours. This solution, again, has been reacting and kept in the same condition as above. The scaffolds were then washed and freeze-dried.

The interlaced network synthesis soon replaced the composite scaffold synthesis method mentioned above, as the interlaced scaffolds showed a more consistent and defined wall structure. In the composite Coll-CS however, the wall structure was more discontinuous and the pores appeared to be less complete, possibly due to the fact that Coll did not form a complete network in composite Coll-CS scaffolds. The difference in microstructure is shown by figure 3.1 below.

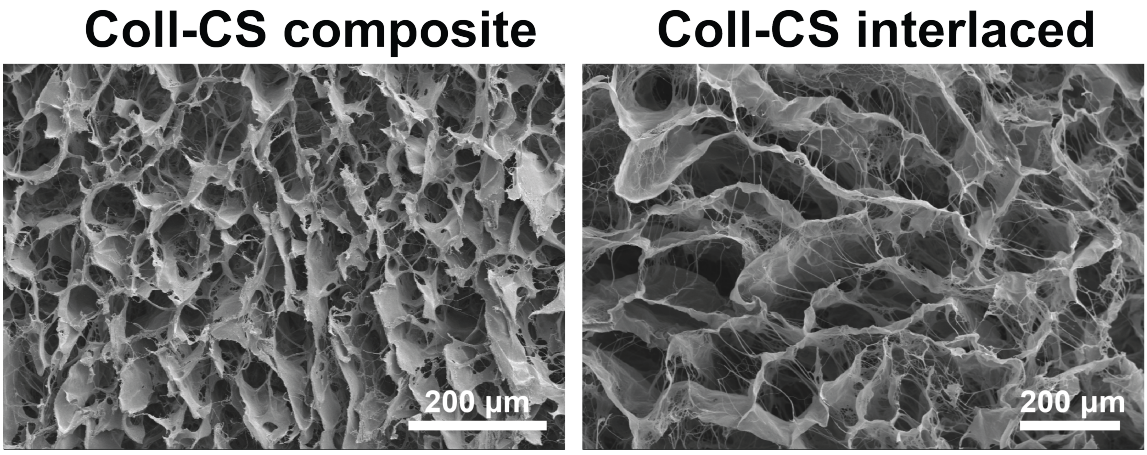


Figure 3.1 – SEM microstructure of Coll-CS scaffolds created via the composite scaffold and interlaced scaffold approach. Scale bars = 200 µm

Dehydrothermal (DHT) crosslinking was also attempted to crosslink Coll. It is an effective crosslinking method that has been widely used to crosslink Coll-Coll and Coll-GAGs [12, 13]. To crosslink, 1.0wt and 1.5wt% Coll were placed in vacuum at 110°C for 20, 45 and 65 hours in a Heraeus Vacutherm vacuum dryer. The option of using DHT crosslinking was quickly abandoned as the resultant Coll scaffolds appeared pale yellow, suggesting a denaturation of Coll into gelatine.

Table 3.1 below shows the scaffolds studied in this section. Coll, Coll-CS, Coll-HA and Coll-CS-HA were chosen for cell studies. Other scaffolds below were studied as a comparison in subsequent studies.

Table 3.1 – A summary of all Coll and interlaced scaffolds synthesised and studied in this section and their abbreviations. Solution concentrations were expressed as wt%

Abbreviations	**Coll solution concentration**	**CS solution concentration**	**HA solution concentration**	**Studies performed**
Coll	1.0	0	0	Cell studies
Coll-CS	0.75	0.25	0	Cell studies
Coll-HA	0.75	0	0.25	Cell studies
Coll-CS-HA	0.75	0.25	0.25	Cell studies
0.5%Coll-0.5%HA	0.5	0	0.5	Histology
0.5%Coll	0.5	0	0	Mechanical studies
0.75%Coll	0.75	0	0	Mechanical studies and interlaced scaffolds
1.5%Coll	1.5	0	0	Mechanical studies

3.2.3 Fourier transformed infrared spectroscopy

FTIR studies the states of vibrations of moieties within materials by measuring absorption (or reflection) as a function of wavelength. Beer-Lambert law below shows a linear relationship between the concentrations of molecular species to the absorption:

$$A(\lambda) = \varepsilon(\lambda)bc \qquad 1$$

where A is the wavelength-dependent absorbance, ε is the wavelength-dependent absorptivity coefficient, b is the path length and c is the analyte concentration [14].

In this study, FTIR was used to characterise the presence of HA and/or CS in the interlaced scaffolds, and any potential distortions to the original Coll triple helix structure following processing. FTIR spectroscopy was performed via a software DigiLab Resolutions Pro. The scaffolds were carefully sliced into 1 mm thin slices using a double edge razor blade (Wilkinson Sword Classic), and folded in quarters to ensure a maximum interaction with the infrared. For comparison, CS and HA powder, as obtained, were also studied. Spectra from 500 to 4000 cm^{-1} were recorded for each scaffold. The scan times were 32 and spectrum resolution was 5 cm^{-1}. For analysis, the data was exported and analysed in Excel. The main difficulty of using FTIR in this study was the overlapping peaks of Coll, CS and HA due to their similar molecular structure. However, incorporation of new materials into Coll would create slight peak shifts. Following accepted procedure, we determined a shift of 4 cm^{-1} to be significant [15]. In addition, peak intensities were also measured to reflect changes in molecular structure.

Furthermore, second derivative analysis was also performed to distinguish more subtle changes to FTIR spectrum and to separate out shoulders due to overlapping peaks. Savizky-Golay algorism in OriginPro 9.1 (OriginLab) was used for our second derivative analysis.

3.2.4 Histology

Histology using alcian blue was used to characterise the presence and distribution of HA in the interlaced scaffolds. Although FTIR and NMR were both able to pick out HA signals, histology helped to generate a visual representation of HA distribution. In addition, this technique studied whether or not HA could form a network within Coll. It was therefore important to help understand the micro-architecture of our Coll-HA scaffolds

Alcian blue stain kit was obtained from Clin-Tech Limited (#631045). Scaffolds were sectioned, washed in distilled water, and stained with alcian blue for 15 minutes. Alcian blue stained negatively charged materials, such as HA in blue, and left neutral molecules in grey. The stained sections were then washed in a running tab for 2 minutes, rinsed in distilled water, and was treated with periodic acid for 5 minutes. The sections were kept on glass coverslips and imaged with an optical microscope to determine the colour.

3.2.5 Energy dispersive X-ray spectroscopy

Energy dispersive X-ray spectroscopy (EDX) was used to determine the sulfur content and distribution in the interlaced scaffolds in an attempt to measure CS distribution. The

sulfur should be directly proportional to the amount of CS, since sulfur is generally present in CS and absence in Coll and HA. Strictly speaking, it is possible for other sulfur-containing amino acids to attach to Coll glycine molecules that could affect our results. Hence Coll here was also studied as a comparison.

During an EDX study, a high energy electron beam impacts the specimen, where electrons from the specimens are excited and ejected from the atom. While another electron fills the vacancy, X-ray of a specific energy is released. The detector then detects the energy, which is the difference in energy between the two electron shells, and is therefore able to distinguish the element composition of the atom [16].

In order to compare the CS content on interlaced scaffolds, pure CS scaffolds were synthesised using a similar freeze-drying method. 2wt% CS was dissolved in distilled water consisting the same concentration of EDC, NHS, ADH and MES. The solution was allowed to react for 12 hours, following by casting in -80°C and then freeze-dried for 24 hours. Prior to EDX analysis, the scaffolds were carefully sliced into thin slices of approximately 1 mm.

Freeze-dried Coll, CS, Coll-CS and Coll-CS-HA were gold-coated by a Bio-Rad ES400 sputter coater at 20 mA for 45 seconds and evaluated using a Zeiss EVO SEM. The scaffolds were analysed in a SE mode with EDX, where electrons were accelerated at a voltage of 15 kV. Three scans per scaffold were performed at different magnifications, and each lasted for 20 minutes. It was also important to ensure that the analysis of element contents had stopped fluctuating. Sulfur contents were analysed digitally from the EDX spectra by software AZtec, and were expressed in atomic percentage.

3.2.6 Nuclear magnetic resonance spectroscopy

Nuclear magnetic resonance (NMR) spectroscopy was used to analyse the release of fragments of HA and CS molecules. The aim of this experiment was to further validate the presence of HA and CS within the three interlaced scaffolds, and to characterise the release of fragments after the previously-performed 28 days of degradation studies described later in section 3.2.9. NMR studies were conducted with the help of Ms Yi Ni from Department of Chemistry, University of Oxford.

^{1}H, ^{13}C and 2D NMR spectra were recorded using a Bruker AV500 MHz spectrometer at ambient temperature. After 28 days' of incubation in phosphate-buffered solution (PBS) at 37°C, Coll-CS, Coll-HA and Coll-CS-HA scaffolds were placed in a fresh PBS and incubated at 37°C for one month. The surrounding PBS was removed after one month and NMR was performed on the PBS obtained. ^{1}H, $^{13}C(^{1}H)$ NMR spectra were referenced internally to residue protio-solvent (^{1}H) or solvent (^{13}C) resonances, and were reported relative to tetramethylsilan.

3.2.7 Pore size and morphological analysis

Scanning electron microscopy (SEM) was used to study the morphologies of scaffolds. An SEM is a type of electron microscope that images a surface by scanning it with a focused electron beam. The electrons in this study were produced from a tungsten filament, which were then accelerated towards the specimen via a controlled magnetic field. Secondary electrons emitted back from the specimens were then collected and processed

into an image. SEMs provide higher magnifications and resolutions with a greater depth of field compared to light microscopes and are therefore desirable for detailed analysis of scaffolds with small pore sizes.

To prepare samples for SEM, freeze-dried scaffolds were sliced using a razor blade into approximately 1 mm thin slices and mounted on a carbon sticky pad on an aluminium stub (Agar Scientific). These slices were coated with gold using a Bio-Rad ES400 sputter coater at 20 mA for 45 seconds, and imaged under the Zeiss EVO SEM. SEM images were taken in a SE mode, with an accelerating voltage of 10 kV, probe current of 100 pA and a vacuum of approximately 6.0×10^{-6} mbar.

To measure the pore size, at least 5 field-of-view images of scaffolds were taken, each constituting at least 20 pores. An average was taken to measure the pore size of the scaffolds. Three batches of scaffolds were measured and an average was then taken on the average of the three batches. Pore sizes were measured using ImageJ by manually outlining the pores and measuring the average diameter.

3.2.8 Compression tests

The stiffness of a scaffold is able to direct neural cell differentiation into a glial or a neuronal linage [17-19] . Therefore, it is important to study if the mechanical properties of scaffolds are suitable for NSC culture and consistent throughout the scaffolds. Previous literature concluded that the mechanical properties of 1.0wt% Coll scaffolds were the most

similar to rat's brains [20]. The objective of this study was thus to establish that the stiffness of the interlaced scaffolds remained similar to the Coll.

Compression testing was performed on a parallel-plate compressor (Denison Mayes Group, 6160) and analysed on a Rubicon software (Denison Mayes Group). Freeze-dried scaffolds had been previously casted into a cylindrical shape. To ensure better contact to the plates, the top and bottom of the scaffolds were carefully flattened by slicing off any uneven surfaces using the razor blades. Compression began from both end at a rate of 500 μm/min and stopped after 20 minutes. Resultant stress-strain curves were plotted on Excel, and compressive moduli were recorded as the gradients of the elastic regions.

3.2.9 Degradation studies

Since our scaffolds were composed of proteins and polysaccharides naturally found in the body, they were expected to degrade over time and be replaced by newly formed tissue. Hence, degradation studies became necessary due to two reasons. One was to demonstrate their ability to degrade within a mimicked physiological environment. Second was to study their rates of mass loss to ensure adequate degradation rates. A rapid degradation may lead to lack of support for cells, and a slow degradation may lead to a potential fibrous encapsulation or other immune reactions.

Degradation studies were carried out in a mimicked physiological environment for 28 days. PBS was prepared by mixing distilled water with 137 mM NaCl, 2.7 mM KCl, 4.3

mM Na_2HPO_4 and 1.47 mM KH_2PO_4. The final pH was adjusted to 7.4 by dropwise addition of HCl.

Scaffolds were weighed on day 0 before testing, and subsequently fully immersed in PBS and stored in a 37°C incubator in an air-tight glass tube. On day 7, 14, 21 and 28, the scaffolds were carefully taken out of the incubator, washed in a large volume of distilled water for 5 minutes to remove any residual salt from the PBS, and subsequently freeze-dried for 24 hours. After weighing the freeze-dried scaffolds, they were placed back to the incubator in a fresh PBS. Scaffold degradation was expressed as the percentage of remaining mass compared to the initial weight.

$$\text{Mass remaining } \% = \frac{\text{Mass remained}}{\text{Initial mass at day 0}} \text{ x } 100\% \qquad 2$$

3.2.10 Statistics

At least 3 groups of scaffolds (n=3) were used per experiment. Results were reported as mean ± standard deviation. Statistical significance was measured by student t-test using the GraphPad software, and a significant level of less than 0.05 was determined to be statistically significant.

3.3 Results

3.3.1 Fourier transformed infrared spectroscopy

In order to demonstrate that the interlaced scaffolds synthesis was successful in incorporating HA and/or CS secondary network within the Coll primary network, we examined the scaffolds under FTIR. Figure 3.2 illustrates the FTIR spectra for pure Coll, HA, CS, and Coll-CS, Coll-HA and Coll-CS-HA.

3.3.1.1 Pure components analysis

Coll under FTIR showed its characteristic peaks including Amide I (1636 cm^{-1}), amide II (1549 cm^{-1}) and amide III (1244 cm^{-1}). Amide I and II peaks represent the stretching vibrations of C=0 bonds, N-H bonding vibrations and C-N stretching. Amide III represents a combination of C-N stretching, N-H bending, C-C stretching and CH_2 wagging vibrations. Peaks around 2850 cm^{-1} and 2920 cm^{-1} were due to amide N-H stretching vibrations. Absorbance due to pyrolidonic ring of hydroxyproline occurred at 1450-1454 cm^{-1}. The spectrum of Coll was consistent to many previously published findings [21-24]

Sugar groups of CS led to an absorbance spectrum near the 1000-1200 cm^{-1} region. Sulfate groups led to a sulfate stretching vibrations that causes absorbance at 1240 cm^{-1}. This overlapped with amide III of Coll (1244 cm^{-1}). Carboxylate groups also caused absorbance at 1410 cm^{-1} and 1610 cm^{-1} which also overlapped near the amide I region. These data were also consistent with previously published findings [25].

HA also led to an amide peak around 1610 cm^{-1} due to C=O stretching and N-H bending. Consistent to literature, peaks around 1375-1404 cm^{-1} represent C-H_2 bending, and peaks between 1000 cm^{-1} and 1200 cm^{-1} represent C-O stretching of proteoglycan sugar ring [26].

Within the spectra, amide I, II and III contributed to the highest absorption intensities. C=O, N-H and C-N bondings were present in Coll, HA and CS and therefore the peaks were expected to overlap around these regions.

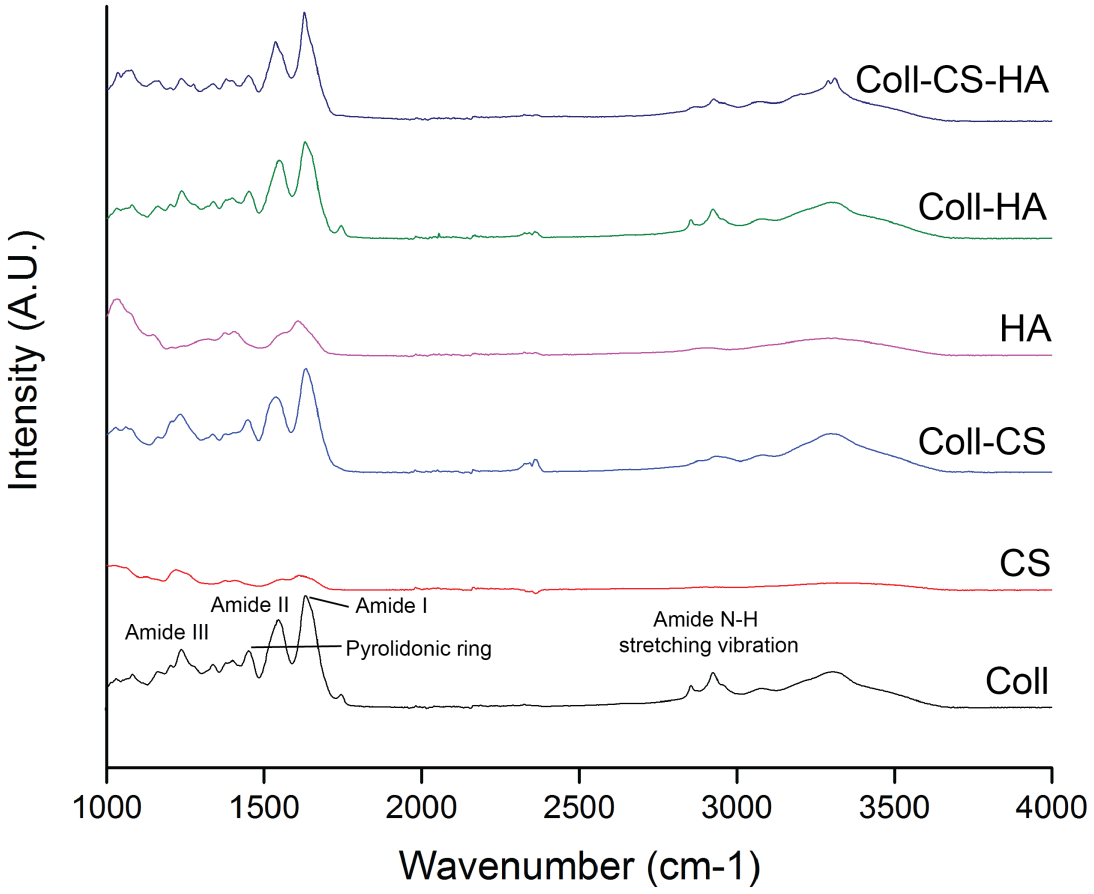


Figure 3.2 - FTIR spectrums of interlaced scaffolds and their pure components. The spectrums were measured from 1000 cm^{-1} to 4000 cm^{-1} and intensities measured by absorbance units (A.U.)

3.3.1.2 Interlaced scaffolds analysis

Spectra of the interlaced scaffolds were remarkably similar to that of Coll. However, small shifts and changes in intensity still revealed subtle changes due to the addition of GAGs. For example, superimposed FTIR spectra revealed that the interlaced scaffolds caused amide I and II to shift slightly to lower frequencies as shown in figure 3.3A and 3.3C, and decreased absorption intensities in most peaks, as shown in figure 3.3C and 3.3D. Peak shifts are likely due to the change in relative intensities of adjacent peaks, resulting in the overlapping peaks to appear shifted.

Apart from peaks at 1078-1080 cm^{-1} on Coll and Coll-HA, another peak was found on Coll-CS and Coll-CS-HA near 1061 cm^{-1}, as shown in figure 3.3B. This was due to the highly sulfated CS [24]. The increase in peak intensities of all interlaced scaffolds, especially Coll-HA and Coll-CS-HA at around 1080 cm^{-1} region, also reflected the carboxylic groups of the uronic acid moiety of GAGs [23]. Coll-CS-HA had the highest intensity here, which was most likely due to the addition of HA and CS together.

Between 1000 cm^{-1} and 1100 cm^{-1} shown by figure 3.3B, Coll-CS and Coll-CS-HA both had higher intensities compared to Coll and Coll-HA. Coll-CS-HA had the highest intensity, indicating a higher concentration of the polysaccharides [27].

As shown by figure 3.3E, the broad bands around 3100 cm^{-1} to 3500 cm^{-1}, centred at 3315 cm^{-1}, were due to the O-H stretching mode of polysaccharides and N-H stretching vibration of the N-acetyl side chain. During crosslinking, hydrogen bonds were formed by joining C=O on HA and CS with N-H on ADH-modified HA or joining C=O on Coll

with N-H on Coll. This formation broadened the bands around this region, and was reflected by the figure. Coll-CS-HA did not show an increase but a somewhat narrower band here [23]. This behaviour is mostly likely due to the prior crosslinking which had taken place between CS and ADH-modified HA before the addition of Coll.

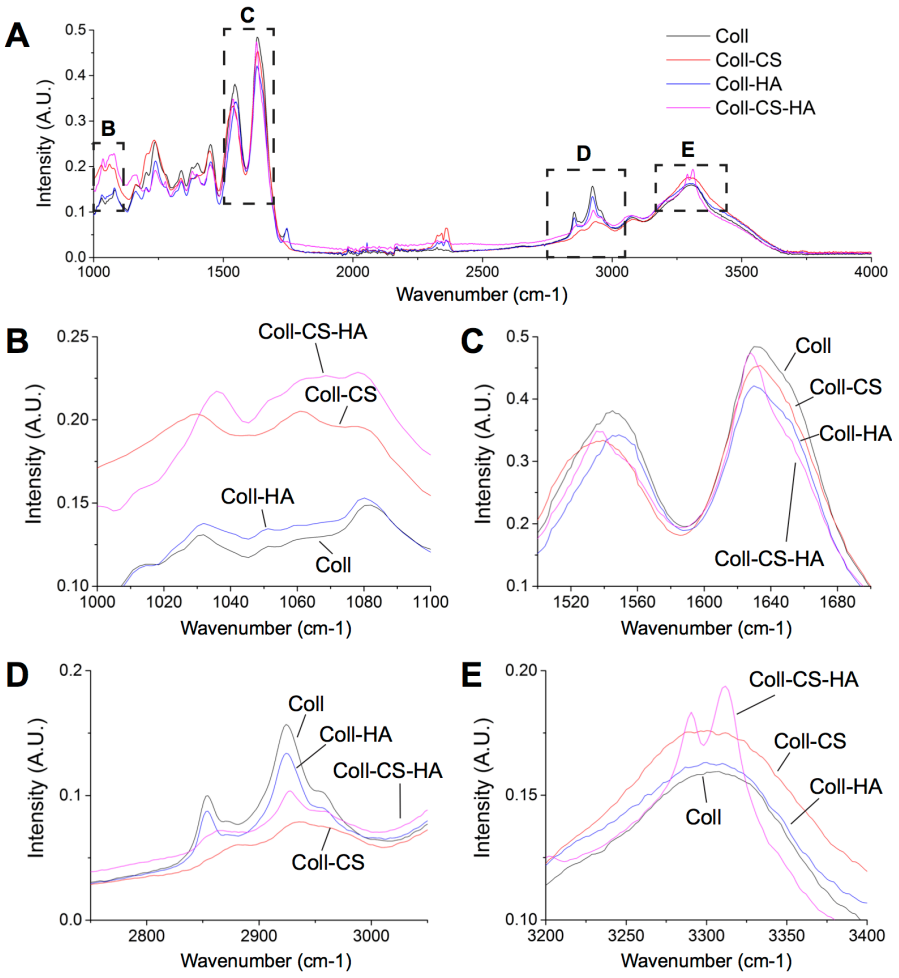


Figure 3.3 – A) FTIR spectrums of the interlaced scaffolds and Coll superimposed from 1000 cm^{-1} to 4000 cm^{-1}. B) FTIR spectrums of interlaced scaffolds and Coll from 1000 cm^{-1} to 1100 cm^{-1}. C) FTIR spectra from 1500 cm^{-1} to 1700 cm^{-1} showing amide I and amide II. D) FTIR spectra from 2750 cm^{-1} to 3050 cm^{-1} showing amide B. E) FTIR spectrums of interlaced scaffolds and Coll from 3200 cm^{-1} to 3400 cm^{-1}.

3.3.1.3 Second derivatives of FTIR spectroscopy

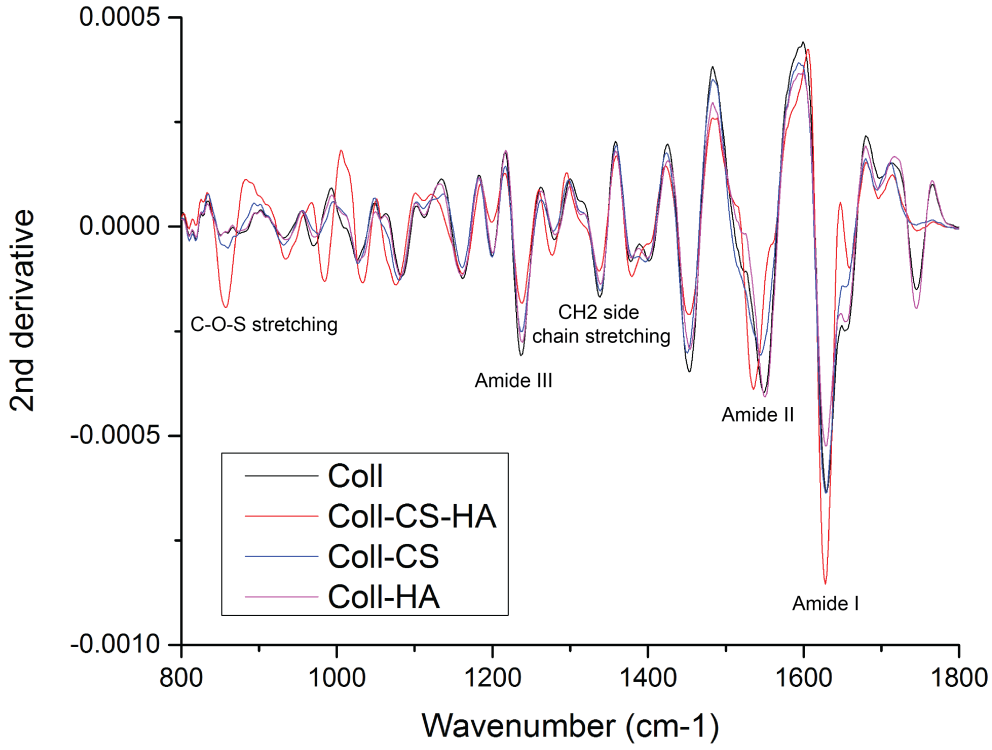


Figure 3.4 - Second derivatives of FTIR spectra for Coll and interlaced scaffolds between 800 cm^{-1} and 1800 cm^{-1}

Second derivatives of FTIR spectra were studied by differentiating the spectra twice using the Savizky-Golay algorithm. Since a second derivative reveals the concavity of a function, it is very effective in resolving subtle differences due to overlaps from Coll and CS [27].

Figure 3.4 above illustrates the second derivatives spectra of Coll and interlaced scaffolds between 800 cm^{-1} and 1800 cm^{-1}. Typical Coll peaks were again obvious, as shown in 1628 cm^{-1}, which corresponds to amide I, in 1549 cm^{-1}, which corresponded to amide II, and in 1339 cm^{-1}, which corresponded to CH_2 side chain vibration [15]. These peaks were

found in all interlaced scaffolds, further validating our previous observation that the original Coll structure remained unchanged. In addition, S-O-C bonds were found on Coll-CS and Coll-CS-HA at around 858-862 cm^{-1}. Peaks at this region shifted away from Coll and Coll-HA. S-O-C is a characteristic bond of CS, indicating the presence of CS within Coll-CS and Coll-CS-HA. Unsurprisingly, Coll-HA overlaps with Coll around this region.

Overall, Coll-CS-HA showed higher peak intensities in second derivatives. Coll-CS and Coll-CS-HA also showed a slight shift to lower wavelength at amide II peak, which was consistent to the FTIR findings. Peaks of Coll-HA however, did not show any significant differences compared to Coll.

Table 3.2 – Band assignment for FTIR secondary derivatives between 800 cm^{-1} and 1800 cm^{-1}. Units are in cm^{-1} and bands with significant differences to Coll are underlined

Bond vibration	**Coll**	**Coll-CS**	**Coll-HA**	**Coll-CS-HA**	**References**
Amide I	1628	1628	1628	1628	[15, 27, 28]
Amide II	1549	<u>1543</u>	1552	<u>1537</u>	[15, 27, 28]
CH_3 asymmetric bending	1452 1379	<u>1448</u> <u>1383</u>	1452 1381	1450 1381	[15, 27, 28]
CH_2 side chain	1339	1339	1336	1334	[15, 24, 27, 28]
Amide III	1238 1279	<u>1234</u> 1279	1236 1281	1236 1277	[15, 27]
C-O-S asymmetric stretching	849	<u>862</u>	849	<u>858</u>	[15]

Band assignments for secondary derivatives are shown in table 3.2. As mentioned previously, band shift of 4 cm^{-1} was determined significant. Compared to Coll, a number of significant shifts from Coll-CS were seen, namely at amide I (-6 cm^{-1}), CH_3 asymmetric bending (+4 cm^{-1} and -6 cm^{-1}), amide III (-4 cm^{-1}), and C-O-S asymmetric stretching (+13 cm^{-1}). Similarly, Coll-CS-HA also caused a number of peak shifts at amide II (-12 cm^{-1}) and C-O-S asymmetric stretching (+9 cm^{-1}). Coll-HA on the other hand, did not shift extensively at these peaks.

3.3.2 Histology

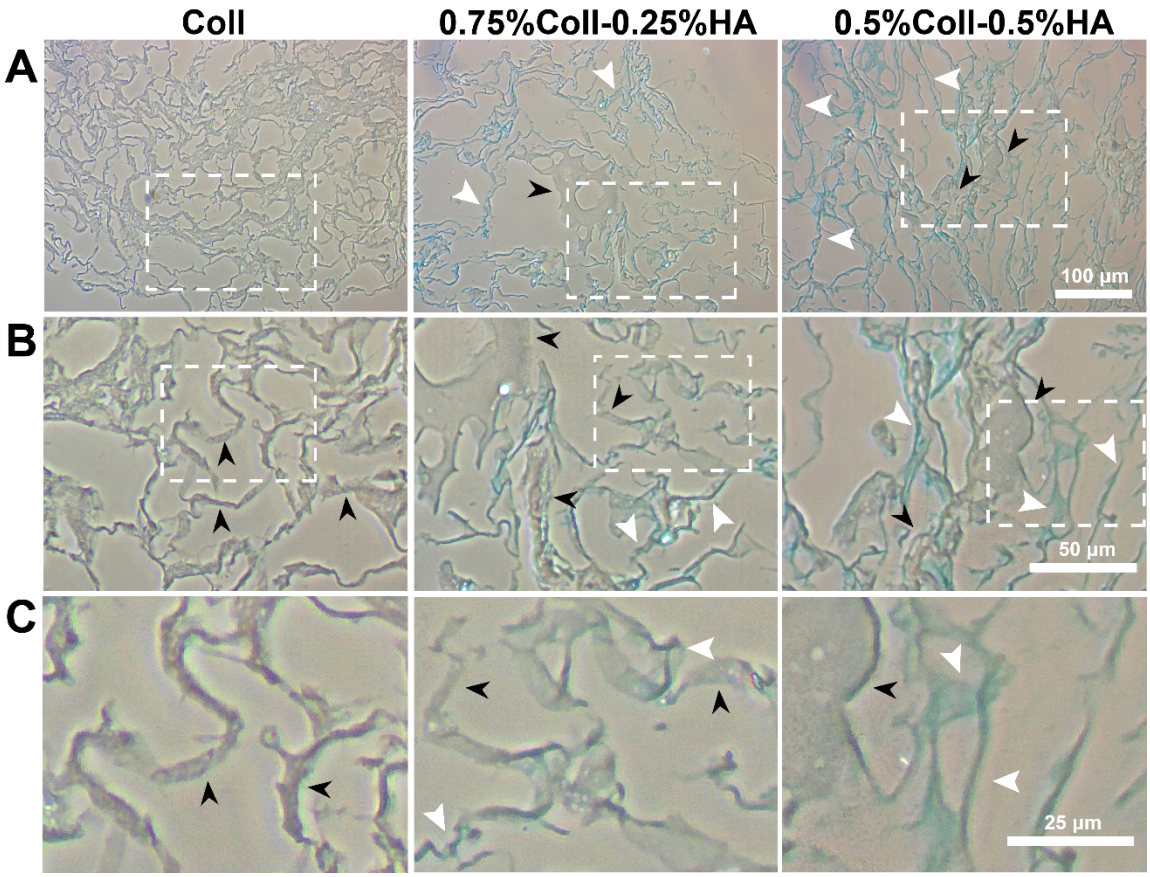


Figure 3.5 – Histology studies using alcian blue for analysis of HA on Coll, 0.75%Coll-0.25%HA and 0.5%Coll-0.5%HA. A) Slices of scaffolds under a light microscope at a lower magnification. B) Higher magnification images of A) showing more detailed microstructure. C) Higher magnification of B) showing individual struts of scaffolds. Alcian blue stains HA in blue, and Coll in grey. Black arrowheads point at Coll and white arrowheads point at HA

Figure 3.5 above illustrates the alcian blue staining of HA on Coll and two different concentration of HA interlaced scaffolds: 0.75%Coll-0.25%HA and 0.5%Coll-0.5%HA.

Notably, 0.75%Coll-0.25%HA was the Coll-HA used in other studies of this chapter and *in vitro* studies in chapter 4.

Alcian blue is a pH-controlled staining that stained cations in GAGs in blue, and neural components, such as Coll, in grey. Alcian blue staining indicated a successful incorporation of HA onto Coll, as shown by the obvious blue branches on the surface of two Coll-HA scaffolds. Higher magnification images showed that HA networks could coexist with Coll struts and were also able to construct independent networks. This was shown by white arrowheads pointing at HA-rich regions and black arrowheads pointing at Coll-rich regions. Blue struts on interlaced scaffolds might not always indicate pure HA networks, as they may merely be HA forming over Coll branches.

Unsurprisingly, increasing HA concentrations led to an increased blue area on the scaffolds. Comparing the two interlaced scaffolds, 0.75%Coll-0.25%HA had more struts where both Coll and HA co-exist, which suggests that the HA concentration was low enough for both Coll and HA to be exposed. On 0.5%Coll-0.5%HA however, most struts, apart from the two black arrowheads, appeared to be completely blue.

3.3.3 Energy dispersive X-ray spectroscopy

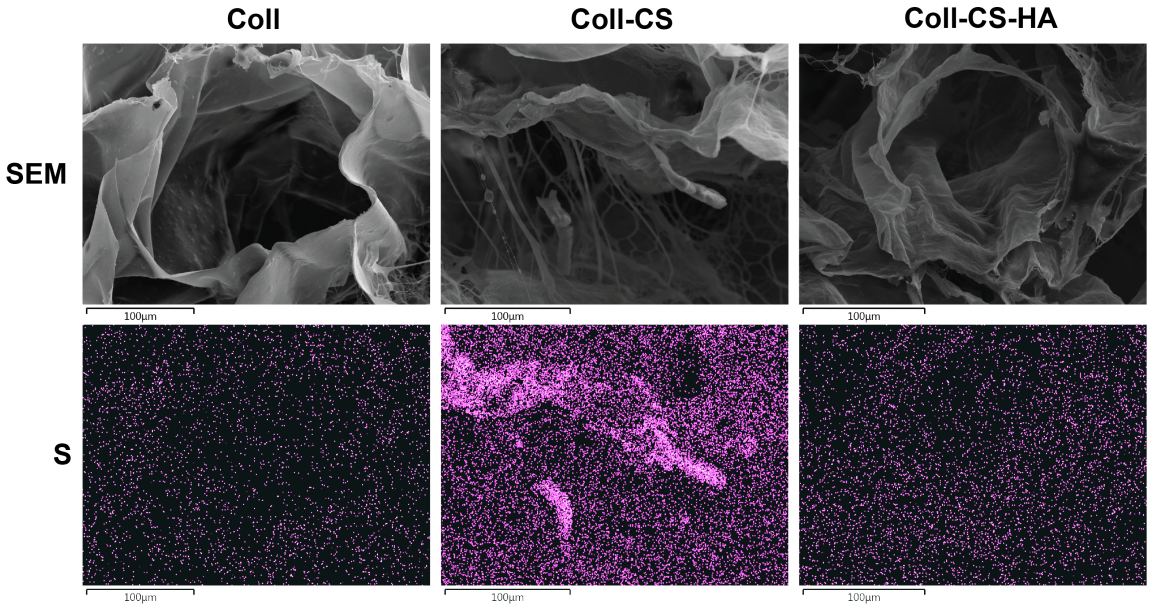


Figure 3.6 – SEM images of scaffolds and corresponding EDX analysis of sulfur distribution on Coll, Coll-CS and Coll-CS-HA scaffolds. Scale bars = 100 µm

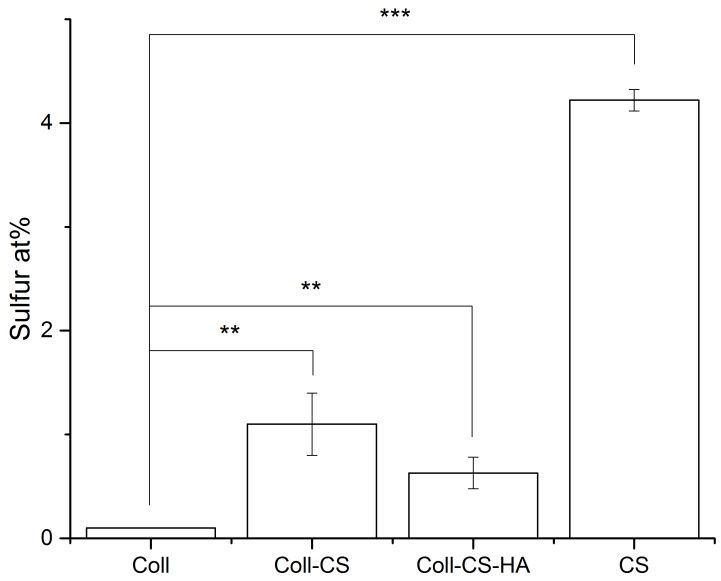


Figure 3.7 – Sulfur content on Coll, Coll-CS, Coll-CS-HA and CS scaffolds measured by EDX. Results are expressed in atomic percentage. (n=3) (**p<0.005, ***p<0.0005)

EDX analysis reviewed sulfur content on Coll, Coll-CS, Coll-CS-HA and CS scaffolds. The average atomic percentages of sulfur found on Coll, Coll-CS, Coll-CS-HA and CS were 0.10%, 1.10%, 0.63% and 4.22% respectively. Small amount (0.1at%) of sulfur was found on Coll. This was most likely due to impurities present on Coll and sulfur-containing proteins attached to its glycine molecule. There was no standard deviation shown for Coll because all three measurements were all 0.1at% S. An EDX with a better resolution may further distinguish any variations.

Sat% on other scaffolds was significantly higher, suggesting a successful incorporation of CS onto Coll. In addition, these water soluble CS was found after at least 3 hours of

continuous washing in PBS and distilled water, indicating a strong incorporation into Coll structure. Compared to a pure CS, the S% is much smaller on the interlaced scaffolds, suggesting that still large surface area of Coll was exposed. Coll-CS-HA had almost half of S% than Coll-CS. The statistics however, was insignificant ($p=0.073$). The difference in sulfur percentage can be reflected on the EDX images of Coll-CS and Coll-CS-HA.

CS distribution was not completely homogeneous on Coll-CS, as indicated by different intensities of sulfur found on Coll-CS. Regions that appeared to be higher in topography did not reveal higher sulfur concentration. These regions with smaller amount of sulfur may be composed by mostly Coll. Histology images of Coll and Coll-HA also revealed this similar inhomogeneous distribution of HA.

The atomic percentage of sulfur discovered on pure CS was much more than what had been expected from a CS monomer. This may be due to inaccuracies of the EDX system on lighter atoms, which will be discussed more in details later on in section 3.4.4.

3.3.4 Nuclear magnetic resonance spectroscopy

In NMR studies, Coll-CS, Coll-HA and Coll-CS-HA samples from degradation studies were used. Instead of analysing the scaffolds, we analysed the surrounding PBS in which the scaffolds were incubated in. This helped us understand the release of HA and CS as Coll's primary structure degraded.

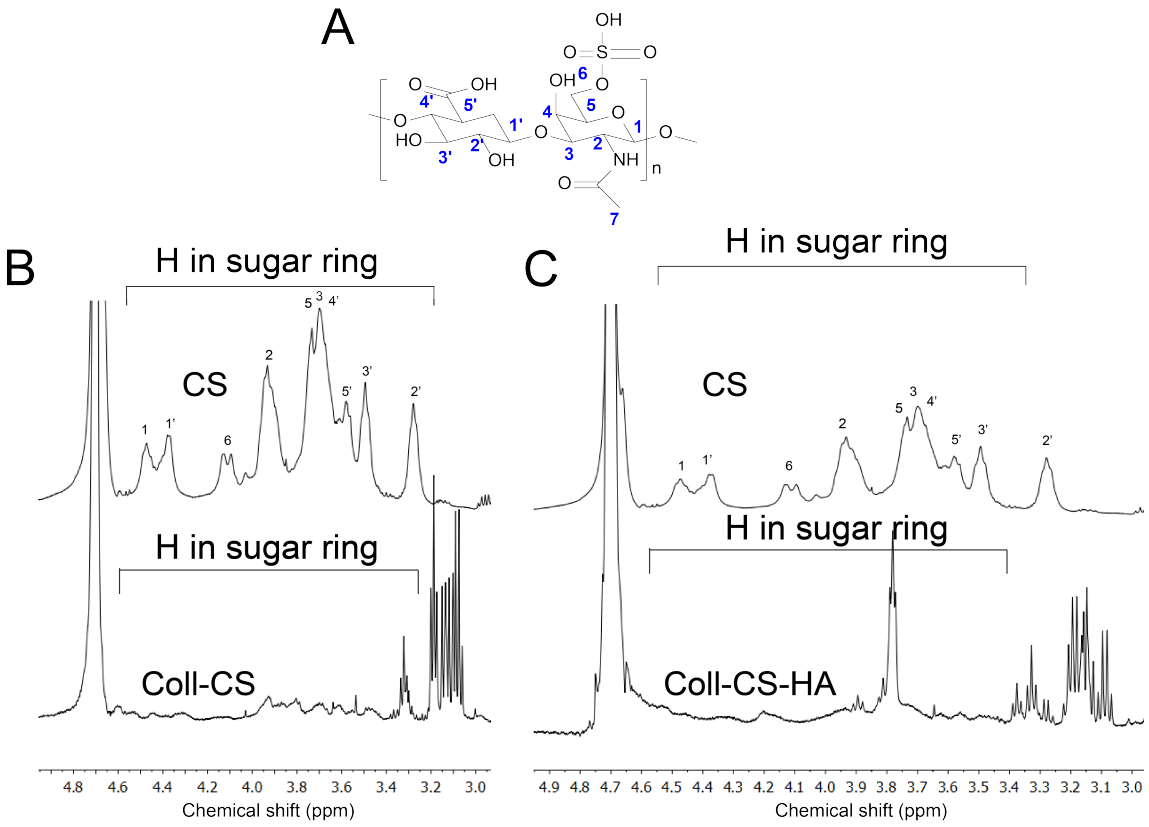


Figure 3.8 – ^{1}H NMR spectra for Coll-CS and Coll-CS-HA in D_2O (500MHz). A) A molecular structure of C6S, B) stacked NMR spectra of CS and Coll-CS, and C) stacked NMR spectra of CS and Coll-CS-HA. The numbers on CS spectra corresponds to the H atom in A)

Figure 3.8 above illustrates stacked ^{1}H NMR spectra of CS, Coll-CS and Coll-CS-HA from 3.0 to 4.9 ppm. NMR peaks of CS matched with previous literature [29]. The large peak at 4.7 ppm corresponded to D_2O. Numbered peaks on CS spectrum correspond to the hydrogen atoms depicted in figure 3.8A. In general, hydrogen atoms in the CS sugar ring were found in Coll-CS and Coll-CS-HA. However, NMR signals were extremely weak since the scaffolds had been previously incubated for 28 days.

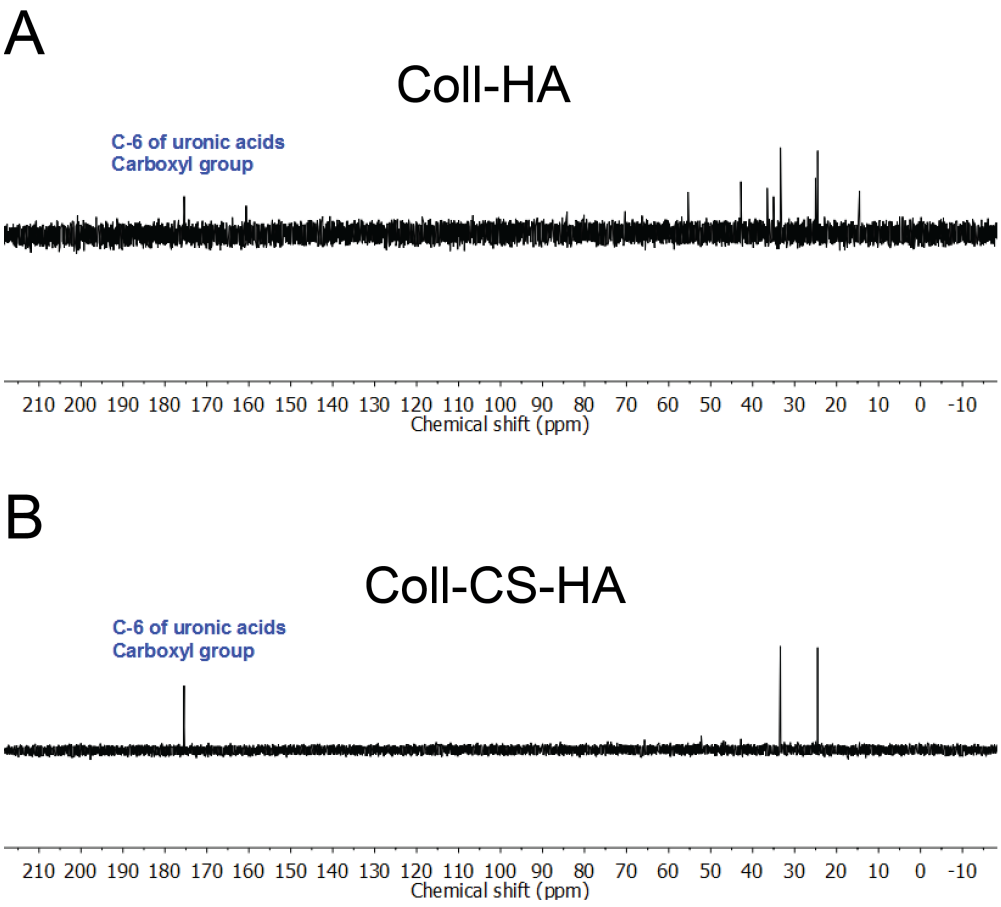


Figure 3.9 – ^{13}C NMR spectra of PBS from A) Coll-HA and B) Coll-CS-HA degradation tests. Chemical shift was recorded from -20 to 220 ppm (500MHz).

Figure 3.9 above illustrates the ^{13}C NMR spectra of PBS from Coll-HA and Coll-CS-HA. Spectra measured chemical shifts from -20 to 220 ppm. The release of HA was implied by depicting the C-6 peak of uronic acids group at around 175 ppm, which was likely part of the degradation product of HA. In addition, peaks around 25 ppm were consistent to previous literature [30]. Signals in general were again weak due to the same reason as CS scaffolds, but signals on Coll-CS-HA was relatively stronger, possibility due to the degraded CS.

NMR results here imply successful incorporations of CS and HA into the interlaced scaffolds. However, degradation of the primary Coll network would also release C atoms around the regions illustrated in figures 3.8 and 3.9, as Coll was also composed by mostly carbon and hydrogen. Thus, the NMR results here would only serve to suggest the fact that there could be a long term release of HA and CS from the interlaced scaffolds.

3.3.5 Scanning electron microscopy

Although previous researches have determined that 1.0wt% Coll had the most optimal mechanical properties for NSC growth, we characterised the pore structure of different Coll concentration to determine whether or not this concentration would lead to a suitable pore structure. Here we synthesised 0.5wt%, 0.75wt%, 1.0wt%, and 1.5wt% Coll solutions. The resultant scaffolds were sectioned and imaged under an SEM.

Figure 3.10 below illustrates the effect of Coll concentration on scaffold pore size. As expected, a higher Coll concentration led to lower pore sizes. 1.5wt% led to the lowest average pore size of 79 μm while 0.5wt% led to the highest of 161 μm. The average pore sizes of 0.75wt% and 1.0wt% Coll were both around 100 μm. 0.75wt% Coll had a slight higher pore size of 105 μm while 1.0wt% Coll had a pore size of 97 μm. The difference however, was not statistically significant.

Due to the relatively larger standard deviations, the differences between 0.75wt% and others were not statistically significant either. However, there were significant differences between 0.5wt% and 1.0wt%, and 0.5wt% and 1.5wt%.

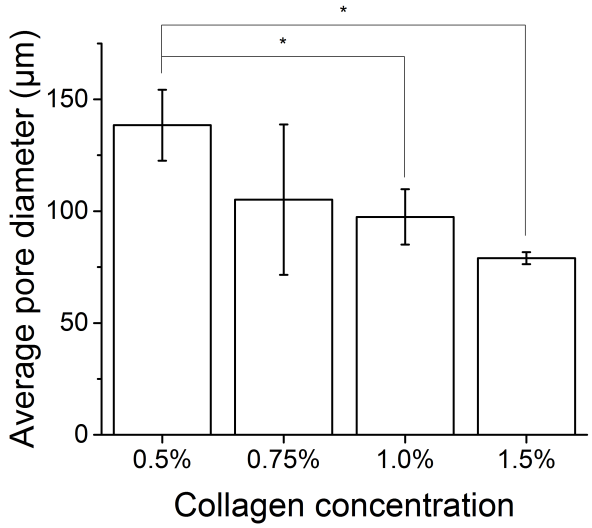


Figure 3.10 - Effect of Coll concentration from 0.5wt% to 1.0wt% on the average pore diameter of scaffolds (n=3). (*p<0.05)

Coll scaffolds in general had a consistent pore structure. Very few closed pores or very large open structure were seen. Having satisfied with the Coll structure, we then synthesised and imaged the interlaced scaffolds.

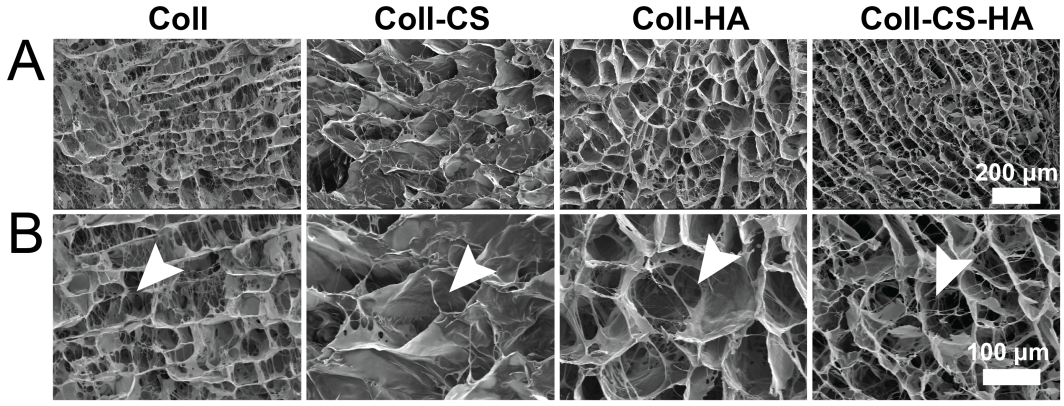


Figure 3.11 - SEM images and pore size analysis of scaffolds. A) SEM images of scaffold cross-sections and B) higher magnification images showing open pores and secondary pores structure (white arrowheads)

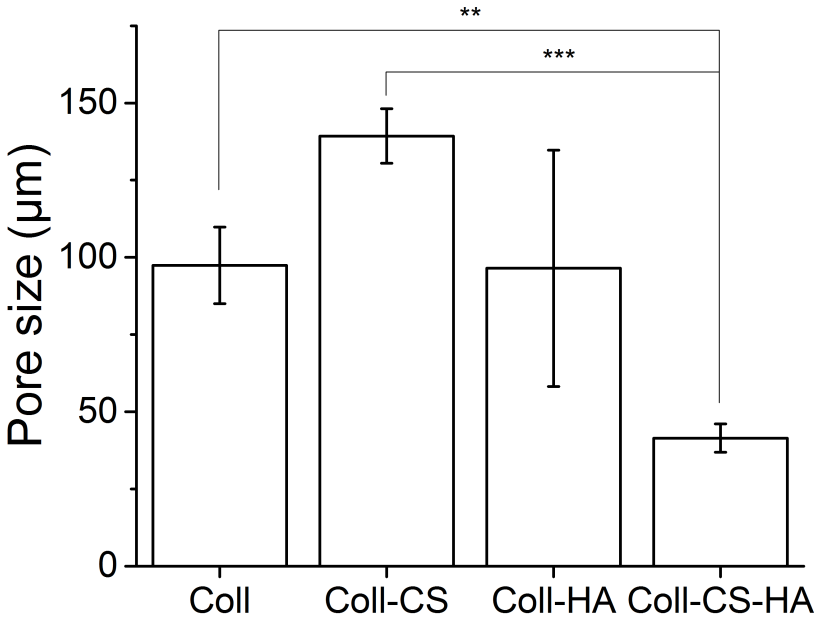


Figure 3.12 - Average pore size of Coll and interlaced scaffolds measured by ImageJ (n=3) (**p<0.005, ***p<0.0005)

SEM images of the cross-sections of 1.0wt% Coll and its interlaced scaffolds are shown in figure 3.11A and B. All interlaced scaffolds were synthesised based on the 0.75wt% Coll scaffolds. Images in panel A and B were taken at different magnifications to reveal their overall and internal pore structure.

It is obvious that all interlaced scaffolds exhibited highly porous foam-like structures similar to that of Coll. The freeze-drying process was effective in producing a highly interconnected porous structure, allowing infiltration of nutrients, growth of NSCs, and connections between cell colonies. When CS and HA were added, their pore structure became more distorted, as evidenced by extensive side-branches within the primary pores. This is more obvious in Coll-CS-HA, as extensive side branches had developed to form individual pores.

Higher magnification images of the scaffolds in figure 3.11B reveal more details. All scaffolds appeared to have defined open pores. Again, secondary pores were also present, evidenced by struts between pores indicated by the arrowheads.

For 1.0% Coll, the pore size was defined by the size of ice crystals formed in the -80°C freezer. Interlaced scaffolds were based on 0.75% Coll, and the addition of CS and/or HA onto 0.75% Coll would create secondary pores within the Coll primary network. It was indeed shown that the addition of CS and HA together had dramatically reduced the pore size of Coll-CS-HA.

Pore sizes varied as a reflection of ice crystals formed and distortion of the original Coll structure. All scaffolds were in the optimal pore diameter range suitable for NSC growth. The differences between Coll, Coll-CS and Coll-HA were not determined to be statistically significant, although the avearge pore size of Coll-CS was roughly 139 μm compared to Coll of 97 μm. Coll-HA had a very similar pore diameter to Coll of 96 μm, although its pores were more distorted, as evidenced by a larger standard deviation. Addition of CS and HA simulataneously however, had led to an extensive growth of struts and secondary pores within the Coll structure, which in turn reduced the average pore diameter to approximately 41 μm.

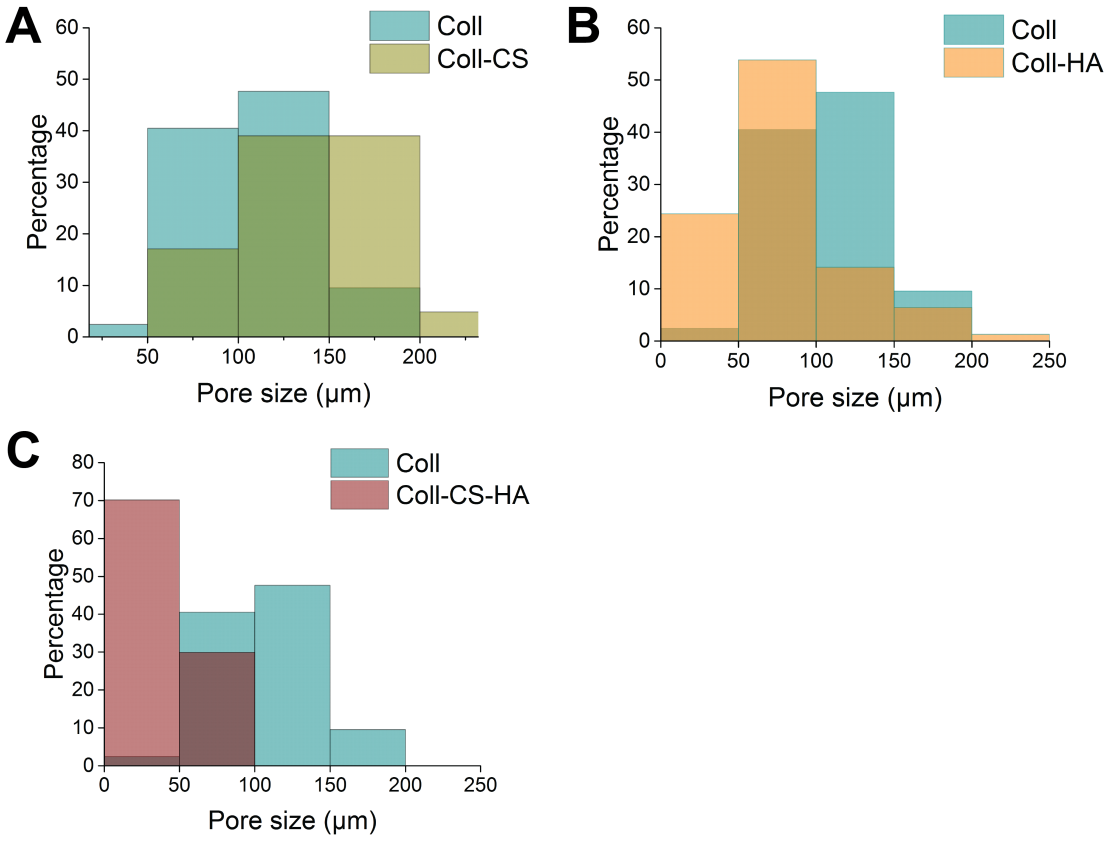


Figure 3.13 – Overlapping bar charts showing comparisons of pore size distributions between Coll and A) Coll-CS, B) Coll-HA, and C) Coll-CS-HA

Figure 3.13 above illustrates the differences in pore size distributions between Coll and its interlaced scaffolds. Noticeably, most pores of Coll, Coll-CS and Coll-HA were within the 50-200 μm range. Bars generally overlap between these three scaffolds. Coll-CS-HA however, accumulated mostly in between 0-50 μm. To better understand the reason for such reduction, we looked at Coll-CS-HA at a higher magnification illustrated by figure 3.14 below.

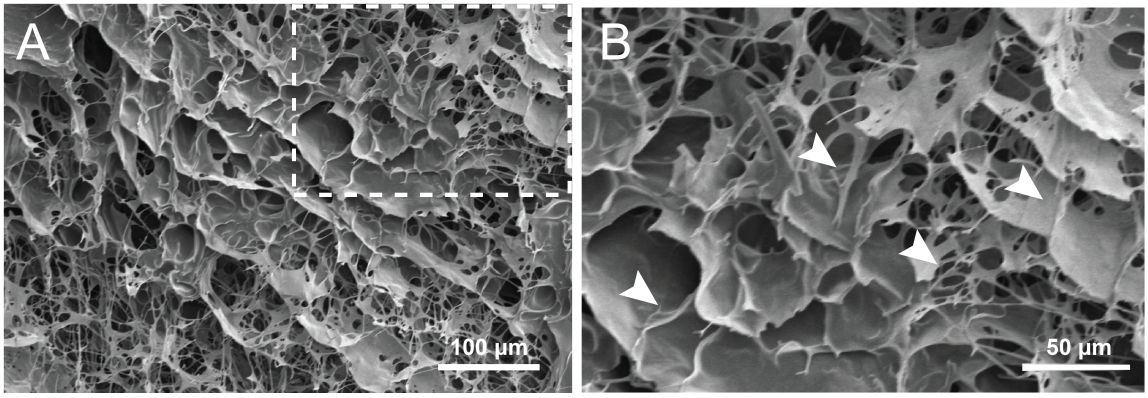


Figure 3.14 – Close-up SEM images of Coll-CS-HA. A) The image shows an overall more distorted pore structure, and B) a higher magnification of A) that reveals extensive struts in between pores and forming secondary pores, as indicated by white arrowheads.

Figure 3.14 above showed a more distorted pore structure and an extensive growth of struts that led to a formation of secondary pores (arrowheads) on Coll-CS-HA. The original Coll structure was still observable by the thicker walls between the primary pores. Hence, it is implied that the growth of secondary pores has led to a reduction in the average pore size of Coll-CS-HA.

3.3.6 Compression testing

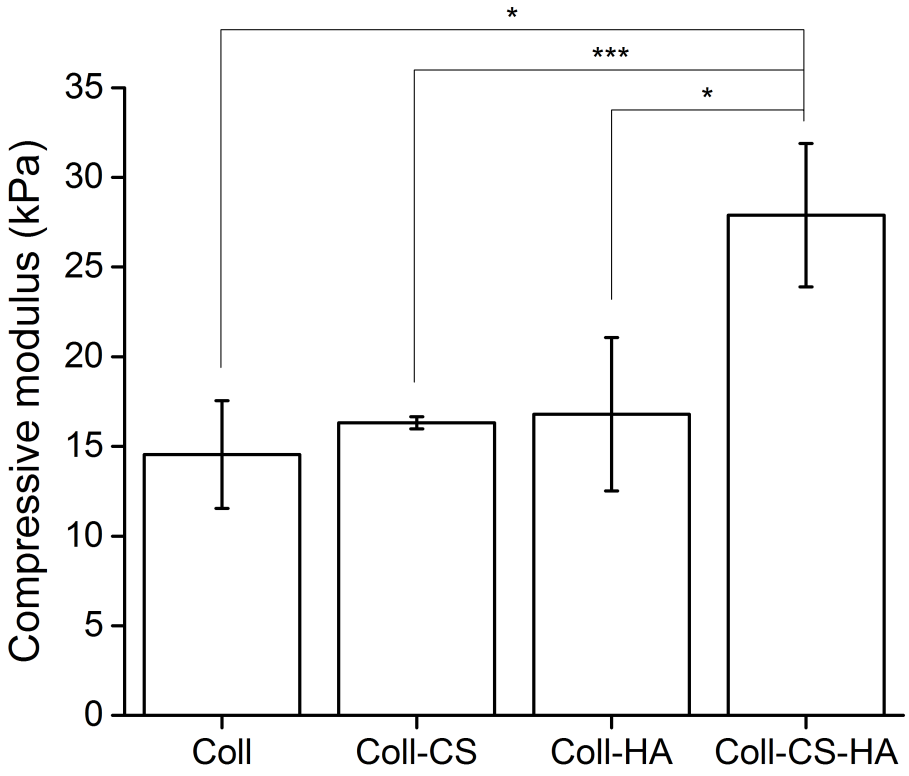


Figure 3.15 – The elastic moduli of a foam phase of all scaffolds measured by compression tests (n=3). (*p<0.05, ***p<0.0005)

Reduction in pore size also affected the overall compressive modulus. Figure 3.15 illustrates the compressive modulus of porous scaffolds. The elastic modulus of Coll-CS-HA in a foam phase was 27.9 kPa, which was statistically significantly higher than those of Coll, Coll-CS and Coll-HA, whose modulus were 14.6 kPa, 16.3 kPa and 16.8 kPa respectively.

3.3.7 Degradation studies

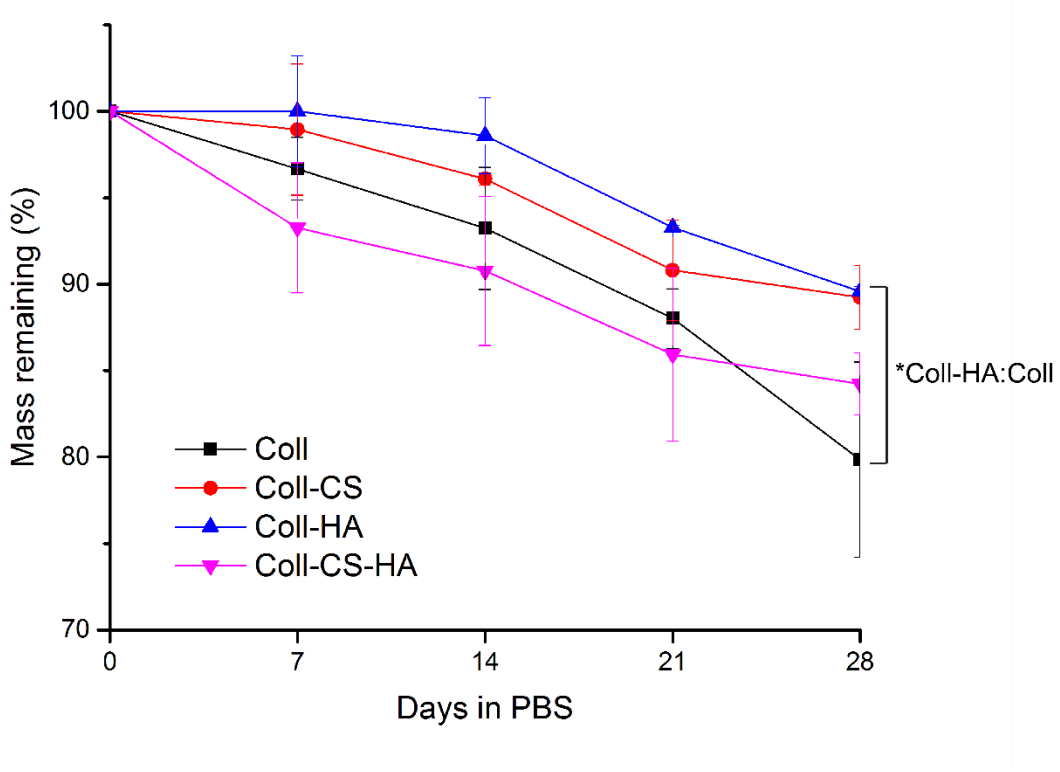


Figure 3.16 – Degradation of scaffolds in a pH 7.4 PBS at 37°C, over a 28 day period. Results were measured every 7 days and expressed as the percentage of their initial mass (n=3). (*$p<0.05$)

Figure 3.16 above shows the degradation profile of scaffolds during a 28-day period. Degradation studies were carried out at a mimicked physiological environment. At the end of 28 days, all scaffolds had lost approximately 10-20% of their original mass. Scaffolds exhibited a slow and smooth degradation curve as no rapid loss in mass was found. The smooth decline in mass generally matches the growth rate of cells observed in chapter 4.

At the end of day 28, Coll had lost the most mass among the scaffolds, followed by Coll-CS-HA, and Coll-CS and Coll-HA. In terms of percentage however, these differences were subtle. Degradation of scaffolds generally did not show any significant differences in between, except Coll and Coll-HA at day 28, where the p value was 0.0407.

It is also worth noticing that, although 80-90% of their initial nass remained at the end of 28 days, all scaffolds had become very soft and fragile. It was possible that during stirring, some parts might have disintegrated into the surrounding PBS. In addition, we also paid close attention to any colour changes to the scaffolds and the PBS, which might indicate infection. All scaffolds remained white and PBS remained transparent at the end of the experiment.

3.4 Discussion

In previous literature, there have been various studies on using interlaced scaffolds as scaffolds for tissue engineering [31]. However, the direct comparison between HA and CS as a scaffold for TBI was barely studied. Also, an interlaced Coll-CS-HA scaffold was also the first to be constructed and studied in this thesis. Thus, characterisations of these scaffolds were imperative for further cell studies. This chapter hence serves to characterise the compositions, morphologies, mechanical properties and degradation profile of the scaffolds synthesised in this thesis.

3.4.1 EDC/NHS crosslinking

EDC/NHS crosslinking involved connecting carboxylic acid groups (-COOH) to amine groups ($-NH_2$) to form amide bonds, or otherwise called peptide bonds (O=C-N-H). EDC/NHS crosslinking started with a modification of the carboxylic acid groups on HA and/or CS. EDC forms unstable reactive o-acylisourea esters with the carboxylic groups.

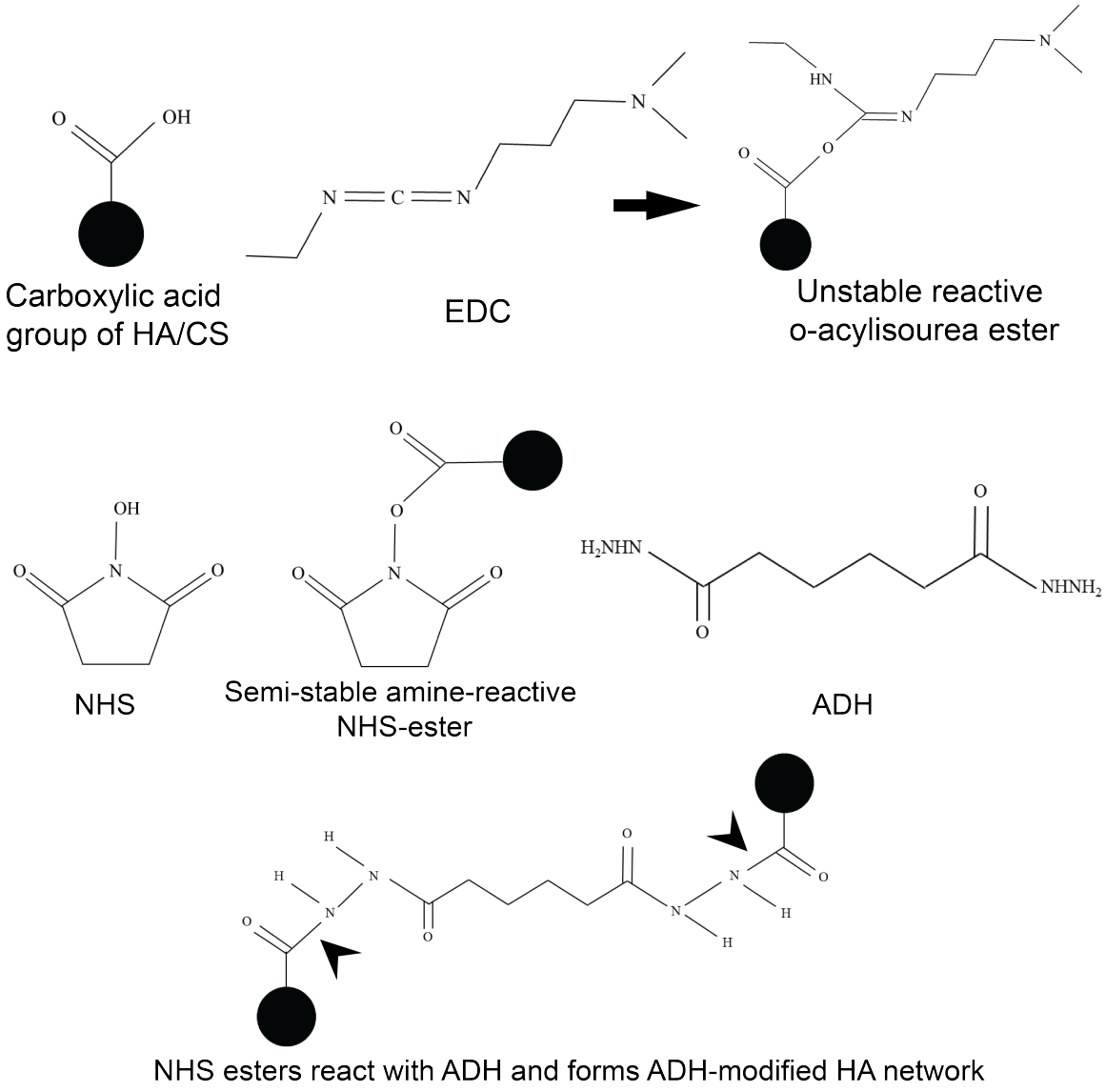


Figure 3.17 – Carboxylic groups of HA/CS reacting with EDC to form unstable reactive o-acylisourea esters. NHS reacts with the unstable o-acylisourea esters and replaces them to form a semi-stable amine reactive NHS-ester. ADH modification provides NH_2 anchoring points. Arrowheads pointing at the newly formed peptide bond CO-NH. Black sphere here represents the rest of the HA/CS molecule

In order for HA-HA, CS-CS or HA-CS crosslinking to take place, ADH was added as a connector. The NH_2 groups at both ends of ADH molecule reacted with the amine-reactive NHS-esters created in the above process. As a result, amide bonds were formed at the end of ADH molecules and H_2O was produced as a by-product. It is worth noticing that EDC and NHS did not form part of the resultant crosslinked structure whereas ADH did. This step is illustrated by figure 3.17 above. This approach to crosslink HA and/or CS has been widely used in previously [32].

$$HA \cdots COOH + H_2N \cdots ADH \cdots NH_2 \rightarrow HA - ADH \cdots NH_2 + H_2O$$

$$HA \cdots COOH + HA - ADH \cdots NH_2 \xrightarrow{EDC+NHS} HA - ADH - HA + H_2O$$

Figure 3.18 – Balanced chemical equation of EDC/NHS crosslinking reaction of HA in the presence of ADH. HA here can also be replaced by CS.

Figure 3.18 above illustrates balanced chemical equation of the reaction shown in figure 3.17. the sign "⋯" represents moieties within the HA or ADH molecule. For example, HA⋯COOH indicates the COOH moiety within the HA molecule.

As mentioned above, EDC/NHS crosslinking led to the formation of hydrogen bonds between C=O and N-H groups. In all interlaced scaffolds, Coll-Coll crosslinking might have also taken place as excess crosslinkers were added to CS and/or HA solution.

Crosslinking was necessary in this study because the networks needed to be stable over a period of weeks to months in order to match the recovery periods of TBI patients. Such crosslinking should not alter the primary network structure, or cause any detrimental

biological effects. One major benefit of EDC/NHS crosslinking is that they do not form part of the resultant network and they dissolve in water, thus can be readily removed by washing. EDC/NHS crosslinking is a common chemical crosslinking approach [33-35]. EDC reacts with the carboxylic acids groups of HA/CS, converting into an amine-reactive o-acylisourea ester. Although the ester could react with amine bonds, they are susceptible to hydrolysis and therefore lead to low efficiency. To stabilise, NHS is added to form a semi-stable amine-reactive NHS ester. Addition of NHS was shown to improve the crosslinking efficiency by 10-20 fold [34, 36].

ADH modification has been widely used in various cell culture, including preadipocytes [37], nucleus pulposus cells [38], breast, colon and ovarian cancer cells, fibroblasts [39], and induced pluripotent neural precursor cells [40]. Most of these studies demonstrated an excellent biocompatibility of ADH, although some studies have occasionally found ADH to slightly increase cytotoxicity [41]. In our studies, we decided to use ADH as part of our crosslinking process because of its biocompatibility and relatively easy process.

Our interlaced scaffolds attempted to avoid any chemical crosslinking between the primary and secondary network, and linked the two networks by physical entanglement as much as possible. If the crosslinking sites of HA or CS were used to crosslink Coll rather than itself, its capability of forming an independent network reduces.

Hence, physical crosslinking was the major mechanism that linked the two networks together and prevented dissolution of HA and/or CS. In this study, we attempted to achieve this by two steps. Firstly, excess amount of EDC, NHS and ADH were used to crosslink HA and CS. This step aimed to react as many carboxylic acid groups as possible, thus

forming an independent network before adding Coll. It is understandable that not all carboxylic acids groups would react due to physical impediment of the large molecules of HA and CS. Thus, we subsequently stored HA and CS solutions in a fridge overnight to ensure that EDC had lost most of its activity before Coll was added. Previous studies have demonstrated that, due to hydrolysis, the half-life of EDC in a pH 5 aqueous solution can be as low as 4 hours [42].

One major benefit of such construction is that it allowed better manipulation over independent networks. The crosslinking densities of HA and/or CS for example, could be easily altered without affecting Coll. The same applied to crosslinking of Coll, as dialysis can help remove crosslinking agents and avoid Coll crosslinking completely. Mixing various materials in one step however, would be more difficult to change the crosslinking density of one material without affecting the other.

Our previous attempt to crosslink HA or CS after constructing Coll-GAGs composites proved to be difficult, as EDC/NHS crosslinking takes place in an aqueous environment, where we could not prevent HA or CS from dissolving prior to being crosslinked. In addition, crosslinking often requires vigorous stirring, which further enabled HA and CS dissolution. Thus, our sequential construction approach provided an easier method to attached GAGs onto Coll.

We need to clarity that our interlaced scaffolds, although very likely, might not fully adhere to the definition of an IPN. In an IPN, there is no direct chemical crosslinking between the primary network and the secondary network [43, 44]. Current technologies limit the direct detection of IPNs, since it is not possible to examine every Coll molecule

in a nanoscale to exclude any Coll-GAG crosslinking in the scaffolds. The above method only serves to exclude possibilities as much as possible. Realistically, there could be non-degraded EDC molecules that crosslinked unreacted carboxylic acids groups on HA/CS to Coll, leading to a small number of chemically crosslinked amide bonds between Coll and GAGs. The pyrolidonic ring to amide III ratios of Coll-GAGs in table 3.3 below showed a reduction compared to Coll, which could be due to some degree of chemical crosslinking. However, we are confident that most of the attachments were due to physical entanglement rather than chemical crosslinking, and adhered to a classical IPN as much as possible.

3.4.2 Fourier transformed infrared spectroscopy

Addition of CS and HA was further confirmed by FTIR. The increased intensities at 1080 cm^{-1} due to carboxylic groups of uronic acids and at 1061 cm^{-1} due to sulfated GAGs were identified. Second derivatives also revealed S-O-C bonds on Coll-CS and Coll-CS-HA, which were previously unidentified due to overlapping peaks in FTIR. S-O-C bonds are characteristic bonds of CS and therefore should be a convincing evidence for the successful incorporation of CS within the two scaffolds.

In general, discrepancies of Coll-CS and Coll-CS-HA compared to Coll were more significant than Coll-HA to Coll. This was because most HA bonds overlapped with Coll and the differences were smaller. CS molecule was more distinct due to its S-O-C bonds. The distinctions were shown in both FTIR spectra and their second derivatives. Coll-HA

had an almost overlapping second derivatives spectrum to Coll, whereas Coll-CS and Coll-CS-HA both showed increased deviations to Coll.

It is also important that the addition of HA and/or CS did not alter the Coll network. As the most abundant protein in human body, Coll has been widely used in encouraging NSC survival and proved to have excellent biocompatibility to NSCs [18, 45, 46]. The two largest peaks in Coll, amide I and amide II, arose from C=O stretching vibrations coupled to N-H bending vibration and from N-H bending vibrations coupled to C-N stretching vibrations respectively, were obvious in the FTIR results of the interlaced scaffolds [47], indicating that the structure of Coll was not disturbed during the synthesis process.

The ratio of pyrolidonic ring and amide III provided information about the denaturation of Coll triple helix, as pyrolidonic rings stabilise the secondary structure of Coll. Denatured Coll triple helix has an amide III/pyrolidonic ring ratio of approximately 0.6 [6]. The ratio is shown in table 3.3 below.

Table 3.3 – Intensities of pyrolidonic ring and amide III peak and their ratios

Spectrum	**Pyrolidonic ring**	**Amide III**	**Amide III/pyrolidonic ring ratio**
Coll	0.248	0.254	1.21
Coll-CS	0.234	0.258	1.10
Coll-HA	0.210	0.212	1.01
Coll-CS-HA	0.204	0.192	0.94

Table 3.3 above shows a reduction in the ratio of amide III (1244 cm^{-1}) to pyrolidonic ring (1452 cm^{-1}) as GAGs were added. Ratios for all scaffolds were around 1, which were consistent with previous findings [46]. Coll had the highest ratio of 1.21. Addition of GAGs reduced the ratio from 1.21 to 0.94 in Coll-CS-HA. These results clearly showed that the synthesis method of the interlaced scaffolds well preserved the original Coll triple helix structure.

However, addition of GAGs did led to a decrease in the overall FTIR intensity. The reduction in intensity, especially in amide II, corresponded to the crosslinking reaction in which $–NH_2$ groups became –N-H [6]. Addition of CS-HA also led to the most remarkable reduction in the amide III/pyrolidonic ring ratio. Previous literature has discovered that EDC/NHS crosslinking could reduce this ratio [6]. Therefore, Coll-Coll crosslinking during an interlaced scaffold synthesis was likely to be the main reason for the reduction.

Following the addition of HA and CS onto Coll, Coll-Coll crosslinking took place under the effect of EDC/NHS crosslinkers. Although crosslinking led to a higher C=O and N-H vibration in the new molecule, these bondings were not reflected by an increase in absorbance in interlaced scaffolds. This was because the newly formed N-H groups from $–NH_2$ were weaker in intensity than the prior $–NH_2$ group. This result was confirmed by Wang *et al*., [45]. In addition, washing step after crosslinking can also led to a loss of non-crosslinked Coll, leading to a decrease in C=O bonding and thus amide I bond [49].

3.4.3 Histology

Alcian blue consists of a soluble form of copper phthalocynine, where the blue colour comes from its copper ions. Alcian blue dye has four positive charges per molecule, and therefore binds strongly to the negatively charged HA [50].

Unlike NMR, alcian blue staining showed a strong evidence of the presence of HA within the scaffolds. This was also because the samples used for histology were fresh. Consistent with literature, very little blue staining were found on Coll [50], and the figure showed a mixture of grey and blue networks within the two Coll-HA scaffolds. Independent blue struts appeared on Coll-HA scaffolds. This suggests that the HA was able to form independent network within Coll. However, it is also worth noticing that the blue struts may not always indicate pure HA network, as they could also be HA networks covering Coll struts. This could happen while freezing the crosslinked Coll-HA scaffolds, ice crystals might have pushed the independent HA struts onto the thicker Coll walls. In addition, CD44, a surface receptor commonly found on HA, was found to bind to Coll type I *in vitro* [51]. These factors might lead to HA binding to Coll struts rather than forming independent struts.

The increase in blue staining was consistent to the increase in HA concentration. On 0.5%Coll-0.5%HA, one could barely see any exposed Coll, whereas Coll was more obvious in 0.75%Coll-0.25%HA.

The distribution of CS and HA has shown interesting results. Localisation of HA and sulfur atoms, studied by alcian blue staining and EDX, proved to be inhomogeneous. This

is important in cell culture. Although CS and HA had effects on improving cell activities, exposed Coll has excellent cell attachment abilities [52-55]. Other techniques that mixed Coll and GAGs together would often result in a homogeneous distribution of GAGs.

Following our discussion in section 3.4.1., there is no current technology that is able to directly depict the absence of all chemical bonds between Coll and GAGs in a scaffold. Histology images here, although showing the two materials closely packed to each other, cannot exclude any chemical bonds either. However, the staining does show that on a 2D level, two networks were able to interpenetrate into each other and form which were very likely independent networks.

3.4.4 Energy dispersive X-ray spectroscopy

EDX results of scaffolds revealed higher sulfur content on Coll-CS and Coll-CS-HA compared to Coll. Small amount of sulfur found on Coll was likely due to impurities while extracting Coll from bovine tendon, which consisted of largely CS. Also, Coll molecules -[Glycine-X-Y]$_n$- often attracted other proteins rather than proline or hydroxyproline. These factors have possibly contributed to the 0.1at% sulfur found on Coll.

It is highly likely that the sulfur atoms found on Coll-CS and Coll-CS-HA were due to the CS networks within the scaffolds. The atomic percentage of sulfur found proved to be significantly higher and consistent throughout each scaffold. Although the CS-HA solution for Coll-CS-HA synthesis had the same concentration with the CS solution for Coll-CS synthesis, there were less sulfur atoms found on top of Coll-CS-HA. This could

be because some HA had masked CS on the surface of Coll-CS-HA. Alcian blue staining indicated many exposed HA on Coll-HA. Since the EDX only scanned the top surface of the scaffold, it could not detect the CS covered by HA and hence the signals found were slightly less (although the difference was statistically insignificant).

The accuracy of EDX quantification could be affected by a variety of factors. Overlapping peaks in EDX for example, could contribute to inaccuracies. In this study, the Kα peak of sulfur occurred at 2.307 keV, and the M peak of gold (from coating) occurred at 2.120 keV. The adjacent peaks could lead to overlaps and thus rendered calculations of peak area, which was proportional to concentration, difficult. In future, this can be improved by using carbon coatings instead of gold, since carbon's Kα peak locates at 0.277, which is much farther away.

Also, analysis of light elements has always been a challenge for EDX. Generally speaking, quantification of elements below sodium tends to be poorer [56]. Although sulfur (atomic weight of 32.06 u) is heavier than sodium (atomic weight of 22.99 u), carbon, nitrogen and hydrogen studied here all have smaller atomic weights. Hydrogen atoms were non-detectable by EDX in our study. These factors contributed to potential inaccuracies of sulfur atomic percentage within the scaffolds. For example, there are 47 atoms per CS monomer (see figure 2.5 in literature review) and thus the theoretical atomic percentage of sulfur would be 2.13at%. Excluding hydrogen atoms, there are 26 atoms, raising the percentage to 3.85at%. The sulfur at% we calculated using EDX was 4.22±0.10at%. This suggests that the discrepancies to the theoretical value might very likely be due to the limitation of lighter element detection. Nevertheless, although such limitation exists,

detection of sulfur is a common practice [57-59]. Thus, we are fairly confident to conclude that, qualitatively, an increase in sulfur content on Coll-CS and Coll-CS-HA was shown.

3.4.5 Nuclear magnetic resonance spectroscopy

Although CS and HA had already been found in FTIR, EDX and histology, samples used for these experiments were relatively fresh. In a TBI implant, recovery or disease progression take place in months. A rapid release of GAGs cannot support long term cell activities. Thus, it is beneficial for these bioactive materials to be released slowly. Other systems utilising a controlled-release system were also widely mentioned in previous literature [60-62].

As mentioned, the samples used in NMR were previously tested for degradation, where scaffolds had been immersed in PBS for 28 days with weekly change of fresh PBS. Although not a water soluble material, degradation of Coll would have taken place during the incubation period, and interfered with the NMR peaks.

Degradation products of HA are generally uronic acids, which were the main targets for many degradation studies involving HA [41, 63]. Coll-CS-HA had a higher signal of C6 from uronic acids compared to Coll-HA. This was likely due to the degradation of CS within Coll-CS-HA. CS also led to the peak at approximately 175 ppm. Another explanation for this is that Coll-CS-HA had a denser pore structure, evidenced by a smaller average pore size. Hence, the infiltration of PBS and thus dissolution of HA during

degradation would be more difficult. After degradation tests, there were simply more HA molecules remained on the scaffold, thus more HA was released in Coll-CS-HA solution.

On Coll-CS and Coll-CS-HA however, the signals were too weak to distinguish. Coll-CS had a number of peaks overlapped with CS. However, Coll-CS-HA did not. This was likely due to the change in environment or alteration from the crosslinking with HA.

As mentioned, NMR here was used merely to illustrate a possible dissolution of HA and CS during the scaffolds degradation. Assessment of the degraded products were inconclusive due to the interference from Coll and a low signal-to-noise ratio. Although similar chemical environments were observed for the degradation products in the region depicted by figures 3.8 and 3.9, it is worth mentioning that the interpretation of these result should be accompanied by EDX, FTIR and histology results. These results were shown here merely for the purpose of suggesting that a long-term release of CS and HA might have taken place. For more thorough studies in future, a quantitative study utilising a solid state NMR may be a more reliable option.

3.4.6 Pore size and morphological studies

SEM images of interlaced scaffolds indicated similar morphologies to pure Coll scaffolds. The scaffolds showed a well-mixed morphology, i.e. no phase separation of Coll and GAGs were observed. Upon cell culturing, these pores would act as ‘living rooms’ for cells to attach and proliferate. Interconnected porous structure is vital as it creates space for NSCs to grow yet allows connection of cell colonies and diffusion of nutrients.

Pore sizes were largely controlled by freezing temperature, which controlled the rate of nucleation of ice crystals. It is known that while water crystallises, the nucleation fronts repel the Coll until it reaches the grain boundaries. As ice sublimed in a freeze-dryer, Coll stayed intact and formed the pore structure observed. Previous literatures have suggested that a Coll pore size between 20 and 125 μm to be suitable for neural cell growth [6, 7]. Thus, we determined to use our interlaced scaffolds and Coll for cell culture, as their pore sizes were within the required range.

Apart from freezing temperature, water viscosity also controls the nucleation rates and thus pore sizes. A concentrated HA solution is highly viscous, thereby exerting a resistance to water nucleation and thus lowering grain sizes. To avoid the effect of viscosity on pore sizes, the scaffolds were washed extensively in PBS and distilled water to remove any free floating GAGs.

We only studied 0.5wt% to 1.5wt% Coll concentration mainly due to handling reasons. Scaffolds with a concentration lower than 0.5wt% became extremely fragile and thus difficult to section using a razor blade. On the other hand, scaffolds with concentration over 1.5wt% were too viscous to be casted in a mould. Therefore, studies of Coll concentration were chosen between 0.5 and 1.5wt%.

Scaffolds studied in this section were composed by mostly air. This was reflected by their low density – all well within 25 kg/m^3. This allowed maximum diffusion of nutrients and growth of NSCs, and a large surface area to volume ratio for maximum cell-material interactions.

3.4.7 Mechanical properties

Mechanical properties are vital while designing scaffolds for tissue engineering. As discussed in the previous chapter, scaffold stiffness can direct cell differentiation, which are essential in encouraging functional recoveries of patients.

Compressive modulus of Coll-CS-HA was almost two-fold of those of Coll, Coll-CS and Coll-HA. This discrepancy in compressive modulus was likely due to an increase in Coll-CS-HA density from the addition of HA and CS together, which led to an increase in the bulk compressive modulus. SEM images of Coll-CS-HA showed the formation of secondary pores. During compression testing, these struts would increase the scaffold's resistance to compression. Therefore, we were interested in whether or not the increase of bulk compressive modulus of Coll-CS-HA was correlated to an increase in its local stiffness. Gibson-Ashby equation followed was used to further study the local moduli of the scaffolds [64]:

$$\frac{E}{E_y} = C\left(\frac{\rho^*}{\rho_s}\right)^{3/2} \quad (3)$$

Where

E = Elastic modulus of a foam

E_y = Elastic modulus of a solid

C = Parameter

ρ^* = Density of the foam

ρ_s = Density of the solid

The formula can be thus rearranged to:

$$E_y \propto E \times \rho^{*(-3/2)} \quad 4$$

The exponent of the power law in the equation depends on the shape and of the cellular materials. The exponent of 3/2 was commonly used for open-cell structures [65], while, the exponent of 2 was commonly used for buckling-dominated behaviour, transforming the above equation to equation 5 below [66].

$$E_y \propto E \times \rho^{*(-2)} \quad 5$$

Both equations study the compressive moduli of solid materials by eliminating the effects from pore size or density. Densities of the scaffolds were measured by dividing the weights by their volumes. The density of Coll was 16.4 ± 4.3 kg/m^3, Coll-CS was 17.6 ± 4.0 kg/m^3, Coll-HA was 21.1 ± 3.9 kg/m^3 and Coll-CS-HA was 24.8 ± 2.3 kg/m^3.

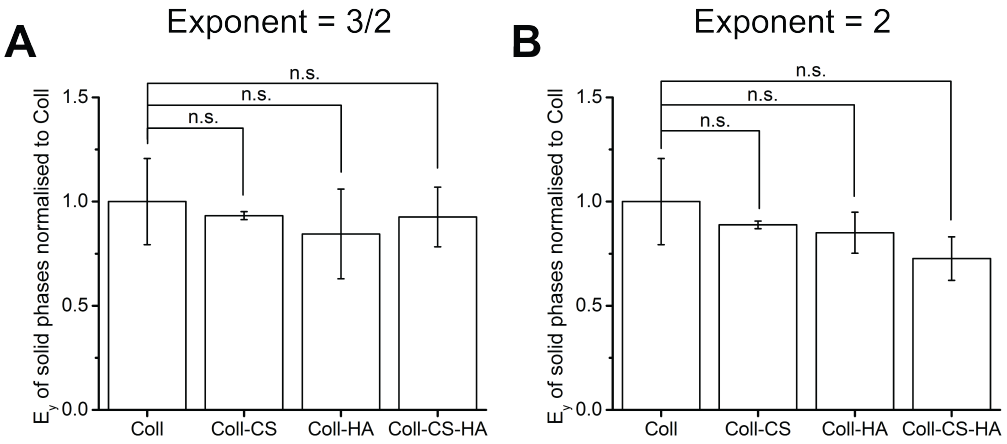


Figure 3.19 – Elastic moduli of the solid phases of scaffolds normalised to Coll, calculated by the Gibson-Ashby equation, where the exponent equals to A) 3/2, and B) 2 respectively (n=3). (n.s. = non-significant)

As expected, when densities of scaffolds were considered and taken into the Gibson-Ashby equations, there was no significant differences between the interlaced scaffolds and Coll, as illustrated by figure 3.19 above. While the exponent equalled to 3/2, the normalised compressive moduli of the solid phases of Coll-CS, Coll-HA and Coll-CS-HA were 0.93±0.02, 0.84±0.21 and 0.93±0.14. Coll-HA showed a decline in its normalised modulus despite a similar compressive modulus at the foam phase. One reason for this decline could be an increase in Coll-HA density compared to Coll (16.4 kg/m^3 to 22.6 kg/m^3). Nevertheless, this result indicates that at a microscopic level, the local stiffnesses of the materials remained unchanged.

While the exponent equalled to 2, the normalised compressive moduli of the solid phases of Coll-CS, Coll-HA and Coll-CS-HA were 0.89±0.02, 0.85±0.10 and 0.73±0.10 respectively. Coll-CS-HA in figure 3.19B had a lower normalised compressive modulus compared to in figure 3.19A. This was because the exponent of -2 overpowered the high compressive modulus, and thus appeared to be lower.

Gibson-Ashby equation is a commonly used approach to calculate the stiffness of porous materials [67-69]. The constant local stiffnesses was expected as in our interlaced scaffolds, addition of an additional network should not alter the original primary network, or Coll. The measured stiffness should invariably depends on the individual stiffnesses of Coll or GAGs themselves. The change in scaffold density was likely due to two reasons: the shrinkage of scaffolds during crosslinking, and the newly-formed branches due to the addition of GAGs.

One previous study has suggested that the mechanical properties of 1.0wt% Coll scaffold resembled the most similarity to those of rats' brains [20]. Hence, although the compressive modulus of Coll-CS-HA was statistically significantly higher than that of Coll, its local stiffness, which was more important for cells, was very similar to that of Coll and therefore its mechanical properties were within the appropriate range.

However, one aspect that may be affected by a scaffold's overall compressive modulus is the force it exerts onto the surrounding tissue after implantation into a brain. A stiff material may cause distortion to the injured tissue and worsen intracranial hypertension, a common side effect of TBI [70]. All our compressive testing was carried out on dried scaffolds. When scaffolds are wet, they absorb water and become very soft – in fact, too soft to be measured on our compressive testing machine or on our atomic force microscope (AFM). Hence, although we have measured the compressive moduli of two 4-day postnatal mouse brains, whose moduli were around 1.8 kPa, we cannot directly compare the differences of the brain and wet scaffolds. In addition, it is known that different parts of the brain have different stiffness values. For example, white matter is thought to be stiffer than grey matter [71, 72]. Implantation into different regions, therefore, may require custom-build scaffolds to match their compositions and mechanical properties.

Other mechanical considerations while designing scaffolds may include their flexibility during a wet stage. Ideally, craniotomy would be avoided as it leads to many side effects including acute pain [73], intracranial pressure and hypertension [74]. A flexible scaffold may be moulded to fit the injured site, and injected using a needle through a minimally invasive surgery. The scaffold then expands and fills the cavity. This property combines

the advantage of an injectable gel, but avoids the issue of poor cell and nutrient infiltration. Thus, these experiments could be done in future to further assess the mechanical properties of our scaffolds.

3.4.8 Degradation studies

In degradation studies, we aimed to create a mimicked physiological environment after brain injuries, and to monitor the degradation profiles of scaffolds across a period of 28 days. 28 days were chosen because tissue degeneration tends to become stabilised after 28 days [75] and the timeframe for regrowth of new tissue after a TBI is on the scale of several weeks [76, 77].

Previous research have indicated that, in a human brain injury, the pH of the brain tissue become stable at around 7-7.2 [78, 79]. Therefore, we chose a neutral pH for our degradation study. From the studies we have noticed that, at this pH, scaffolds remained stable over 28 days and were stable even being further kept for several months.

No significant differences were found across different scaffolds except Coll and Coll-HA at D28. Coll appeared to degrade slightly faster than others, reaching a 20% weight loss compared to 10-15% of others. This was probably due to the crosslinking of Coll within the interlaced scaffolds. Crosslinking mechanism connected free NH_2 bonds with C=O bonds, forming covalent bonds, thereby reducing the penetration of water molecules and increasing resistance to hydrolysis. However, at the end of 28 days, still 80-90% of the weight of all the scaffolds remained, allowing a continuous support for the cells.

In PBS, Coll was degraded by hydrolysis of Coll NH-CO bonding, which turned the bonds into COOH-NH_2, forming gelatine [80]. Gelatine was then further degraded by hydrolysis into fragments of peptide bonds. The mechanism of Coll degradation into gelatine is shown by the chemical reaction below.

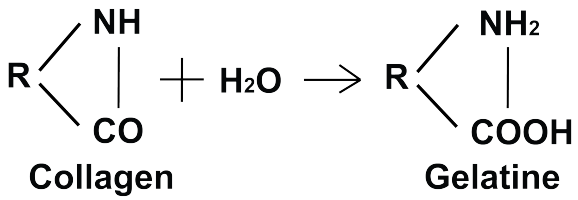


Figure 3.20 – Degradation of Coll into gelatine by hydrolysis

Within a human body, Coll, CS and HA are subject to constant degradation and reconstitution. CS for example, was found to have a biological half-life of 8 to 16 days [81]. The degraded products of these biomaterials are common to human's immune system and are safe within the body.

In an actual implant, body fluids facilitate degradation of scaffolds by hydrolysis. Also, other factors, including phagocytosis, enzymatic digestion and pressure, were not considered in this study. The main degradation mechanism of HA, CS and Coll in the body is enzymatic degradation by hyaluronidases, chondroitinases or collagenases [30, 81-83]. Therefore, one would expect the actual degradation to be faster than that in PBS.

The main difference between an enzymatic degradation and hydrolysis is the attack site. Enzymatic degradation tends to occur at the surface and degrades inwards. This is because unlike water, enzymes' macromolecules cannot easily penetrate into the cross-section of materials [84]. Although there are differences between degradation mechanisms in PBS

and in a physiological environment, future *in vitro* degradation studies may not necessarily have to include enzymes, as it is difficult to mimic the constant flow of fluids and other physiological factors, such as macrophages. Future studies should be carried out *in vivo*, allowing a more realistic monitor on degradation of an implant.

3.5 Conclusions

The purpose of this study was to character Coll and its interlaced scaffolds on their composition, micromorphologies, mechanical properties, and degradation behaviour.

The main reasons for constructing interlaced scaffolds were to imitate brain's ECM as much as possible and to allow better control over each network. In our study, we encouraged CS, HA, or CS-HA network to form before Coll was added to the solution. This way, we could avoid as much chemical crosslinking between the GAGs and Coll and limit their interactions to mostly physical crosslinking. This was important to our scaffold construction as it allowed manipulation of the primary and secondary networks independent of each other. Therefore, morphological studies and mechanical properties studies were essential, as we needed to ensure that the addition of secondary network did not disturb the primary network.

Morphologies and mechanical properties of the interlaced scaffolds proved to remain consistent to those of Coll. Addition of CS and HA together onto Coll had reduced the pore size from 100 μm to 40 μm by forming extensive branches and secondary pores, which dramatically increased the compressive modulus from 16 kPa to almost 28 kPa. In future, this may cause different responses in an actual implantation. However, after taking their density into account and measuring the stiffness as a solid material, the change in the local stiffness was insignificant. For *in vitro* studies, local stiffness is more important for cell activities as cells reside on a microscopic level.

Characterising the addition of HA and CS onto Coll, as well as the presence and distribution, were also vital. Without a direct crosslinking between GAGs and Coll, we need to ensure that the water-soluble CS and HA could stay within the network without dissolving. EDX, FTIR, and histology results have demonstrated that the interlaced scaffolds synthesis had been successful in incorporating HA and/or CS onto the Coll primary network.

In our studies, HA and CS were able to withstand vigorous overnight stirring. The final step in the synthesis contained washing off the crosslinking agents. EDX results revealed 1.1at% and 0.7at% of sulfur on Coll-CS and Coll-CS-HA respectively, compared to a mere 0.1at% on Coll. Histology of HA showed the presence of HA after vigorous washing, and FTIR studies also indicated the presence of S-O-C and uronic acid moiety of HA and CS in the interlaced scaffolds.

Hence, our studies above have proved that HA and CS have been successfully incorporated into the interlaced scaffolds, and the scaffolds remained consistent to Coll in terms of morphology and mechanical properties. In order to show the biological effect of HA and CS, *in vitro* cell behaviour studies have been carried out, and will be discussed in the next chapter.

3.6 References

1. Hopkins AM, DeSimone E, Chwalek K, Kaplan DL. 3D *in vitro* modeling of the central nervous system. Progress in Neurobiology. 2015;125:1-25.

2. Lee J, Cuddihy MJ, Kotov NA. Three-dimensional cell culture matrices: state of the art. Tissue Engineering: Part B. 2008;14(1):61-86.

3. Clements IP, Munson JM, Bellamkonda RV. Neuronal Tissue Engineering. In: Ratner BD, Hoffman AS, Schoen FJ, Lemons JE, editors. Biomaterials Science: An Introduction to Materials in Medicine. 3rd ed: Academic Press; 2012. p. 1291-306.

4. McUsic AC, Lamba DA, Reh TA. Guiding the morphogenesis of dissociated newborn mouse retinal cells and hES cell-derived retinal cells by soft lithography-patterned microchannel PLGA scaffolds. Biomaterials. 2012;33:1396-405.

5. Elias PZ, Spector M. Implantation of a collagen scaffold seeded with adult rat hippocampal progenitors in a rat model of penetrating brain injury. Journal of Neuroscience Methods. 2012;209:199-211.

6. Pietrucha K. Physicochemical properties of 3D collagen-CS scaffolds for potential use in neural tissue engineering. International Journal of Biological Macromolecules. 2015;80:732-9.

7. Yannas IV. Emerging rules for inducing organ regeneration. Biomaterials. 2013;34(2):321-30.

8. Huang K-F, Hsu W-C, Chiu W-T, Wang J-y. Functional improvement and neurogenesis after collagen-GAG matrix implantation into surgical brain trauma. Biomaterials. 2012;33:2067-75.

9. Ni Y, Tang Z, Cao W, Lin H, Fan Y, Guo L, *et al*. Tough and elastic hydrogel of hyaluronic acid and chondroitin sulfate as potential cell scaffold materials. International Journal of Biological Macromolecules. 2015;74:367-75.

10. Lau LW, Cua R, Keough MB, Haylock-Jacobs S, Yong VW. Pathophysiology of the brain extracellular matrix: a new target for remyelination. Nature Review. 2013;14:722-9.

11. Davidenko N, Schuster CF, Bax DV, Raynal N, Farndale RW, Best SM, *et al*. Control of crosslinking for tailoring collagen-based scaffolds stability and mechanics. Acta Biomaterialia. 2015;25:131-42.

12. G. HM, J. JM, J. OBF. The effect of dehydrothermal treatment on the mechanical and structural properties of collagen-GAG scaffolds. Journal of Biomedical Materials Research Part A. 2009;89A(2):363-9.

13. Drexler JW, Powell HM. Dehydrothermal crosslinking of electrospun collagen. Tissue Engineering Part C: Methods. 2011;17(1):9-17.

14. Saarakkala S, Rieppo L, Rieppo J, Jurvelin JS. Fourier transform infrared (FTIR) microspectroscopy of immature, mature and degenerated articular cartilage. In: Méndez-Vilas A, Díaz J, editors. Microscopy: Science, Technology, Applications and Education: FORMATEX; 2010. p. 403-14.

15. Tamaddon M, Walton RS, Brand DD, Czernuszka JT. Characterisation of freeze-dried type II collagen and chondroitin sulfate scaffolds. J Mater Sci: Mater Med 2013;24:1153–65.

16. Goldstein J, Goldstein JI, Goldshtain Y, Newbury DE, Joy DC, Echlin P, *et al*. Scanning Electron Microscopy and X-ray Microanalysis: Third Edition: Springer US; 2003.

17. Seidlits SK, Khaing ZZ, Petersen RR, Nickels JD, Vanscoy JE, Shear JB, *et al*. The effects of hyaluronic acid hydrogels with tunable mechanical properties on neural progenitor cell differentiation. Biomaterials. 2010;31:3930-40.

18. Mori H, Ayumi Takahashi, Horimoto A, Hara M. Migration of glial cells differentiated from neurosphere-forming neural stem/progenitor cells depends on the stiffness of the chemically cross-linked collagen gel substrate. Neuroscience Letters. 2013;555:1-6.

19. Georges PC, Miller WJ, Meaney DF, Sawyer ES, Janmey PA. Matrices with compliance comparable to that of brain tissue select neuronal over glial growth in mixed cortical cultures. Biophysical Journal. 2006;90:3012-8.

20. Elias PZ, Spector M. Viscoelastic characterization of rat cerebral cortex and type I collagen scaffolds for central nervous system tissue engineering. Journal of the Mechanical Behavior of Biomedical Materials. 2012;12:63-73.

21. Dinescu S, Galateanu B, Albu M, Lungu A, Radu E, Hermenean A, *et al*. Biocompatibility assessment of novel collagen-sericin scaffolds improved with hyaluronic acid and chondroitin sulfate for cartilage regeneration2013.

22. Potter K, Kidder LH, Levin IW, Lewis EN, Spencer RGS. Imaging of collagen and proteoglycan in cartilage sectionsusing fourier transform infrared spectral imaging. Arthritis & Rheumatism. 2001;44(4):846-55.

23. Lungu A, Albu MG, Florea NM, Strancu IC, Vasile E, Iovu H. The influence of glycosaminoglycan type on the collagen-glycosaminoglycan porous scaffolds. Digest Journal of Nanomaterials and Biostructures. 2011;6(4):1867-75.

24. Vidal BdC, Mello MLS. FT-IR microspectroscopy of rat ear cartilage. PLoS ONE. 2016;11(3).

25. David-Vaudey E, Burghardt A, Keshari K, Brouchet A, Ries M, Majumdar1 S. Fourier transform infrared imaging of focal lesions in human osteoarthritic cartilage. European Cells and Materials. 2005;10:51-60.

26. Fischer R, McCoy MG, Grant SA. Electrospinning collagen and hyaluronic acid nanofiber meshes. Journal of Materials Science Materials in Medicine. 2012;23(7):1645-54.

27. Mader KT, Peeters M, Detiger SEL, Helder MN, Smit TH, Christine L. Le Maitre, *et al*. Investigation of intervertebral disc degeneration using multivariate FTIR spectroscopic imaging. Faraday Discussions. 2016;187(1):393-414.

28. Rieppo L, Saarakkala S, Närhi T, Helminen HJ, Jurvelin JS, Rieppo J. Application of second derivative spectroscopy for increasing molecular specificity of fourier transform infrared spectroscopic imaging of articular cartilage. Osteoarthritis and Cartilage. 2012;20(5):451-9.

29. Volpi N, Mucci A, Schenetti L. Stability studies of chondroitin sulfate. Carbohydrate Research. 1999;315(3):345-9.

30. Pattersona J, Siew R, Herring S, Lin A, Guldberg R, Stayton P. Hyaluronic acid hydrogels with controlled degradation properties for oriented bone regeneration. Biomaterials. 2010;31(26):6772–81.

31. Suri S, Schmidt CE. Photopatterned collagen–hyaluronic acid interpenetrating polymer network hydrogels. Acta Biomaterialia. 2009;5(7):2385-97.

32. Kirker KR, Prestwich GD. Physical properties of glycosaminoglycan hydrogels. Journal of Polymer Science Part B Polymer Physics. 2004;42(23):4344-56.

33. Pieper JS, Hafmans T, Veerkamp JH, van Kuppevelt TH. Development of tailor-made collagen–glycosaminoglycan matrices: EDC/NHS crosslinking, and ultrastructural aspects. Biomaterials. 2000;21(6):581-93.

34. Sehgal D, Vijay IK. A method for the high efficiency of water-soluble carbodiimide-mediated amidation. Analytical Biochemistry. 1994;218(1):87-91.

35. Wissink MJB, Beernink R, Pieper JS, Poot AA, Engbers GHM, Beugeling T, *et al*. Immobilization of heparin to EDC/NHS-crosslinked collagen. Characterization and *in vitro* evaluation. Biomaterials. 2001;22(2):151-63.

36. Staros JV, Wright RW, Swingle DM. Enhancement by N-hydroxysulfosuccinimide of water-soluble carbodiimide-mediated coupling reactions. Analytical Biochemistry. 1986;156(1):220-2.

37. Shoham N, Sasson AL, Lin F-H, Benayahu D, Haj-Ali R, Gefen A. The mechanics of hyaluronic acid/adipic acid dihydrazide hydrogel: Towards developing a vessel for delivery of preadipocytes to native tissues. Journal of the Mechanical Behavior of Biomedical Materials. 2013;28:320-31.

38. Su W-Y, Chen Y-C, Lin F-H. Injectable oxidized hyaluronic acid/adipic acid dihydrazide hydrogel for nucleus pulposus regeneration. Acta Biomaterialia. 2010;6(8):3044-55.

39. Luo Y, Prestwich GD. Synthesis and selective cytotoxicity of a hyaluronic acid-antitumor bioconjugate. Bioconjugate Chemistry. 1999;10:755−63.

40. Nih LR, Moshayedi P, Llorente IL, Berg AR, Cinkornpumin J, Lowry WE, *et al*. Engineered HA hydrogel for stem cell transplantation in the brain: Biocompatibility data using a design of experiment approach. Data in Brief. 2017;10:202-9.

41. Schramm C, Spitzer MS, Henke-Fahle S, Steinmetz G, Januschowski K, Heiduschka P, *et al*. The cross-linked biopolymer hyaluronic acid as an artificial vitreous substitute. Investigative Ophthalmology & Visual Science. 2012;53(2):613-21.

42. Gilles MA, Hudson AQ, Borders CL. Stability of water-soluble carbodiimides in aqueous solution. Analytical Biochemistry. 1990;184(2):244-8.

43. Sperling LH. Interpenetrating Polymer Networks: An Overview. Interpenetrating Polymer Networks. Advances in Chemistry. 239: American Chemical Society; 1994. p. 3-38.

44. Alemán JV, Chadwick AV, He J, Hess M, Horie K, Jones RG, *et al*. Definitions of terms relating to the structure and processing of sols, gels, networks, and inorganic-organic hybrid materials (IUPAC Recommendations 2007). Pure and Applied Chemistry2007. p. 1801.

45. Egawa EY, Kato K, Hiraoka M, Nakaji-Hirabayashi T, Iwata H. Enhanced proliferation of neural stem cells in a collagen hydrogel incorporating engineered epidermal growth factor. Biomaterials. 2011;32:4737-43.

46. Koutsopoulos S, Zhang S. Long-term three-dimensional neural tissue cultures in functionalized self-assembling peptide hydrogels, Matrigel and Collagen I. Acta Biomaterialia. 2013;9:5162-9.

47. X.H.Wang, D.P.Li, W.J.Wang, Q.L.Feng, F.Z.Cui, Y.X.Xu, *et al*. Crosslinked collagen/chitosan matrix for artificial livers. Biomaterials. 2003;24(19):3213-20.

48. Plepis SMDG, Goissis G, Das-Gupta DK. Dielectric and pyroelectric characterization of anionic and native collagen. Polymer Engineering and Science. 1996;36(24):2932-8.

49. Chaubaroux C, Vrana E, Debry C, Schaaf P, Senger B, Voegel J-C, *et al*. Collagen-based fibrillar multilayer films cross-linked by a natural agent. Biomacromolecules. 2012;13(7):2128−35.

50. Sugiyama T. The mechanism of specific staining of acid mucopolysaccharide by alcian blue: on the influence of urea treatment on the stainability Acta Histochemica Et Cytochemica. 1968;1(1):16-30.

51. Jalkanen S, Jalkanen M. Lymphocyte CD44 binds the COOH-terminal heparin-binding domain of fibronectin. The Journal of Cell Biology. 1992;116(3):817-25.

52. Clyman RI, McDonald KA, Kramer RH. Integrin receptors on aortic smooth muscle cells mediate adhesion to fibronectin, laminin, and collagen. Circulation Research. 1990;67(1):175-86.

53. Heino J. The collagen family membersas cell adhesion proteins. Bioessays. 2007;29(10):1001-10.

54. Somaiah C, Kumar A, Mawrie D, Sharma A, Patil SD, Bhattacharyya J, *et al*. Collagen promotes higher adhesion, survival and proliferation of mesenchymal stem cells. PLOS ONE. 2015;10(12):e0145068.

55. Klebe RJ. Isolation of a collagen-dependent cell attachment factor. Nature. 1974;250:248.

56. Herrington CR. Quantitative EDS and WDS X-ray Microanalysis of Semiconductor Materials: Principles and Comparisons Journal of Electron Microscopy Technique. 1985;2:471-9.

57. Kinoshita H, Tanaka N, Jamal M, Kumihashi M, Okuzono R, Tsutsui K, *et al*. Application of energy dispersive X-ray fluorescence spectrometry (EDX) in a case of methomyl ingestion. Forensic Science International. 2013;227(1):103-5.

58. Li N, Gan F, Wang P, Chen K, Chen S, He X. In situ synthesis of 3D sulfur-doped graphene/sulfur as a cathode material for lithium-sulfur batteries. Journal of Alloys and Compounds.

59. Doyle A, Saavedra A, Tristão MLB, Aucelio RQ. Determination of S, Ca, Fe, Ni and V in crude oil by energy dispersive X-ray fluorescence spectrometry using direct sampling on paper substrate. Fuel. 2015;162:39-46.

60. Duan H, Li X, Wang C, Hao P, Song W, Li M, *et al*. Functional hyaluronate collagen scaffolds induce NSCs differentiation into functional neurons in repairing the traumatic brain injury. Acta Biomaterialia. 2016;45:182-95.

61. Moncion A, Lin M, O'Neill EG, Franceschi RT, Kripfgans OD, Putnam AJ, *et al*. Controlled release of basic fibroblast growth factor for angiogenesis using acoustically-responsive scaffolds. Biomaterials. 2017;140:26-36.

62. Sun J, Mou C, Shi Q, Chen B, Hou X, Zhang W, *et al*. Controlled release of collagen-binding SDF-1α from the collagen scaffold promoted tendon regeneration in a rat Achilles tendon defect model. Biomaterials. 2018;162:22-33.

63. Burdick JA, Chung C, Jia X, Randolph MA, Langer R. Controlled degradation and mechanical behavior of photopolymerized hyaluronic acid networks. Biomacromolecules. 2005;6(1):386–91.

64. Gibson LJ, Ashby MF. Cellular Solids: Structure and Properties. 2 ed. Cambridge: Cambridge University Press; 1997.

65. Evans AG, Hutchinson JW, Ashby MF. Cellular metals. Current Opinion in Solid State and Materials Science. 1998;3(3):288-303.

66. Ashby MF. The properties of foams and lattices. Philosophical Transactions of the Royal Society A. 2006;364:15-30.

67. Liu L-Z, Jin H-J. Scaling equation for the elastic modulus of nanoporous gold with “fixed” network connectivity. Applied Physics Letters. 2017;110(21):211902.

68. Hodge AM, Biener J, Hayes JR, Bythrow PM, Volkert CA, Hamza AV. Scaling equation for yield strength of nanoporous open-cell foams. Acta Materialia. 2007;55(4):1343-9.

69. Hedayati R, Sadighi M, Aghdam MM, Zadpoor AA. Mechanical properties of additively manufactured thick honeycombs. Materials. 2016;9(8):613-35.

70. Roux PL. Intracranial Pressure Monitoring and Management. In: Laskowitz D, Grant G, editors. Translational research in traumatic brain injury. 15. Boca Raton: CRC Press/Taylor and Francis Group; 2016.

71. Kaster T, Sack I, Samani A. Measurement of the hyperelastic properties of ex vivo brain tissue slices. Journal of Biomechanics. 2011;44(6):1158-63.

72. van Dommelen JAW, van der Sande TPJ, Hrapko M, Peters GWM. Mechanical properties of brain tissue by indentation: interregional variation. Journal of the Mechanical Behavior of Biomedical Materials. 2010;3(2):158-66.

73. Benedittis GD, Lorenzetti A, Migliore M, Villani RM. Postoperative pain in neurosurgery: a pilot study in brain surgery. Neurosurgery. 1996;38(3):466-9.

74. Gray LCD, Matta BF. Acute and chronic pain following craniotomy: a review. Anaesthesia. 2005;60(7):693-704.

75. Ali Erturk, Mentz S, Stout EE, Hedehus M, Dominguez SL, Neumaier L, *et al*. Interfering with the chronic immune response rescues chronic degeneration after traumatic brain injury. The Journal of Neuroscience. 2016;36(38):9962–75.

76. Williams AJ, Hartings JA, Lu X-CM, Rolli ML, Tortella FC. Penetrating ballistic-like brain injury in the rat: differential time courses of hemorrhage, cell death, inflammation, and remote degeneration. Journal of Neurotrauma. 2006;23(12):1828-46.

77. Fitch MT, Doller C, Combs CK, Landreth GE, Silver J. Cellular and molecular mechanisms of glial scarring and progressive cavitation: *in vivo* and *in vitro* analysis of inflammation-induced secondary injury after cns trauma. The Journal of Neuroscience. 1999;19(19):8182-98.

78. Clausen T, Khaldi A, Zauner A, Reinert M, Eoppenberg E, Menzel M, *et al*. Cerebral acid–base homeostasis after severe traumatic brain injury. Journal of Neurosurgery. 2005;103:597–607.

79. Gupta AK, Zygun DA, Johnston AJ, Steiner LA, Al-Rawi PG, Chatfield D, *et al*. Extracellular brain ph and outcome following severe traumatic brain injury. Journal of Neurotrauma. 2004;21(6):678–84.

80. Bogue RH. Conditions affecting the hydrolysis of collagen to gelatin1. Industrial And Engineering Chemistry. 1923;15(11):1154-9.

81. Wasteson A, Lindahl U, Halltn A. Mode of degradation of the chondroitin sulphate proteoglycan in rat costal cartilage. Journal of Biochemistry. 1972;130:729-38.

82. Inoue Y, Nagasawa K. Preparation, by chemical degradation of hyaluronic acid, of a series of even- and odd-numbered oligosaccharides having a 2-acetamido-2-deoxy-d-glucose and a dglucuronic acid residue, respectively, at the reducing end Carbohydrure Reseurch. 1985;141:99-110.

83. Krane SM. Collagenases and collagen degradation. The Journal of Investigative Dermatology. 1982;79:83-6.

84. Okada T, Hayashi T, Ikada Y. Degradation of collagen suture *in vitro* and *in vivo*. Biomaterials. 1992;13(7):448-54.

Chapter 4 – *In Vitro* Cell Studies

4.1 Introduction

In this chapter, *in vitro* cell studies using neural stem cells (NSCs) from the subventricular zone (SVZ) were performed on Coll and the interlaced scaffolds. The main objective of this thesis was to develop knowledge of NSC growth on engineered scaffolds as a potential future therapy for treating TBI. It is known that SVZ NSCs play an important role in TBI recovery. As reviewed by Chang *et al*., after a TBI, the number of 5-Bromo-2′-deoxyuridine (BrdU) labelled cells are significantly increased in the SVZ, indicating an increase in proliferation, and SVZ-derived neuroblasts migrate towards the injured sites [1]. Therefore, studies on *in vitro* cell behaviours, including proliferation, differentiation, migration and survival of SVZ NSC on the scaffolds are important to understand.

We divided our cell culture into proliferation studies, migration studies and differentiation studies. In proliferation studies, we observed phosphohistone-3 (PHi3) expression and overall cell colony sizes of 7-day cultures. In cell survival studies, we used Caspase-3 (Casp3) for the measurement of cell death. For migration studies, we observed migration from neuroblast spheroids and SVZ explants on our scaffolds.

In differentiation studies, we investigated the differentiation behaviours of NSCs on our scaffolds over a 21-day period. NSCs are tripotent cells and can be cued to go down either glial or neuronal lineage, or can be grown in cultures to remain undifferentiated. Although regeneration of functional neurons are important for brain recovery, studies have found that glial cells also hold essential roles in brain repair [2]. For differentiation studies, this

chapter used multiple markers: nestin (expressed by NSCs), GFAP, (glial fibrillary acidic protein, expressed by astrocytes and NSCs), Dcx, (doublecortin, expressed by neuroblasts), MAP2, (microtubule-associated protein 2, expressed by mature neurons), Olig2 (expressed by oligodendrocytes), and VGLUT1 (expressed by vascular glutamate transporters).

Our hypothesis for this study was that Coll by itself was not capable of inducing significant NSC proliferation, differentiation and migration. Thus, the addition of HA and CS onto Coll-CS-HA would have a beneficial effect and therefore might be a potential candidate for tissue engineering therapy for a TBI.

4.2 Materials and Methods

4.2.1 Isolation and culture of SVZ NSCs

SVZ NSCs were obtained from wide-type postnatal (P3-P5) C57BL6 mice. Mice were cooled to 4°C (on wet ice) to induce unconsciousness and deep anaesthesia from hypothermia, and decapitated using a surgical scissor. The brains were stored in ice-cold Neurobasal® media at all times before and during the dissection. The brains were sliced in the cortical plane using a Mcllwain tissue chopper and the SVZ was carefully dissected away using needles under a Leica MZ12 dissecting microscope. The SVZ tissue was digested by Accutase (Sigma Aldrich, UK) for 15 minutes at room temperature, centrifuged at 1,200 rpm (relative centrifugal force = 334 g) for 5 minutes, and suspended in a Neurobasal medium (Gibco, 10888-022) containing B27 (Gibco, 17504) glutamax (Gibco, 35050-038), PenStrep (Gibco, 15070-063), epidermal growth factor (EGF) (20 ng/mL, Sigma, E9644) and fibroblast growth factor-2 (FGF-2) (20 ng/mL, R&D system, 233-FB-025). The cells were suspended at a concentration of 100,000 cells/mL, and were then incubated in a 37°C, 5.0% CO_2 incubator on tissue culture treated 6-well plates (Corning®, CLS3516).

To obtain purified NSCs, NSCs were allowed to proliferate and expand into neurospheres for 3-4 days before passaging. During passaging, any cells in the supernatant were removed and adhernt neurospheres were obtained, digested with Accutase, and re-suspended at the same concentration of 100,000 cells/mL in a fresh media with growth

factors (GFs). We used tertiary neurospheres for our culture, as debris had been removed and cells were still mostly undifferentiated, the neurospheres mostly consisting of NSC and progenitors. Procedures were carried out with the University of Oxford Research Ethics Committee approval, in accordance with the Animals (Scientific Procedures) Act of 1986 (UK).

4.2.2 Coating

In order to characterise the stem cell phenotype of NSCs and demonstrate their ability to differentiate into neuronal lineages, tertiary NSCs were dissociated and cultured on adherent plates coated with laminin.

8-well chambers were used for adherent cell culture. In sterilised conditions, 150 μL of 0.1mg/mL poly-D-lysine (Sigma, P6403) was added into each well for an hour. Subsequently, poly-D-lysine was removed and the wells were washed three times with sterilised PBS, before adding 10 μg/mL laminin (Life Tech, 23017015). The chambers were incubated at 37°C overnight. Prior to cell culture, laminin was removed and media added to the wells.

4.2.3 Culture of NSCs

A variety of different cell seeding approaches were attempted before we decided the optimal approach for this study. The approach underlined in table 4.1 was determined to be the seeding method for NSC culture on scaffolds in this thesis.

Table 4.1 – Seeding methods tested in this study

Seeding methods	**Scaffolds size**	**Well plates**
Inject 25k NSCs in 250 μL media via a syringe into the centre of scaffolds	Thick scaffolds to allow injection	24 well plate
Add 10 μL media that contains 25k cells on top of the scaffolds, rest for 30 min, followed by adding 240 μL of cell-free media	Large, thin scaffolds that cover the entire well	48 well plate
	Small, thin scaffolds that cover a portion of the well	48 well plate
Add 25k NSCs in 250 μL media on top of the scaffolds in one step	Large, thin scaffolds that cover the entire well	48 well plate

To avoid bacteria etc. contamination, all scaffolds were sterilised by ethanol before seeding. Firstly, freeze-dried scaffolds were sectioned using a double edge razor blade (Wilkinson Sword Classic) into approximately 500 μm slices. The slices were then immersed in a 70% ethanol solution for 15 minutes. Subsequently, the slices were then carefully washed three times with sterilised PBS in a sterilised laminar flow hood. Finally, the slices were washed in medium for 5 minutes before placing into a 48-well plate.

Tissue culture treated 48-well plates (Corning®, CLS3548) were used for the culture of SVZ NSCs on scaffolds. Tertiary neurospheres were dissociated by incubating with Accutase for 10 minutes at room temperature and washed twice in Neurobasal media.

25,000 cells in approximately 250 μL Neurobasal media were added to the scaffolds using pipettes, making a final seeding concentration of 100,000 cells/mL.

The timeline and procedures for proliferation and differentiation studies are illustrated in figure 4.1. In proliferation conditions, 20 ng/mL EGF and 20 ng/mL FGF-2 were added to the media (proliferation media). The plates were then left in a 37°C, 5% CO_2 incubator for 21 days with weekly addition of GFs. Media was changed every 4-5 days. Two scaffolds were taken out on D4, D7, D14 and D21 respectively for fixation and immunohistochemistry.

In the differentiation condition, GFs were added at D0. At D7, the media was replaced by a fresh media with no GFs (differentiation media). The scaffolds were kept in culture for another two weeks. Differentiation studies analysed scaffolds at D14 and D21 post-seeding.

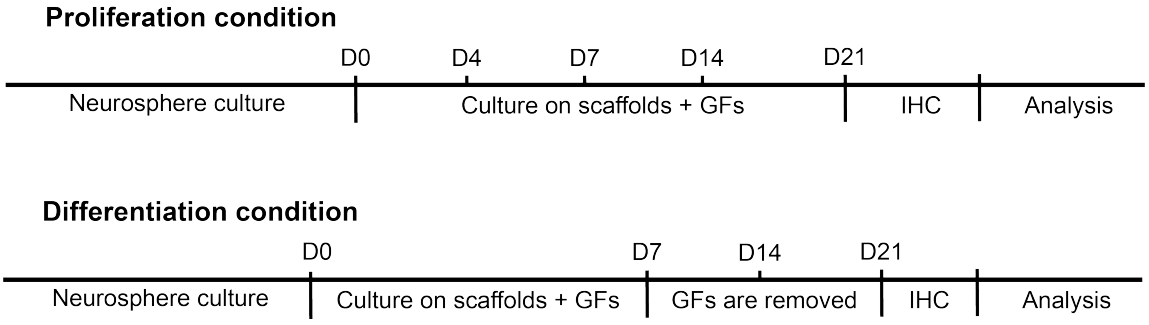


Figure 4.1 – Timeline and procedures for proliferation and differentiation studies

As positive controls, the same number of cells, volume of media and concentrations of GFs were added in two laminin-coated 8-well chambers. In one chamber, cells were incubated overnight to allow attachment to the laminin before fixing and subsequent

labelling with nestin. In the other chamber, cells were allowed to proliferate for 7 days before fixing and labelling with Dcx and MAP2.

In order to characterise other cells grown on scaffolds in culture, ReNcell CX (Millipore, SCC007), a human neural progenitor cell line derived from 14-week human cortical brain tissue, was also used. ReNcells were received as frozen samples in liquid N_2. Cells were thawed and passaged once before culturing on Coll and interlaced scaffolds. Before thawing, 20 µg/mL laminin diluted in DMEM/F12 (Millipore, DF-042-B) was used to coat a T75 flask. Subsequently, ReNcells were thawed and cultured in the laminin-coated flasks, split with trypsin and passaged once until convoluted.

The same concentration as SVZ cells of 100,000 cells/mL was used for ReNcell scaffold cultures. Same amount of EGF and FGF-2 was added to the culture, which was fixed at D7.

4.2.4 Immunohistochemistry

Immunohistochemistry (IHC) is a common process to detect proteins and other antigens within cells antibodies labelled using fluorescence. It is a two-step process that first involves exposing cells expressing a protein of interest with a specific primary antibody, followed by adding a secondary antibody that is bound to a fluorescent molecule of a specific wavelength.

After each time point, two scaffolds from the culture plates were removed and fixed in 4vol% paraformaldehyde (PFA) for 15 minutes in a new 48 well plate. This was followed

by 2 hours' incubation in a blocking solution, named PBS+, containing PBS, 0.1vol% Triton X-100 and 5vol% donkey serum. Scaffolds were labelled with primary antibodies for 24 hours on a shaker at 4°C, washed with PBS, and subsequently incubated with secondary antibodies in a dark environment for 2 hours at room temperature. Incubation with antibodies was prolonged compared to the protocol in the laboratory for immunocytochemistry to ensure maximum infiltration of the reagents into the scaffolds. After that, 0.1vol% of 4',6-Diamidino-2-phenylindole (DAPI) was added to the scaffolds for 15 minutes to label cell nuclei, followed by three washes with PBS. The final scaffolds were sealed and stored at 4°C. Anti-nestin, Dcx and MAP2 antibodies were used.

Table 4.2 - Primary antibodies used for immunohistochemistry

Antibody	**Host**	**Source**	**Dilution**	**Cell type detected**
Dcx	Goat	Santa Cruz SC8066	1:100	Neuroblasts
GFAP	Chicken	AbCam AB4674	1:5000	Astrocytes
Nestin	Mouse	Millipore, MAB353	1:100	NSCs
Casp3	Rabbit	Cell Signalling Technologies, 9661S	1:300	Cell death
MAP2	Chicken	AbCam, AB5392	1:1000	Mature neurons
VGLUT1	Rabbit	Synaptic Systems, 135-303	1:1000	Vascular glutamate transporters
PHi3	Rabbit	Millipore, 06-570	1:400	Proliferation
Olig2	Rabbit	Millipore, AB9610	1:1000	Oligodendrocytes

Table 4.3 - Secondary antibodies used for immunohistochemistry

Antibody	**Source**	**Dilution**
Donkey α-mouse AlexaFluor®568	Life Technologies	1:500
Donkey α-chicken AlexaFluor®488	Jackson ImmunoResearch	1:500
Donkey α-goat AlexaFluor®488	Life Technologies	1:500
Goat α-rabbit AlexaFluor®568	Life Technologies	1:500
Donkey α-goat AlexaFluor®647	Life Technologies	1:500
Chicken α-rabbit AlexaFluor®647	Life Technologies	1:500

To eliminate possible background absorption of antibodies on scaffolds, a no primary control experiment was conducted without the addition of primary antibodies. On a 7D proliferation experiment, after fixing and blocking with PBS+, 0.2vol% of donkey α-chicken AlexaFluor®488, chicken α-rabbit AlexaFluor®647 and goat α-rabbit AlexaFluor®568 respectively were incubated with scaffolds for 2 hours. The scaffolds were subsequently stained with DAPI and imaged under a Zeiss 710 confocal microscope.

4.2.5 Confocal microscopy

The main imaging technique for cells used in this study was confocal microscopy. A confocal microscope is a laser-based microscope that offers many unique advantages over conventional widefield optical epi-fluorescence microscopes, including eliminating out-of-focus signals and an enhanced control over depth of field. The microscopy utilises a

spatial filtering technique that only images signals coming from its focal plane [3]. This was extremely helpful while imaging scaffolds, as the 3D culture environment could lead to background noise from other z planes. Thus, using a confocal microscope in this study led to a tremendous improvement in resolution.

Before imaging, scaffolds were removed from their plate using a tweezer, and placed on a new glass cover slip above the lenses. The images were taken by a Zeiss 710 confocal microscope. For morphology and quantification studies, we used 63x lenses for imaging.

4.2.6 Total colony size measurement

In order to study and compare the number of NSCs on scaffolds, the surface area of DAPI+ cells in 7D proliferation and differentiation studies were measured by an epi-fluorescence microscope. The total surface area of DAPI per scaffold was measured using ImageJ.

4.2.7 Morphological analysis

For a better resolution and analysis of morphology and cell attachment, SEM was used to image dehydrated freeze-dried scaffolds. Scaffolds from D7 proliferation condition and D21 differentiation condition were imaged. In order to prepare dry samples for SEM imaging, scaffolds were first dehydrated using increasing gradient concentrations of ethanol. Scaffolds were washed in distilled water, followed by 30%, 50%, 70% and absolute ethanol for 15 minutes each. The scaffolds were then quenched in liquid nitrogen and stored in a -80 °C freezer prior to freeze drying in the freeze dryer for 24 hours.

Resultant scaffolds were gold-coated using a Bio-Rad ES400 sputter coater at 20mA for 45 seconds, and imaged under a Zeiss EVO SEM. SEM images were taken at 15 kV and 300 pA in SE mode at 8 x 10^{-6} mbar.

4.2.8 Migration studies

Gad65-GFP mice were also used for migration studies for better imaging. Gad65-GFP mice were genetically-modified to naturally express green fluorescence protein (GFP) and were dissected to obtain their SVZ and RMS regions as described in the following.

To ensure the explants and spheroids would not be washed away by media or IHC, we attempted a number of different seeding methods shown in table 4.4. We chose the method underlined as our primary seeding method in this study.

Table 4.4 – Seeding methods of SVZ explants and neuroblast spheroids in this study

Seeding methods	**Scaffolds**	**Fluorescence**
Placing explants or spheroids directly onto scaffolds, followed by adding 250 μL of media	One large, thin scaffold that covers the entire well	IHC
Placing explants or spheroids directly onto scaffolds and incubate for 1 hr for attachment before adding 250 μL of media	Two large thin scaffolds that sandwich the explants or spheroids	Gad65-GFP mice
	Two large thin scaffolds that sandwich the explants or spheroids	NucBlue
	One large, thin scaffold that covers the entire well	NucBlue

4.2.8.1 Isolation and culture of neuroblast spheroids

To obtain neuroblasts, P3-5 mice were sacrificed and dissected. The rostral migratory stream (RMS) region was carefully dissected using a pair of needles and digested by Accutase for 10 minutes at room temperature. After cell counting, 4,000 dissociated neuroblasts, at a concentration of 50,000 cells/mL, were placed per well in an ultra-low adhesion 96-well plate (Greiner, 650970) for 24 hours to aggregate under gravity. After 24 hours, cells formed into spheroids, which were then carefully taken out by a 200 μL pipette and placed carefully in between two sterilised scaffold slices.

In order to compare migration from spheroids, Matrigel was also added to the experiment. Cold Matrigel was first diluted by adding the same volume of cold media. Subsequently, 25 μL of diluted Matrigel was added to the spheroids in the 96 well plate and incubated.

The neuroblast spheroids were allowed to grow for 2 days in GF-free media. At the end of the culture, one drop of NucBlue (Thermo Fisher, R37606) was added to each well before imaging with a confocal microscope. Optical images of spheroids in Matrigel were taken at 0h, 24h and 48h. Neuroblast spheroid culture was carried out under the help from Dr. Martin Ducker in the laboratory.

4.2.8.2 Isolation and culture of SVZ explants

SVZ explants were prepared by dissecting the SVZ tissue from the Gad65-GFP mice into approximately 200 μm x 200 μm explant sections using needles. The sections were stored in ice cold media before transferring onto scaffolds under the dissection microscope. Explants were allowed to grow in GF-free medium for 2 days, before being labelled with NucBlue (Thermo Fisher, R37605) and imaged under the same Zeiss confocal microscope.

4.2.9 Statistical analysis

Results were presented as mean ± standard deviation. Student unpaired t-test from GraphPad and one-way ANOVA from Origin were used to determine the significance of differences between sets of data. $P<0.05$ was used to determine significance. N=3 for all studies were taken unless otherwise stated.

4.3 Results

4.3.1. Isolation of SVZ NSCs

Tertiary NSCs on the laminin-coated chambers were immunostained with anti-nestin antibodies at D0. The rest of these cells were cultured in parallel to those on scaffolds. At D7, their phenotypes were studied with MAP2 and Dcx immunocytochemistry and are shown in figure 4.2 below.

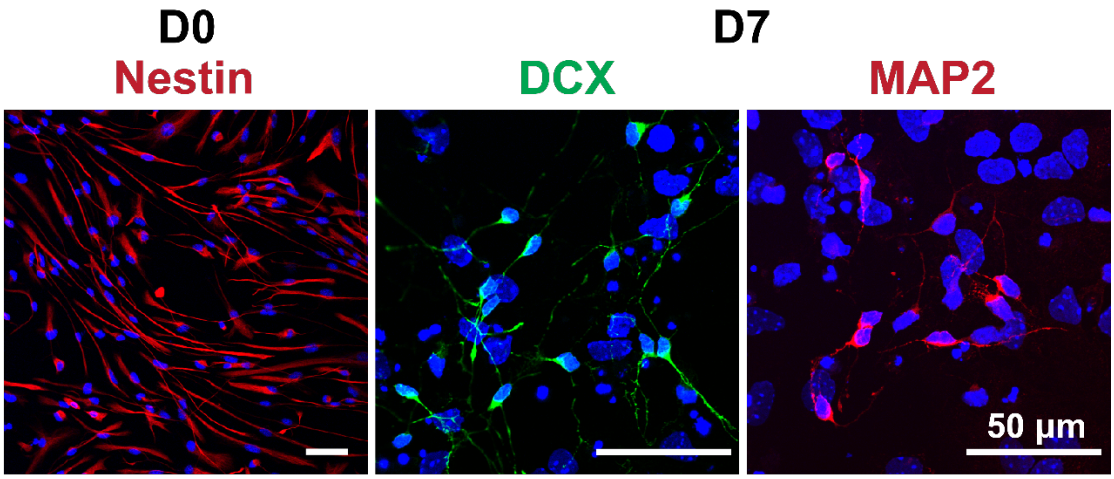


Figure 4.2 – SVZ NSCs cultured on 2D laminin-coated chambers for 0 and 7 days with the addition of EGF and FGF-2 on day 0. DAPI staining, which labelled all cell nuclei, was shown in blue. Scale bar = 50 µm

Before seeding onto the scaffolds, NSCs were first isolated from mouse brains and cultured until they reached tertiary stage neurospheres. Laminin-coated plates allowed cells to attach and thus render immuncytochemistry easier.

Although cells growing in a 3D environment better replicates a natural physiological environment, 2D culture on laminin allowed easier imaging of the morphologies of cells as their neurites and cell bodies were in the same focal plane. Figure 4.2 shows that most tertiary cells expressed nestin at day 0. As well the bipolar morphology observed is usually associated with SVZ NSC. This indicates that the cells seeded onto the scaffolds were mainly expressing stem cell characteristics.

EGF and FGF-2 are commonly used GFs for driving SVZ NSC proliferation and self-renewal [4]. After 7 days' culturing with GFs, notably, NSCs had given rise to young Dcx+ neurons, some of which had matured into MAP2+ neurons. In general, Dcx+ young neuronal morphology exhibited bi-polar structures, indicating a potential migratory phenotype and this was still seen at D7 in some MAP2+ neurons. However, some Dcx+ or MAP2+ cells did not develop neurites, suggesting that they may have stopped migrating and may not yet have extended neurites. Also, multipolar structures were rarely seen. This indicates that although many cells were MAP2+, these cells were relatively immature after 7 days in proliferation media, which would be expected to inhibit differentiation.

4.3.2. Tripotent differentiation capability of SVZ NSCs

To validate the tripotent differentiation capability of SVZ NSCs, we labelled SVZ cells grown in Coll scaffolds in proliferation conditions at D7 with anti-GFAP, MAP2, Dcx and Olig2 antibodies to characterise astrocytes, neurons and oligodendrocytes respectively.

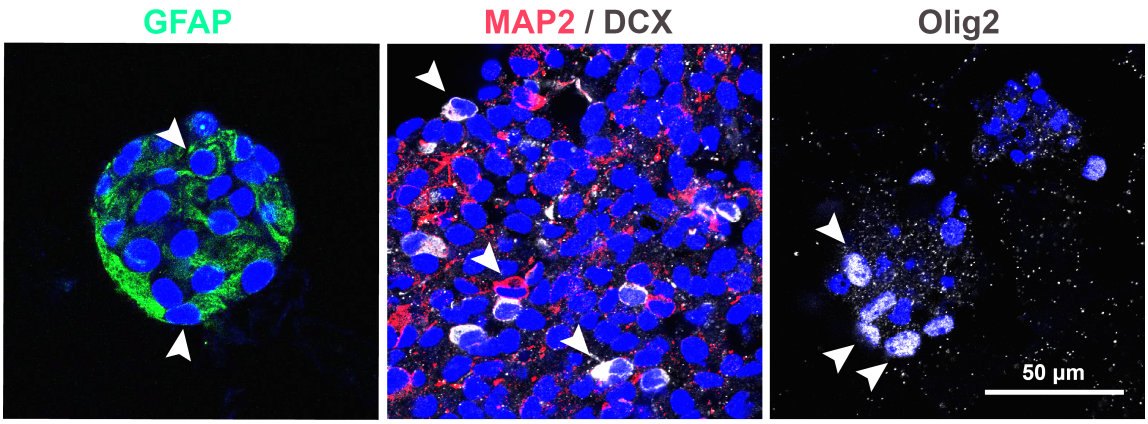


Figure 4.3 – Dissociated tertiary NSCs cultured on Coll scaffolds for 7 days differentiated into GFAP+ (green), MAP2+ (red), Dcx+ (white) and Olig2+ (white) cells. White arrowheads point at DAPI+ cells expressing the cell type specific markers. Scale bar = 50 µm

Figure 4.3 above illustrates the tripotent differentiation of SVZ NSCs. Cells were cultured for 7 days on a Coll scaffold with the addition of GFs at D0. GFAP staining suggested astrocytic differentiation, MAP2/Dcx co-labelling suggested mature and early neuronal differentiation and Olig2 suggested oligodendrocyte differentiation. Anti-GFAP, Dcx and MAP2 antibodies all labelled the cytoplasm while anti-Olig2 labelled nuclei as expected, hence the difference in morphologies. It is also worth noticing that the lack of neurites, especially in Dcx/MAP2 co-labelling, was likely attributed to the 3D environment, where axons or neurites often lied in a different focal plane, hence the apparent morphologies might not fully resemble those in figure 4.2.

In MAP2/Dcx co-labelling, white arrowheads point at DAPI+ cells expressing both MAP2 and Dcx (top left), MAP2 only (middle), and Dcx only (bottom). These stainings illustrate

neurons at different stages of maturation. Cells only expressing Dcx indicated a relatively earlier stage of differentiation, while cells expressing MAP2 indicated a later stage. Cells expressing both indicated somewhere in between. The co-labelling indicates that SVZ NSCs were able to differentiate into neurons of different stages of maturation within the scaffold.

GFAP and Olig2 expression were indicative of glial differentiation. As mentioned, neurons, astrocytes and oligodendrocytes are the most commonly found cell types of the brain. Hence, these positive labellings showed that the SVZ NSCs grown in Coll scaffolds were capable of giving rise to the major types of neural cells found in brain.

4.3.3 No primary control

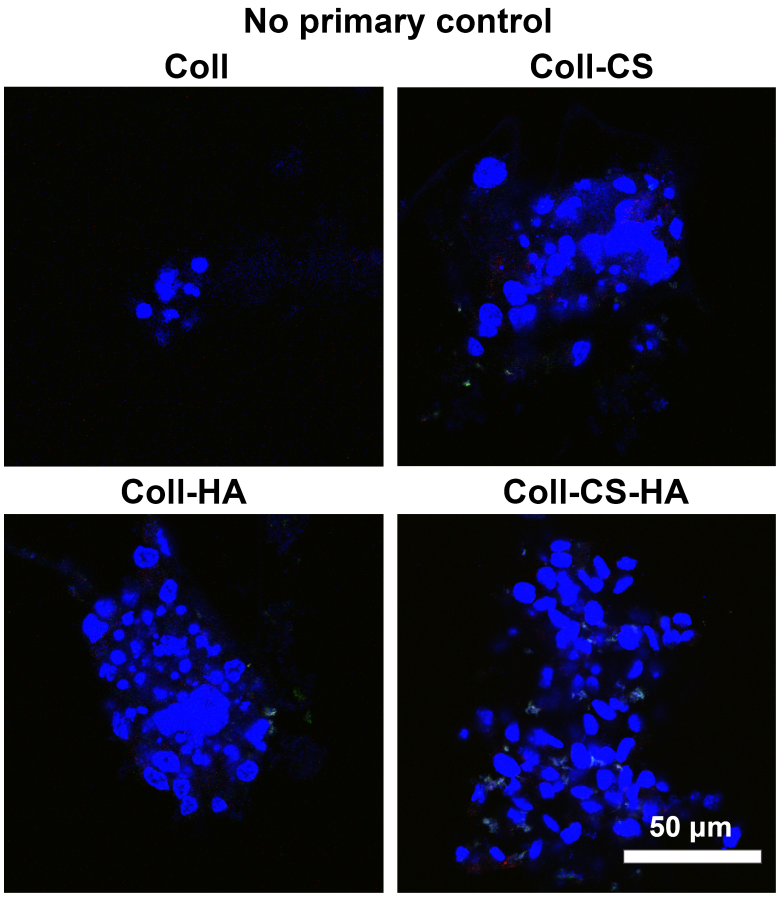


Figure 4.4 – No primary control on a 7D proliferation culture showing no detectable binding of secondary antibodies. Secondary antibodies used were donkey α-chicken AlexaFluor®488 (green), chicken α-rabbit AlexaFluor®647 (pseudo-coloured white) and goat α-rabbit AlexaFluor®568 (red). Blue: DAPI. Scale bar = 50 µm

A no primary control eliminates the confounding fluorescence signal of secondary antibodies in the interpretation of IHC results. Figure 4.4 illustrates a no primary control study over the four scaffolds on a 7D proliferation culture. In this study, the secondary antibodies used in the no primary control also labelled PHi3, MAP2, GFAP, Casp3 and

VGLUT1 expressions. As seen in the figure, no obvious fluorescence was observed around or on nuclei. This indicates that our IHC staining shown later in this chapter was not due to non-specific binding of the secondary antibodies.

4.3.4 ReNcell culture

To determine the viability of alternative cell sources for our study, we also employed ReNcells CX as a comparison to SVZ NSCs. Although cultured on a 3D scaffolds, ReNcells grew in a monolayer at the bottom of the plates. DAPI images are shown in figure 4.5 below.

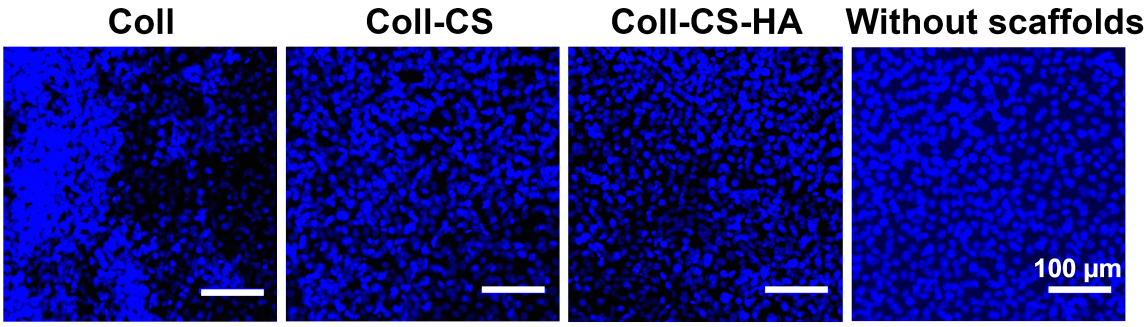


Figure 4.5 – ReNcell cultured 7 days in proliferation condition with scaffolds and without scaffolds. Images were taken at the same focal plane. Scale bar = 100 µm

Figure 4.5 above illustrates a 7D proliferation culture of ReNcells labelled by DAPI. Images were taken at the same focal plane, indicating that ReNcells on Coll, Coll-CS and Coll-CS-HA all grew on the bottom of the plates, rather than within the scaffolds. This an unexpected result shows that ReNcells did not penetrate the scaffolds but preferred

attaching to the plates. Hence, we used SVZ NSCs as the primary cell source for the rest of this section.

4.3.5 Cell death

In order to show that our scaffolds were capable of supporting cell survival, and our sterilisation process did not leave cytotoxic ethanol behind, we stained our 7D cultures with anti-Casp3 antibodies, a protein that is activated during cell death [5] and also a commonly used marker for apoptosis or necrosis. Casp3 immunocytochemistry was used to label cell death on the scaffolds (figure 4.6).

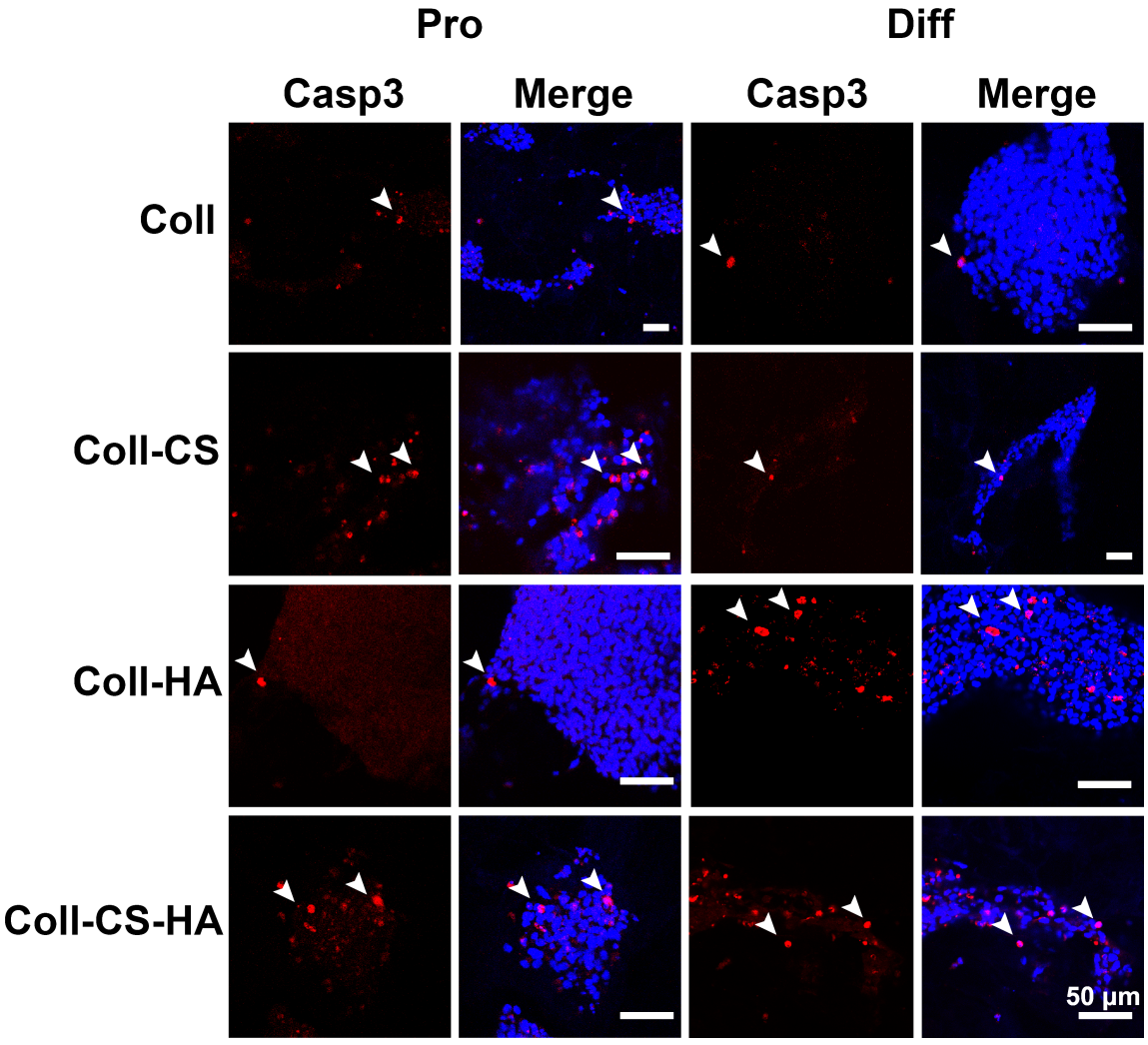


Figure 4.6 – Casp3 staining of Coll and interlaced scaffolds at day 7 in proliferation (Pro) and differentiation condition (Diff). Red: Caspase 3, blue: DAPI. White arrowheads point at Casp3 and DAPI colocalisation. Scale bars = 50 µm (n=1)

Figure 4.6 above illustrates the Casp3 staining for cell death in a 7-day culture in the proliferation and the differentiation condition. Casp3 is a cytoplasm marker and therefore encircled the DAPI staining.

In general, less than 10% of DAPI+ cells expressed Casp3 across all scaffolds in both conditions, indicating healthy colonies throughout all conditions. It is obvious that the total cell death was remarkably low compared to DAPI staining. Unlike in neurosphere cultures, where most cell death occurred at the centre, there was not an observable accumulation of Casp3+ cells within the colonies. Instead, the distribution of Casp3+ cells was random.

Only n=1 for this study was carried out as we only wished to confirm the biocompatibility of our scaffolds and that the sterilisation process was acceptable. However, the morphology of cells and positive detection of marker antigens continued to demonstrate good cell viability throughout the study.

4.3.6 Total colony sizes

The total colony size in scaffolds was measured by summing up the surface area of DAPI+ cells to provide an understanding of the total number of cells. Scaffolds were made in a mould with similar diameters to the well, such that they covered as much of the well as possible to ensure the scaffolds had captured most of the cells seeded. Figures below illustrate representative images of DAPI+ staining on each scaffold for 7 days *in vitro* in both culture conditions. DAPI was shown in white in the figure.

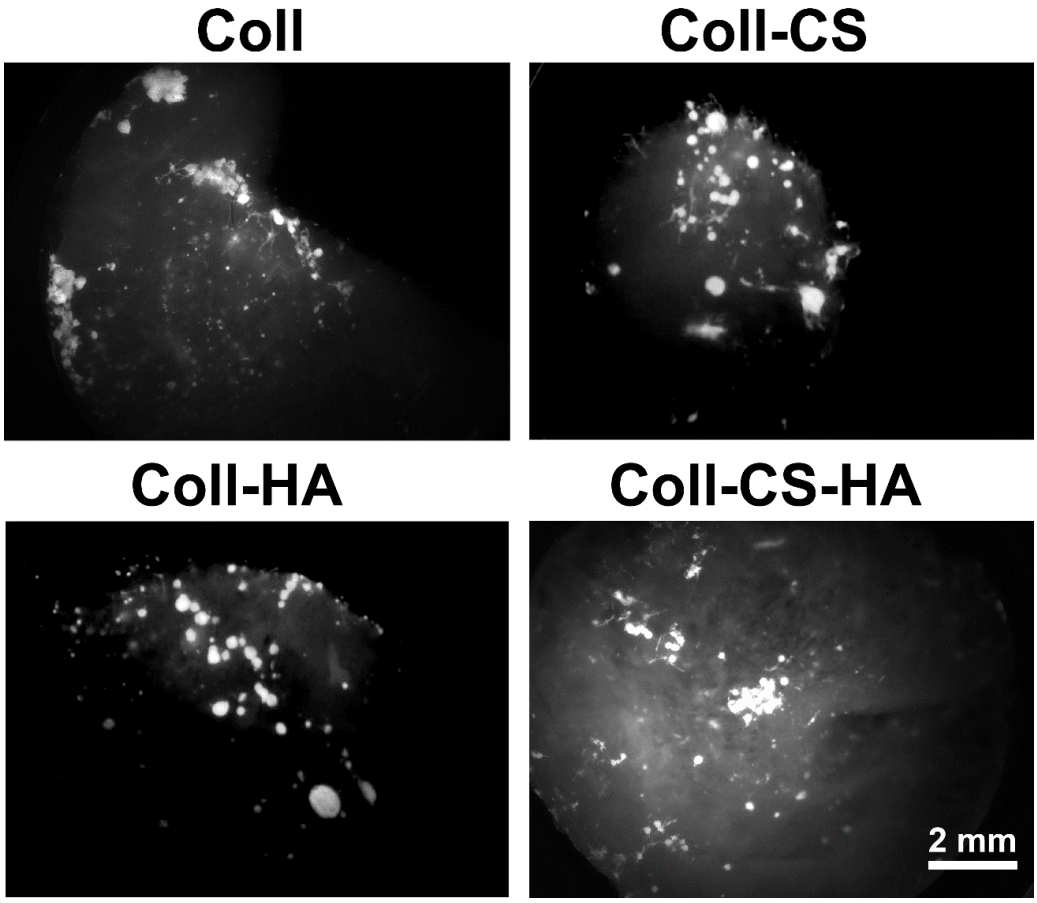


Figure 4.7 - DAPI images of Coll, Coll-CS, Coll-HA and Coll-CS-HA scaffolds cultured with NSCs for 7 days in proliferation conditions. The images were taken with the lowest magnification to illustrate an entire well for total colony size measurement. Coll scaffolds outline visible as background. Scale bar = 2 mm

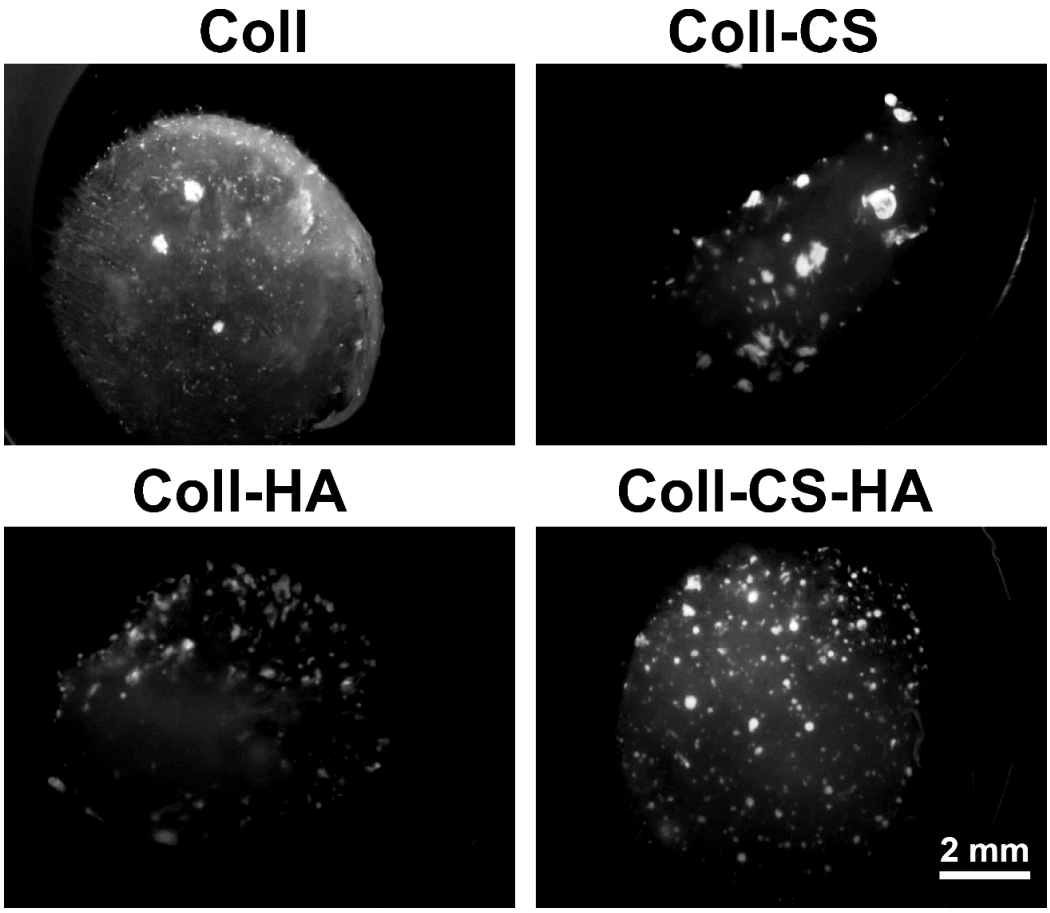


Figure 4.8 - DAPI images of Coll, Coll-CS, Coll-HA and Coll-CS-HA scaffolds cultured with NSCs for 7 days in differentiation conditions. The images were taken with the lowest magnification to illustrate an entire well for total colony size measurement. Coll scaffolds outline visible as background. Scale bar = 2 mm

We hypothesised that the average normalised surface area of colonies is proportional to the number of cells present in the scaffolds, since the amount of DAPI staining reflects the number of cell nuclei. Although the cells reside in a 3D environment with a scaffold thickness of 0.5 – 1 mm, at low magnification the thickness is less significant compared to the field of view. Therefore, we were able to capture all DAPI+ cells in a single image.

Figures 4.7 and 4.8 above illustrate typical colonies grown on scaffolds. The scaffolds were moved to a new plate such that cells attached to the original plate were not included in the analysis. The light grey regions detected showed the scaffold outlines, as collagen reflected minimal light. There was some shrinkage due to continuous washing during IHC. The Coll-CS shown in differentiation conditions had a smaller scaffold size due to the scaffold folding onto itself during staining. The Coll scaffold in differentiation condition also showed a high background but this was excluded while measuring the colony area.

At day 7 *in vitro* culture, dissociated NSCs seeded onto the scaffolds had grown in spherical colonies in both proliferation and differentiation conditions. The normalised surface areas on respective scaffolds are shown in figure 4.9. In general, proliferation conditions had larger colony sizes shown in table 4.5 below. These colonies did not aggregate on the surface or at the edge of the scaffolds. Instead, colonies were distributed homogeneously across the scaffolds, indicating random infiltration of NSCs. In addition, a number of very large colonies (up to 0.5 mm in diameter) were observed on Coll-CS and Coll-HA. On Coll-CS-HA however, colonies followed a more uniform diameter. This is an interesting result as this could be linked to the respective pore sizes.

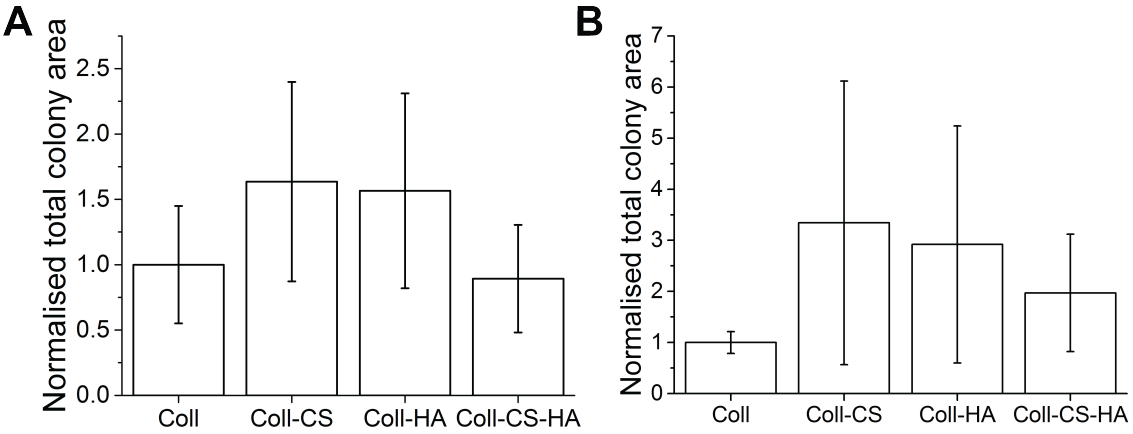


Figure 4.9 – Measurement of total colony surface area of DAPI+ cells on scaffolds in A) proliferation condition, and B) differentiation condition. The results of interlaced scaffolds were normalised to Coll and were not statistically significant from one another.

Table 4.5 – Average colony sizes of scaffolds measured by ImageJ in mm^2

Condition	Coll	Coll-CS	Coll-HA	Coll-CS-HA
7D Proliferation	2.98	4.88	4.67	2.64
7D Differentiation	0.45	1.51	1.31	0.89

Figure 4.9 illustrates the surface areas of all DAPI fluorescence on scaffolds of D7 proliferation and differentiation studies. Results were normalised to Coll to avoid variation from experiment to experiment. Although NSCs on scaffolds grew in 3D, the scaffolds were thin and discrepancies in the focal plane became negligible under the lowest magnification and thus were imaged in mass. The number of cells in the scaffolds was proportional to their surface area under an epi-fluorescence microscope. Therefore, the surface area of DAPI was a good reflection of the number of cells on a scaffold.

Under the proliferation condition shown in figure 4.9A, Coll-CS and Coll-HA scaffolds supported a roughly 50% increase in total colony area compared to Coll scaffolds. The increase was even more dramatic in differentiation condition in figure 4.9B, where the Coll-CS and Coll-HA scaffolds both almost tripled the colony area of Coll. Coll-CS-HA on the other hand, showed a doubled colony area compared to Coll in the differentiation

condition, but a similar area in the proliferation condition. However, due to the large standard deviations, the statistics of all colony areas were not determined to be significantly different from Coll alone.

4.3.7 Morphological analysis

To study the morphologies of colonies and individual cells, we imaged scaffolds from two conditions, D7 proliferation and D21 differentiation, under an SEM. SEM images are shown in figure 4.10 below.

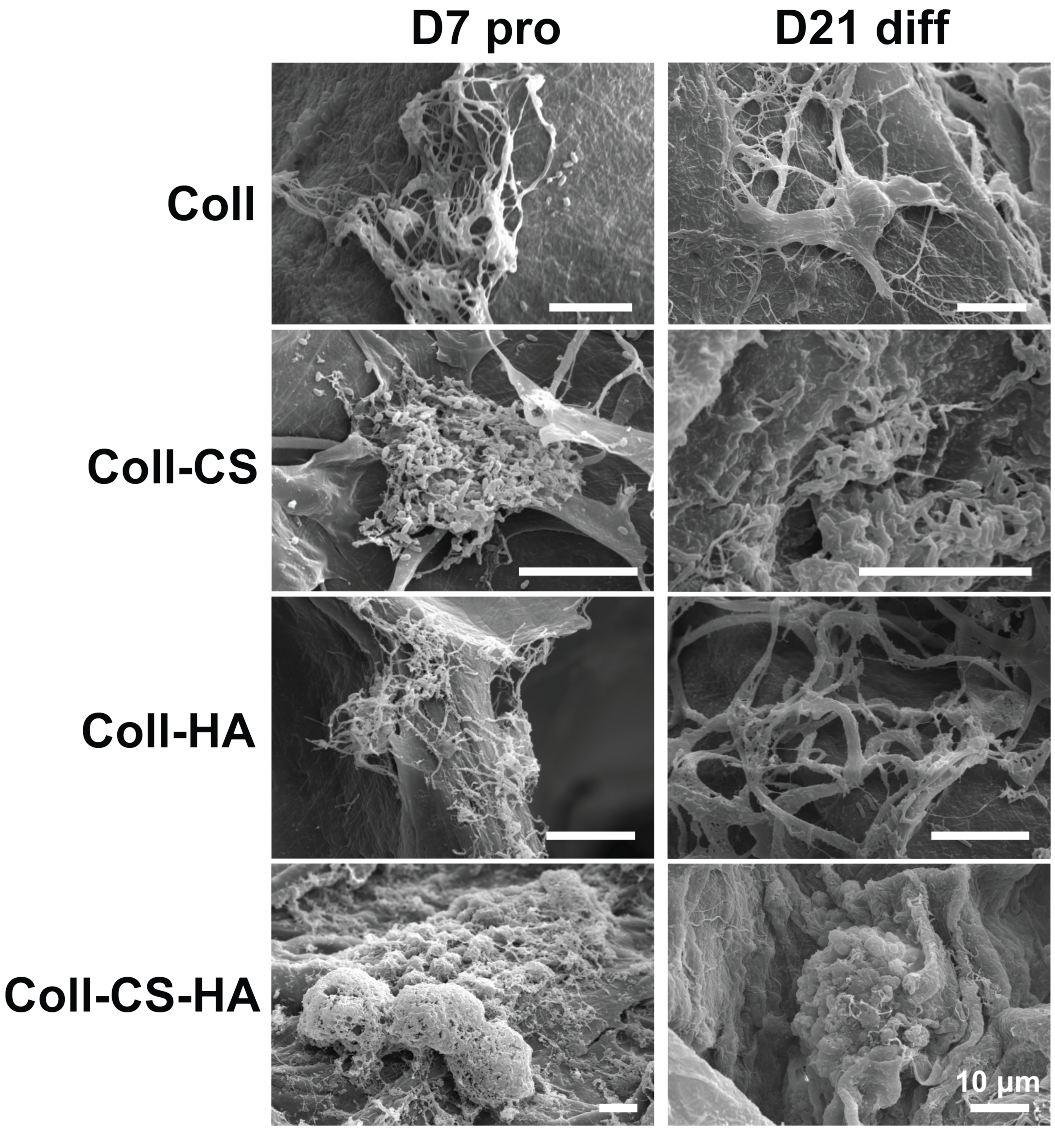


Figure 4.10 - SEM images of SVZ cells seeded onto Coll and interlaced scaffolds under D7 proliferation condition and D21 differentiation condition. Scale bars = 10 µm

Similar to the IHC results, SVZ NSCs seeded proliferated into dense colonies. SEM images showed that these cells were able to attach onto the scaffolds, indicating a good biocompatibility of the scaffolds. It is worth noticing that these scaffolds had been

thoroughly washed during IHC and dehydration, hence a strong bonding between cells and scaffolds is evident.

In terms of morphology, extensive branches were observed on most colonies. Coll scaffolds at the 21D differentiation condition for example, showed one multipolar cell adhering onto the walls of the scaffold. The star shape with four major branches resembled an astrocyte-like morphology. Similar branches were also obvious in other conditions. Most cells found exhibited either bi-polar or spherical morphology. Spherical cells with no branches can be seen in Coll-CS-HA on the 21D differentiation image, although similar morphology was common in other scaffolds and conditions.

Colonies were found to either develop into a spherical shape, forming a neurosphere-like colony, or to grow along the geography of the scaffolds. There was not a clear trend for these morphologies to be found on particular scaffolds or particular conditions observable. Both types of morphologies were found regularly throughout all scaffolds.

In addition to the branches, we also noticed a range of different cell diameters across the scaffolds. Cells on Coll and Coll-CS-HA in the 21D differentiation condition in the figure had considerably larger diameter than others, while cells found on Coll-CS at 7D had an average diameter of less than 1 μm, which was far smaller than our DAPI staining. It is common for cells to sometimes experience significant shrinkage during freeze-dying [6, 7]. As expected, similar shrinkage was not reflected in IHC results, which will be demonstrated later. The spheres shown in Coll-CS-HA in the 7D proliferation condition were indicative of colonies of cells rather than single cells.

4.3.8 Nestin expression

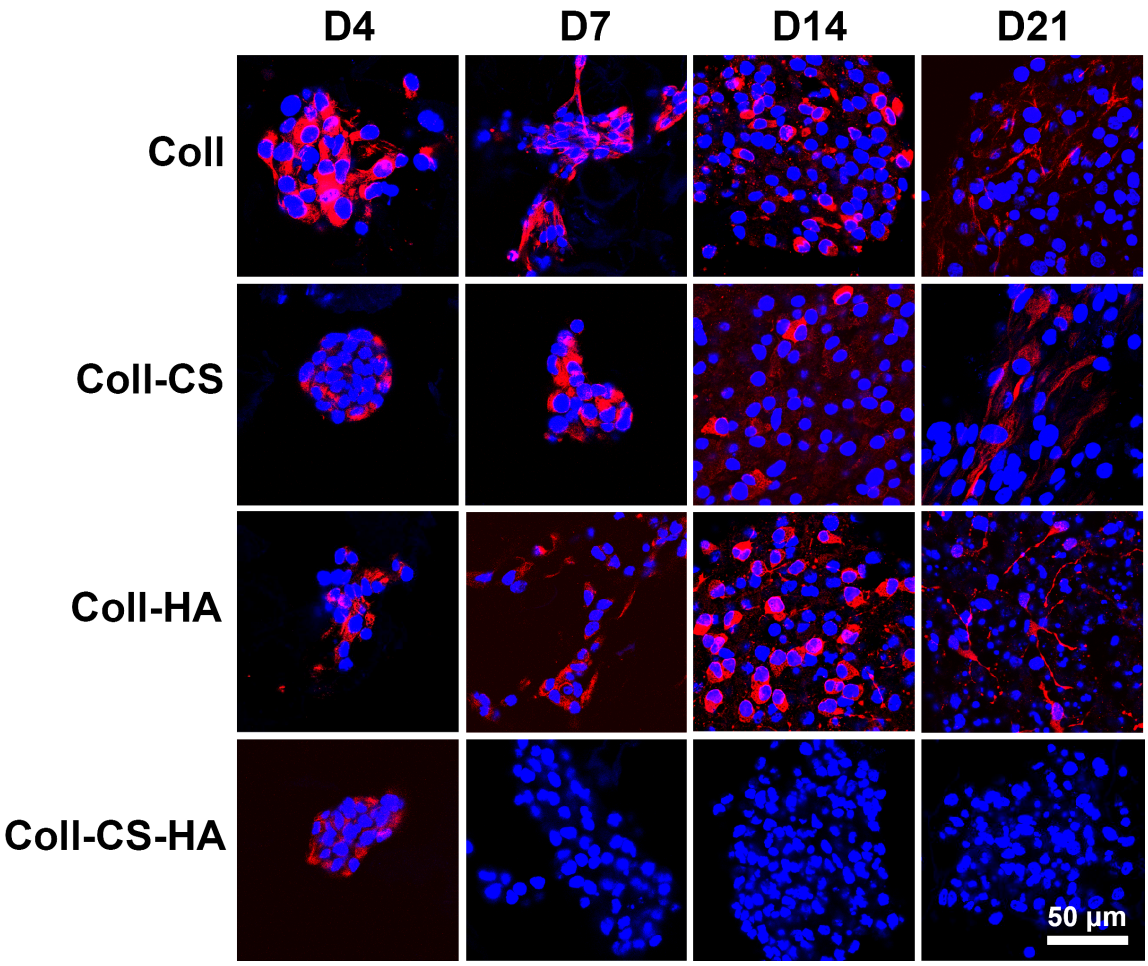


Figure 4.11 – Representative confocal images of nestin+ cells on Coll and interlaced scaffolds at day 4, 7, 14 and 21 after seeding in proliferation condition. Images were taken at 63x. Blue: DAPI and red: nestin. Scale bar = 50 µm

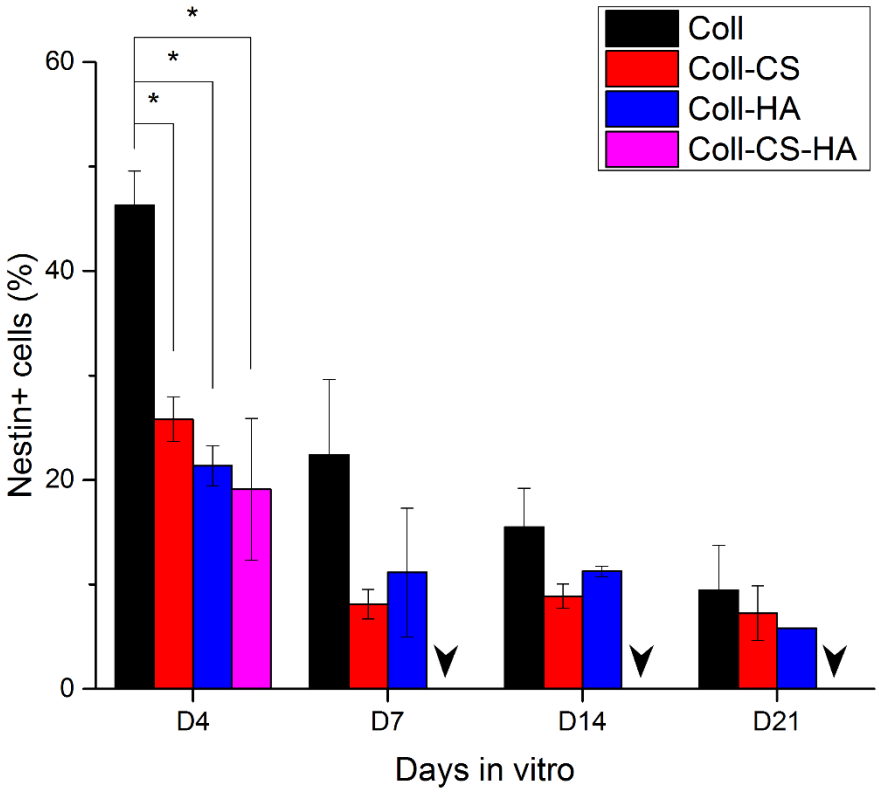


Figure 4.12 – Quantification of nestin+ expression as a percentage of DAPI in proliferation condition. Arrowheads point at Coll-CS-HA scaffolds in which nestin expression was non-detectable (*$p<0.05$)

Nestin is an intermediate filament protein that is expressed by immature stem cells [6]. It has been widely used to study NSCs from SVZ [9,10]. Hence, in this study, we used nestin to distinguish stem cells.

According to figure 4.12 above, over the 21-day period, the percentage of nestin+ cells gradually declined in all scaffolds. This implies that the NSCs seeded had started differentiating and therefore losing nestin expression. It is obvious that cells grown in

Coll-CS-HA scaffolds showed significantly less nestin+ expression compared to Coll throughout the 21-day period. After D4, no nestin+ cells could be found on Coll-CS-HA, suggesting a higher degree of differentiation. Even at day 4, nestin expression on Coll-CS-HA was lower compared to other scaffolds. Coll, on the other hand, retained the most nestin+ cell at D4, where almost half of the cells expressed nestin. Coll-CS and Coll-HA however, only had around 20%. At the other time points, the percentage of nestin+ cells on Coll was no longer statistically significantly higher than Coll-CS or Coll-HA. The final percentage of nestin+ cells at day 21 was around 10% for Coll, and 5-7% for Coll-CS and Coll-HA.

There were no obvious differences in nestin expression of Coll-CS and Coll-HA. Both showed a gradual decline of nestin+ expression during the culture period. From day 7 to day 21 however, the decline was less significant.

NSCs cultured in differentiation condition for 14 and 21 days were also labelled with nestin. However, very few cells were found to be nestin+ on all scaffolds. Thus, results were not imaged nor quantified due to the rarity.

4.3.8.1 Nestin and PHi3 co-expressions

In order to show the proliferative ability of stem cells, we co-stained nestin with anti-PHi3 antibodies on Coll, Coll-CS and Coll-HA in proliferation conditions at 14 and 21 day *in vitro*. PHi3 is an immunomarker for cells undergoing mitosis. It is a nuclear stain that colocalises with DAPI.

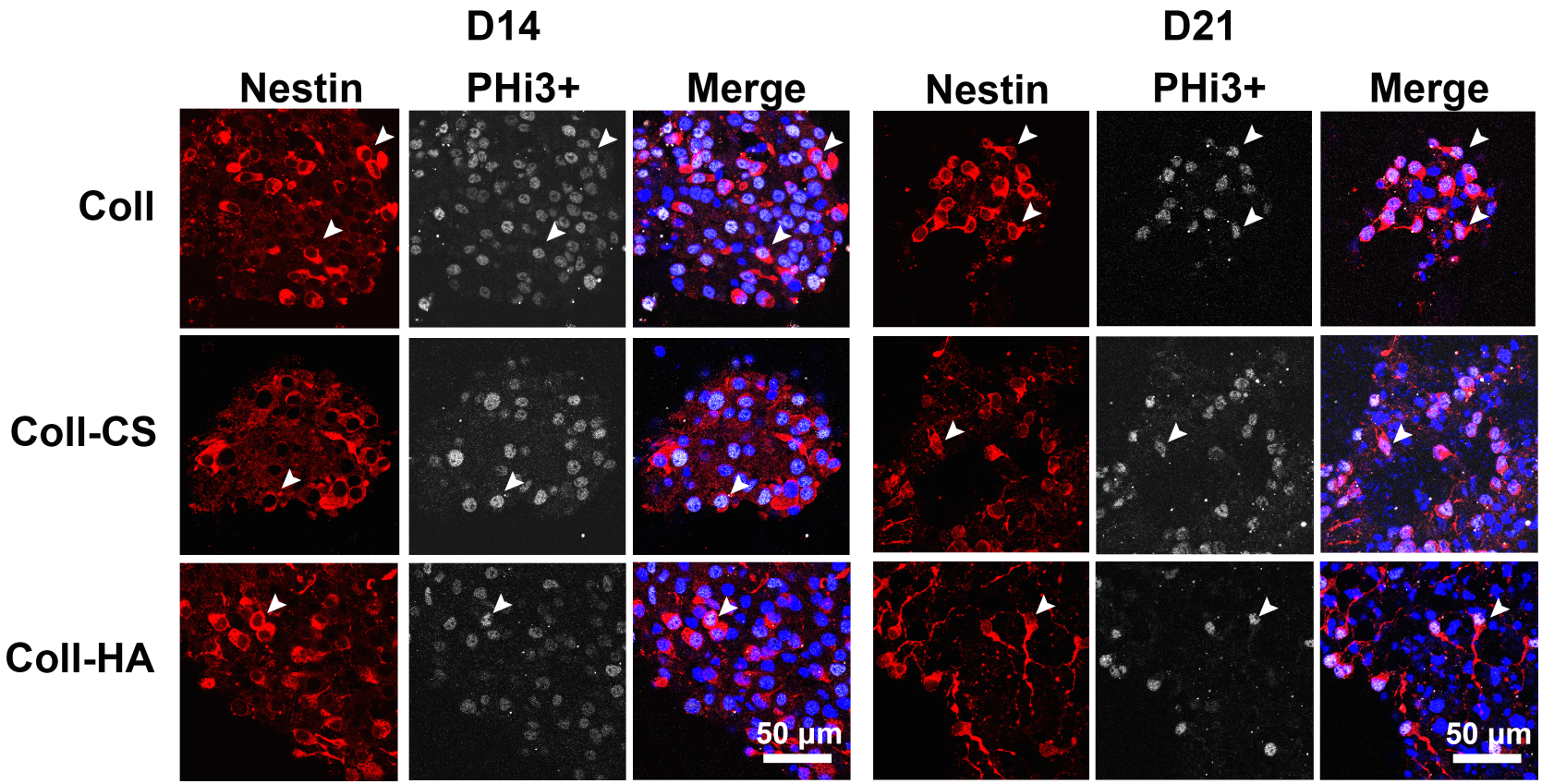


Figure 4.13 – Nestin and PHi3 co-labelling on Coll, Coll-CS and Coll-CS-HA scaffolds at day 14 and 21 after seeding in proliferation condition. White: PHi3+ and red: nestin+. White arrowheads point to co-labelled cells (n=1). Scale bars = 50 µm

Figure 4.13 above illustrates the co-staining of nestin with PHi3. Coll-CS-HA was not shown here because no nestin+ cells were found at D14 and D21. On other types of scaffolds, many cells were found to express both nestin and PHi3. Co-expression indicates a proliferating stem cell. There were also cells expressing only PHi3 or nestin. These were likely proliferating neuroblasts or astrocytes, or nestin+ cells that had started to differentiate.

A range of different PHi3 intensities was observed in figure 4.13. We could eliminate the effect of secondary antibodies based on the no primary control in figure 4.4. The range of intensities was likely due to NSCs at different stages of proliferation, as PHi3 only labels a small part of the proliferating cell cycle. However, it is still possible to distinguish some bright PHi3+ cells.

Comparing 14- and 21-day culture, a slight decrease of PHi3+ intensity towards a later stage can be observed, suggesting a more differentiated population. However, quantification was not taken as only one PHi3 staining was conducted.

Proliferation and differentiation are often conflicting phenomenon. Hence, if a cell starts differentiating, it would often lose its proliferating ability. On Coll, many DAPI+ cells expressed PHi3. This can be correlated with its high nestin+ expression, suggesting that a high proliferation might be responsible for a low differentiation on Coll. We therefore need to examine the differentiation of other cell types further.

4.3.9 GFAP expression

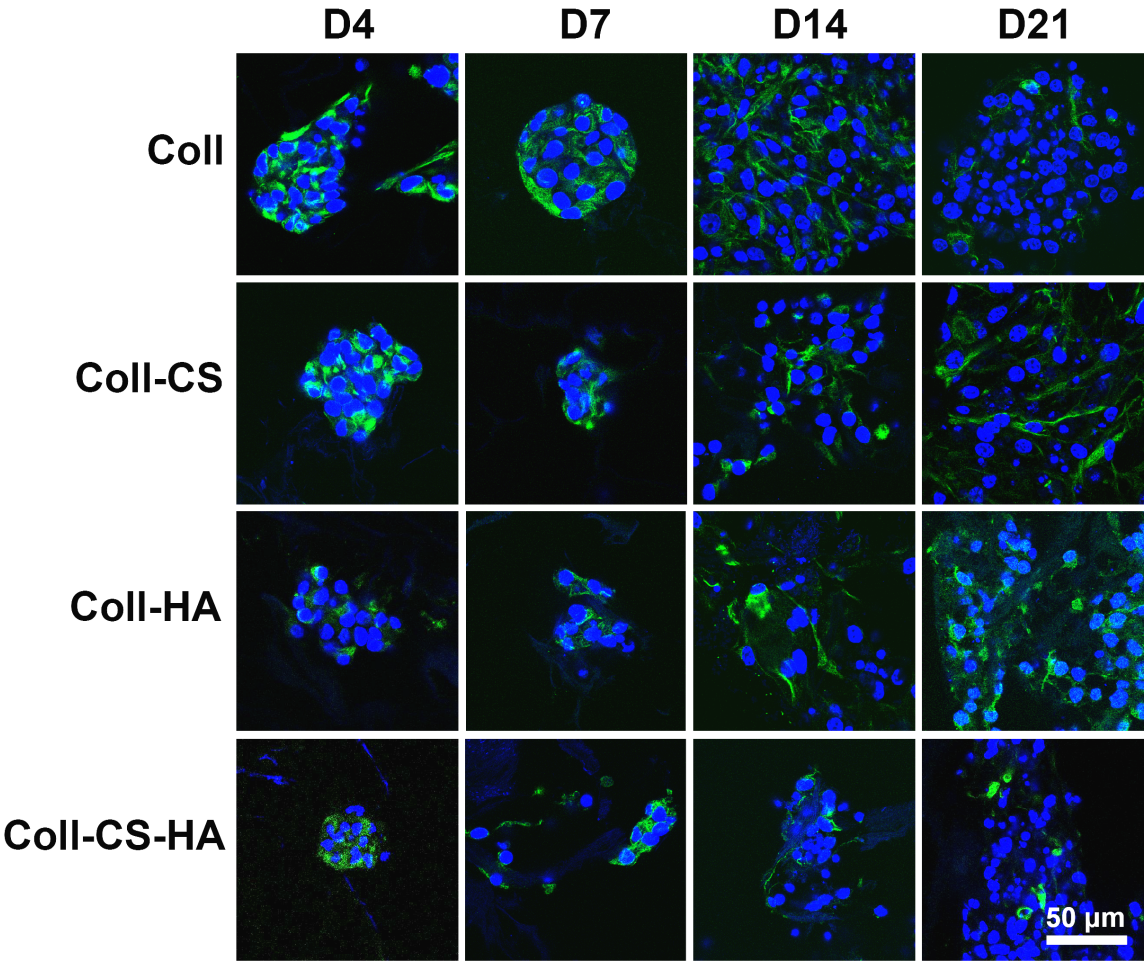


Figure 4.14 - Representative confocal images of GFAP+ cells on Coll and interlaced scaffolds at day 4, 7, 14 and 21 after seeding in proliferation condition. Images were taken at 63x. Blue: DAPI and green: GFAP. Scale bar = 50 µm

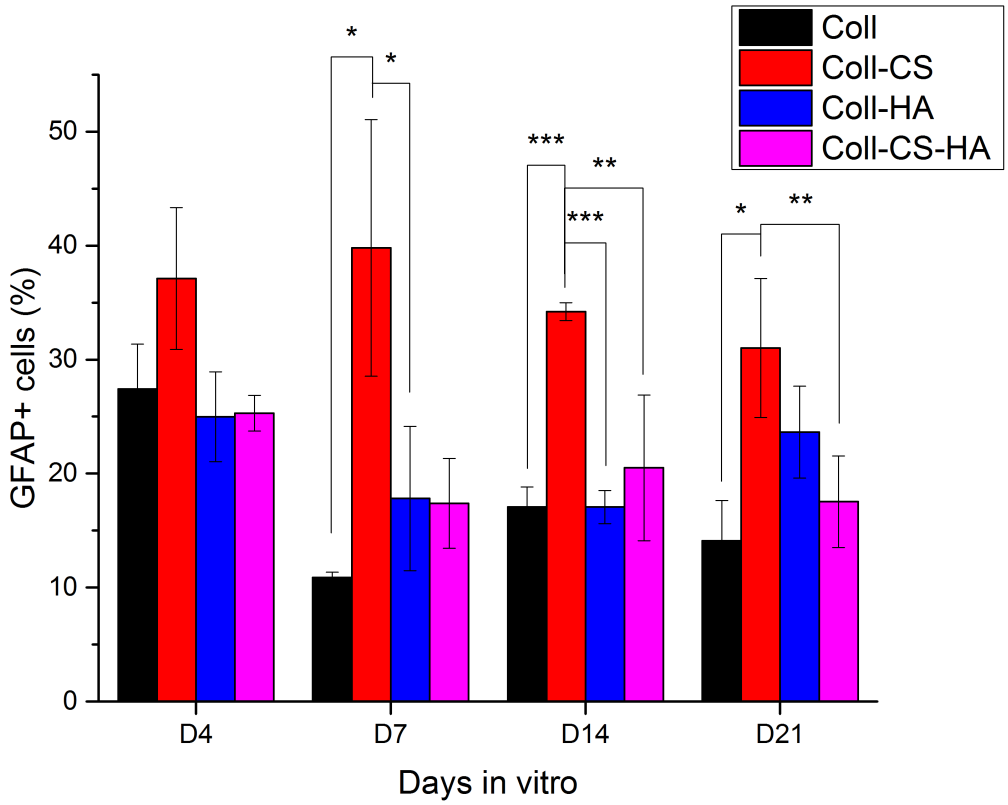


Figure 4.15 - Quantification of GFAP+ expression as a percentage of DAPI in proliferation condition. (*p<0.05, **p<0.005, ***p<0.0005)

To study the degree of astrocytic differentiation, GFAP+ expression was investigated. On D7, D14 and D21, the percentage of GFAP+ cells on Coll-CS showed a significant increase to 30-40% compared with other scaffolds which were associated with 10-20% GFAP+ cells. Coll-CS also increased the GFAP+ cells to 37% at D4, although this was not statistically significant from other scaffolds in which around 25% were GFAP+.

There were no obvious differences in the percent of GFAP+ cells between Coll, Coll-HA and Coll-CS-HA at specific time points. However, GFAP+ expressions at D4 seemed to

be slightly higher on these scaffolds compared to subsequent time points. The differences were not statistically significant.

Morphologies of GFAP+ cells revealed the presence of type 1 and type 2 astrocytes. In general, type 1 astrocytes have a fibroblast-like shape, and type 2 astrocytes have a multipolar morphology [11]. GFAP+ cells were found to exhibit both morphologies, and were consistent to those found by others [11]. As shown in figures 4.16 and 4.17 below, type 1 astrocytes were bi-polar and had two oppositely-aligned fibres spanning outwards, whereas type 2 astrocytes had multiple axons and tended to be more of a star-like shape. Z-stacks were taken to confirm their morphology in 3D. It is worth noticing that most of the GFAP+ cells on all scaffolds expressed type 1 morphology rather than type 2. Quantification was not taken as only few GFAP+ cells resembled type 2 astrocyte morphology.

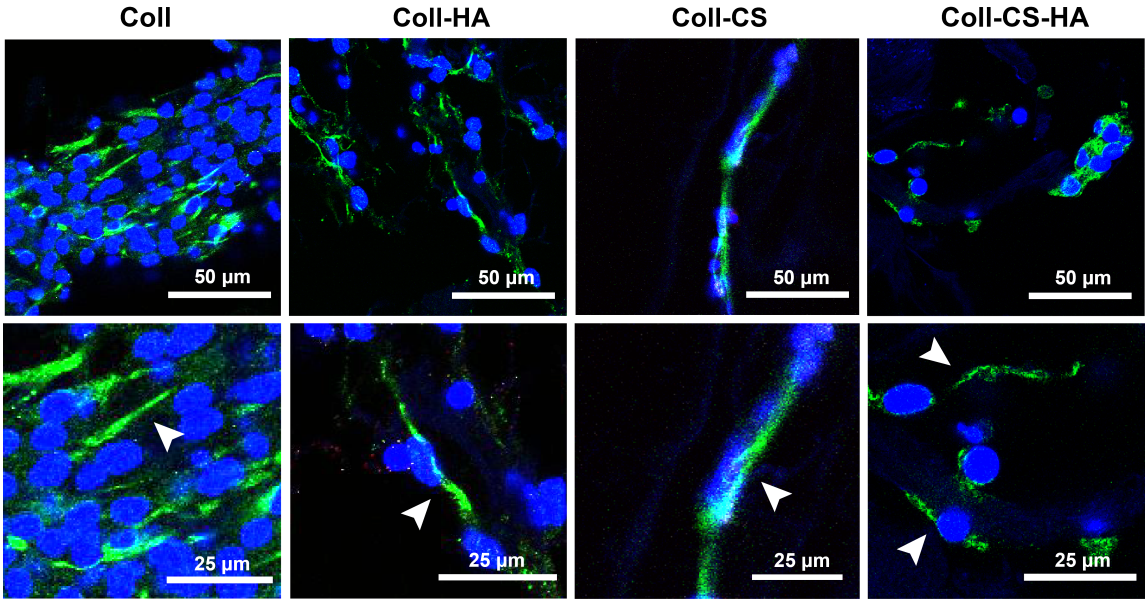


Figure 4.16 – GFAP+ cells expressing type 1 astrocyte morphology on Coll and interlaced scaffolds at day 7 after seeding in proliferation condition. Second row illustrates higher magnification images of GFAP+ cells. White arrowheads point at GFAP+ cells with type 1 astrocyte morphologies.

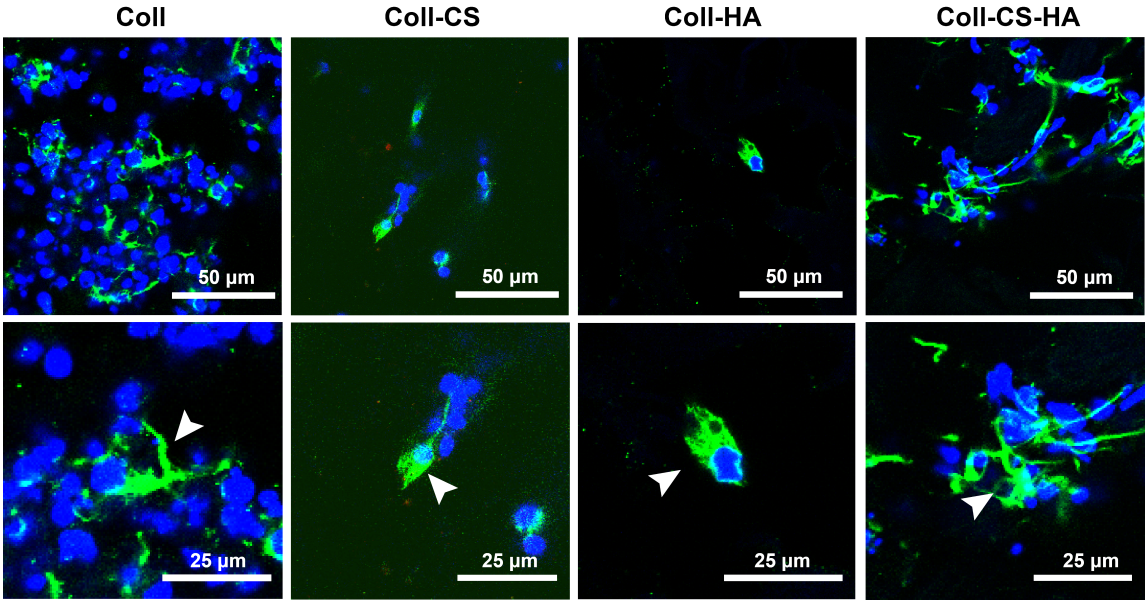


Figure 4.17 - GFAP+ cells expressing type 2 astrocyte morphology on Coll and interlaced scaffolds at day 7 after seeding in proliferation condition. Second row illustrates higher magnification images of GFAP+ cells. White arrowheads point at GFAP+ cells with type 2 astrocyte morphologies

4.3.10 Dcx and MAP2 expressions

Figure 4.18 below illustrates Dcx and MAP2 co-staining on all scaffolds in the proliferation condition. MAP2 was only used in day 14 and 21 because it is generally a marker for later stage neurons.

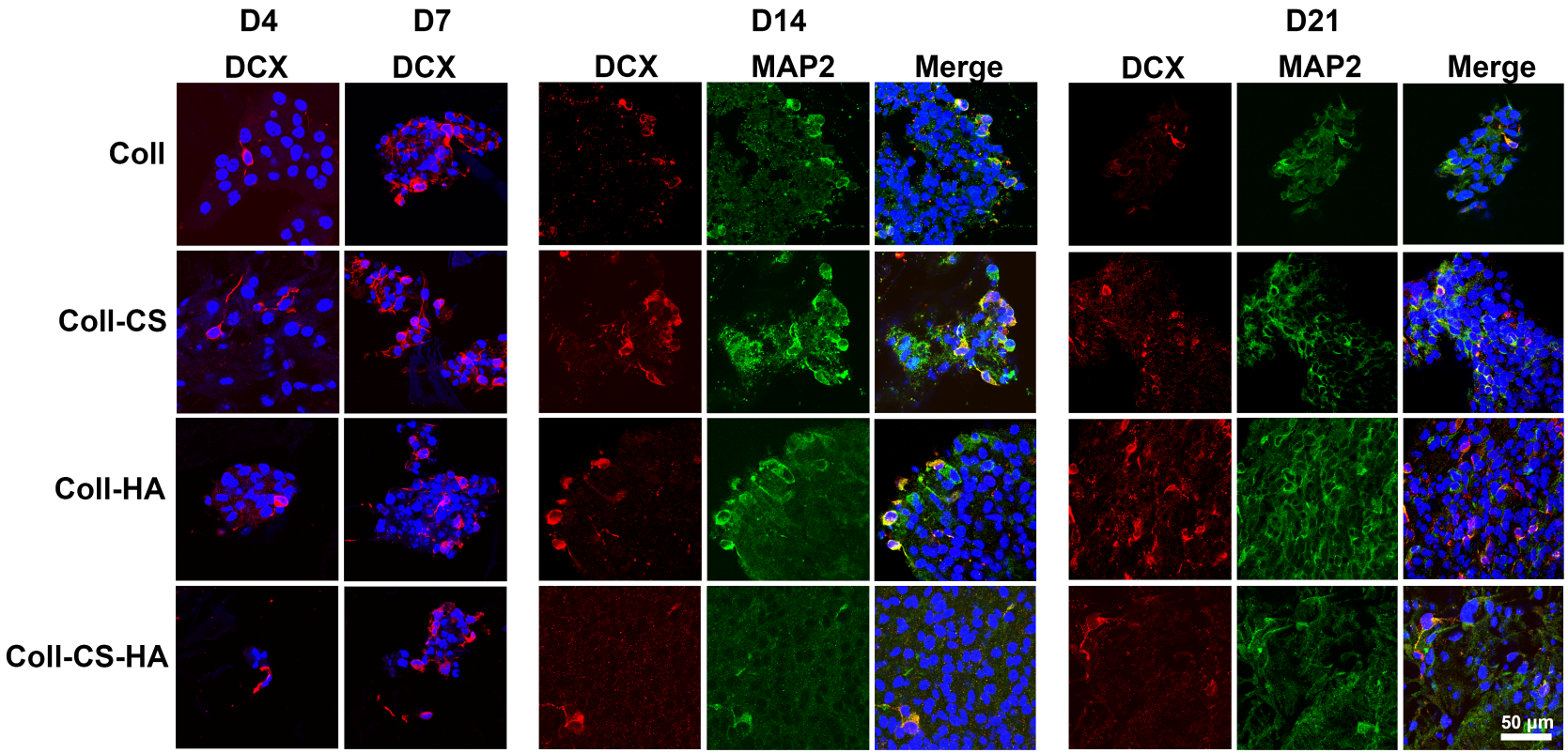


Figure 4.18 - Representative confocal images of Dcx+ cells on Coll and interlaced scaffolds at day 4 and 7, and Dcx+ and MAP2+ cells at 14 and 21 after seeding in proliferation condition. Images were taken at 63x. Blue: DAPI, green: MAP2 and red: Dcx. Scale bar = 50 µm

Compared to the control well in figure 4.2, morphologies of Dcx+ and MAP2+ cells on scaffolds remained similar to those cultured in media only, as they both showed typical bi-polar structure. Similar to figure 4.2, very few cells expressed multipolar morphologies or extended long processes or branches.

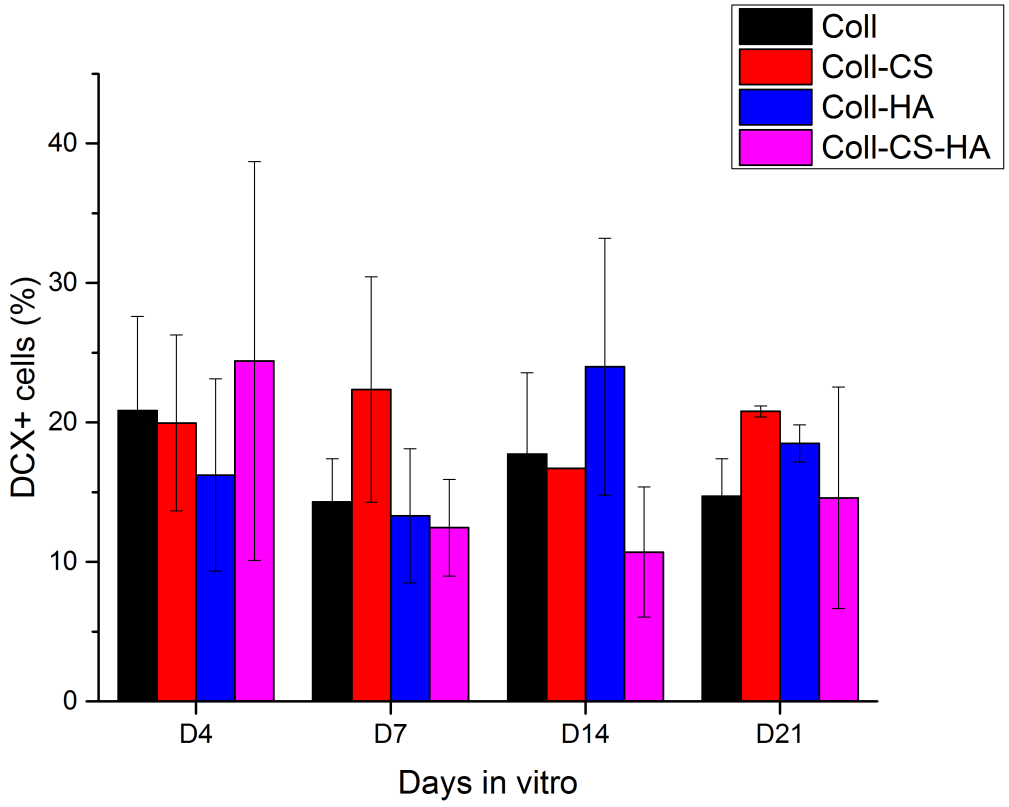


Figure 4.19 – Quantification of Dcx+ expression as a percentage of DAPI+ cells in proliferation condition. No significant differences were observed across the scaffolds (n=3)

Neuronal differentiation from NSCs was studied by two markers: Dcx, which labelled early neurons, and MAP2, which labelled more mature neurons. As a result, we concluded

that around 10-20% of the cells on all scaffolds were Dcx+. Interestingly, no significant differences were seen across the different scaffolds at specific time points. Throughout the 21-day period, the percentages did not decrease or increase significantly either, indicating that the amount of neuroblasts remained generally constant.

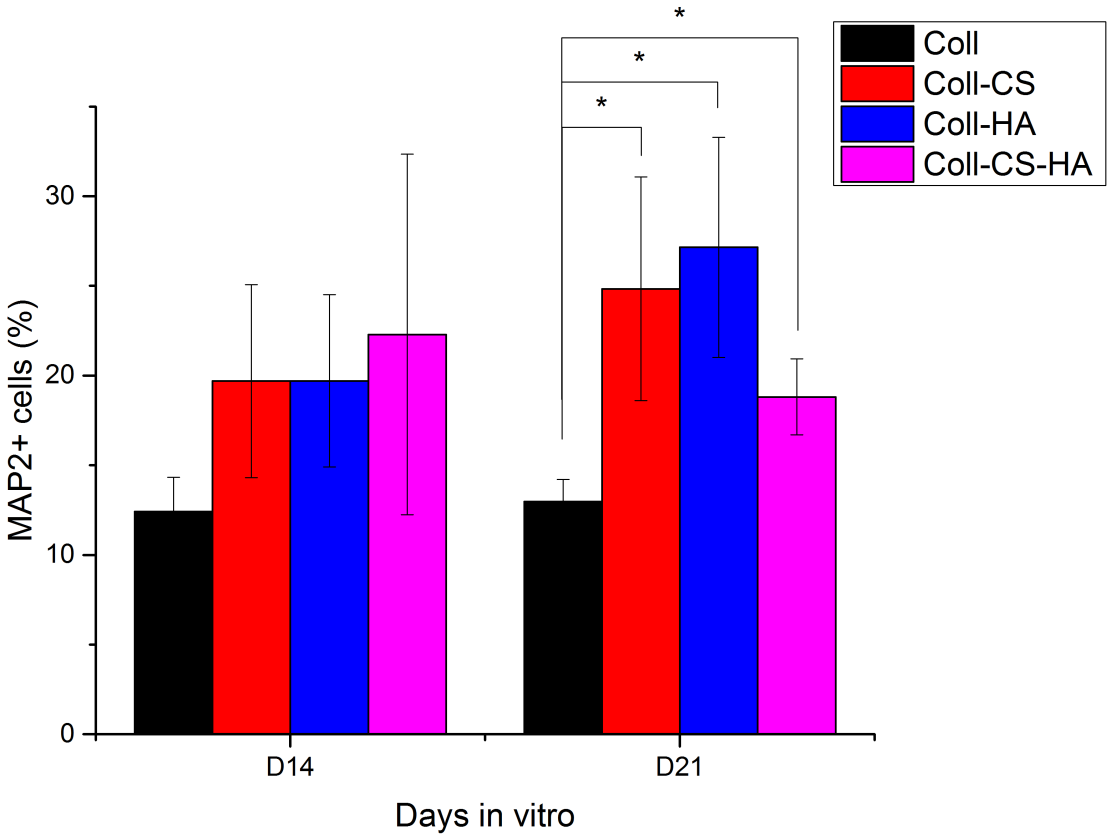


Figure 4.20 - Quantification of MAP2+ expression as a percentage of DAPI+ cells in proliferation condition. (*p<0.05)

Figure 4.20 above illustrates the quantification of MAP2+ cells on Coll and interlaced scaffolds in the proliferation condition. From day 14 to 21, there was a slight increase in the percentage of MAP2+ cells, which may indicate that more cells had matured and

expressed MAP2+. However, this is not shown in Coll-CS-HA. On Coll-CS and Coll-HA, the percentage of MAP2+ cells increased from 20% at D14 to around 25% at D21, compared to Coll which remained around 12%. Coll-CS-HA however, did not also show a significant increase between the two time points.

In day 21, there were significant increases of MAP2+ cells in the interlaced scaffolds compared to Coll. Such differences did not reach statistical significance at day 14, although similar quantitative increases are obvious. Enhancement in MAP2+ differentiation was similar in Coll-CS and Coll-HA. However, the addition of CS and HA did not induce a compound effect.

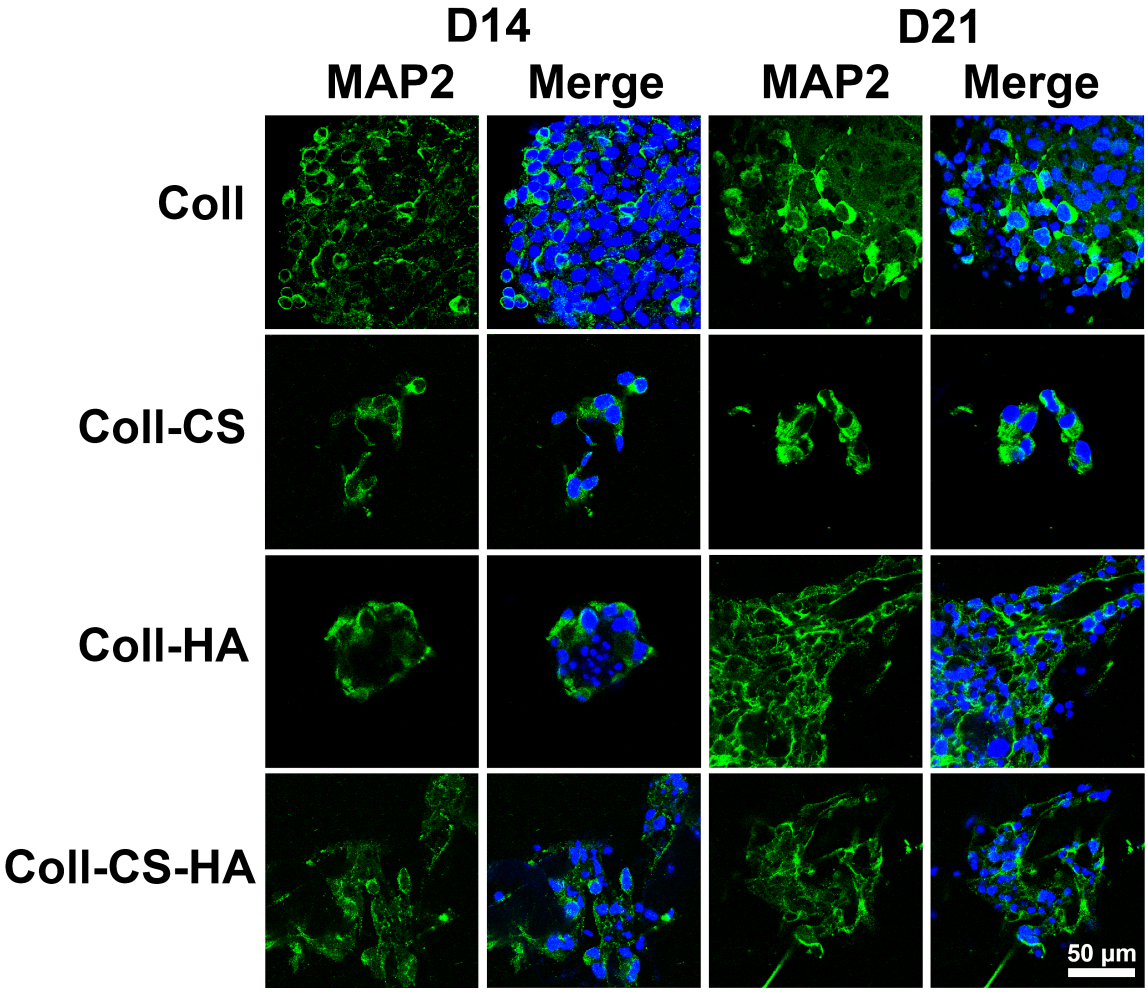


Figure 4.21 - Representative confocal images of MAP2+ cells at 14 and 21 after seeding in differentiation condition. Images were taken at 63x. Blue: DAPI and green: MAP2. Scale bar = 50 µm

MAP2+ expression was also found on all scaffolds in differentiation conditions at 14 and 21 day post seeding. Again, typical neurites were shown by MAP2, indicating a mixture of bi- and multipolar morphology. Long and extending neurites, both within the colonies or extending outwards, were more obvious in the differentiation than in the proliferation.

Apart from these, MAP2+ cells in differentiation conditions generally resembled similar morphologies to those in proliferation conditions.

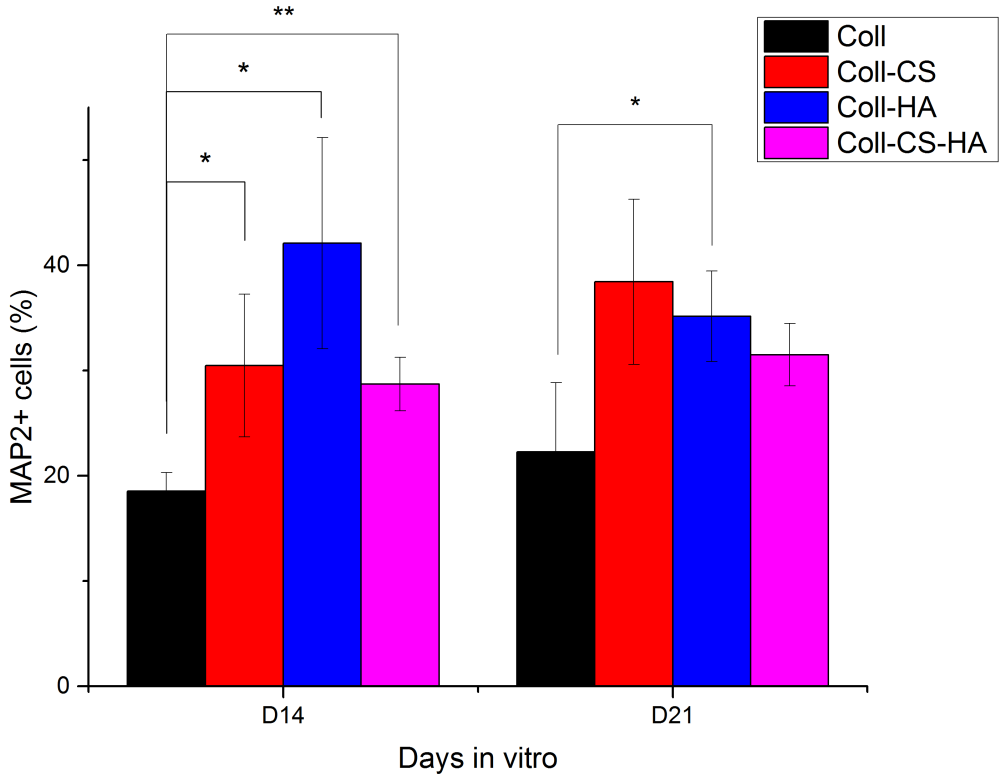


Figure 4.22 - Quantification of MAP2+ expression as a percentage of DAPI+ cells in the differentiation condition. (*p<0.05, **p<0.005)

Similar to the proliferation condition, in the differentiation condition, interlaced scaffolds led to an increase in MAP2+ labelling from around 20% in Coll to 30-40% on day 14 and day 21. On day 21, only Coll-HA showed a statistical significant increase to Coll. Although the differences were not statistically significant on other scaffolds, both Coll-

CS and Coll-CS-HA showed increases in their means. ($p=0.0523$ for Coll-CS:Coll and $p=0.09$ for Coll-CS-HA:Coll).

Comparing the two MAP2 quantifications in figures 4.20 and figure 4.22, MAP2+ cells were more common in the differentiation condition. MAP2+ cells increased from 12% to 20% in Coll, and from 20-25% to 30-40% in the interlaced scaffolds. Within each condition, there were no statistical differences between Coll-CS, Coll-HA, and Coll-CS-HA, although the average of the latter was smaller.

4.3.10.1 MAP2 and VGLUT1 co-expressions

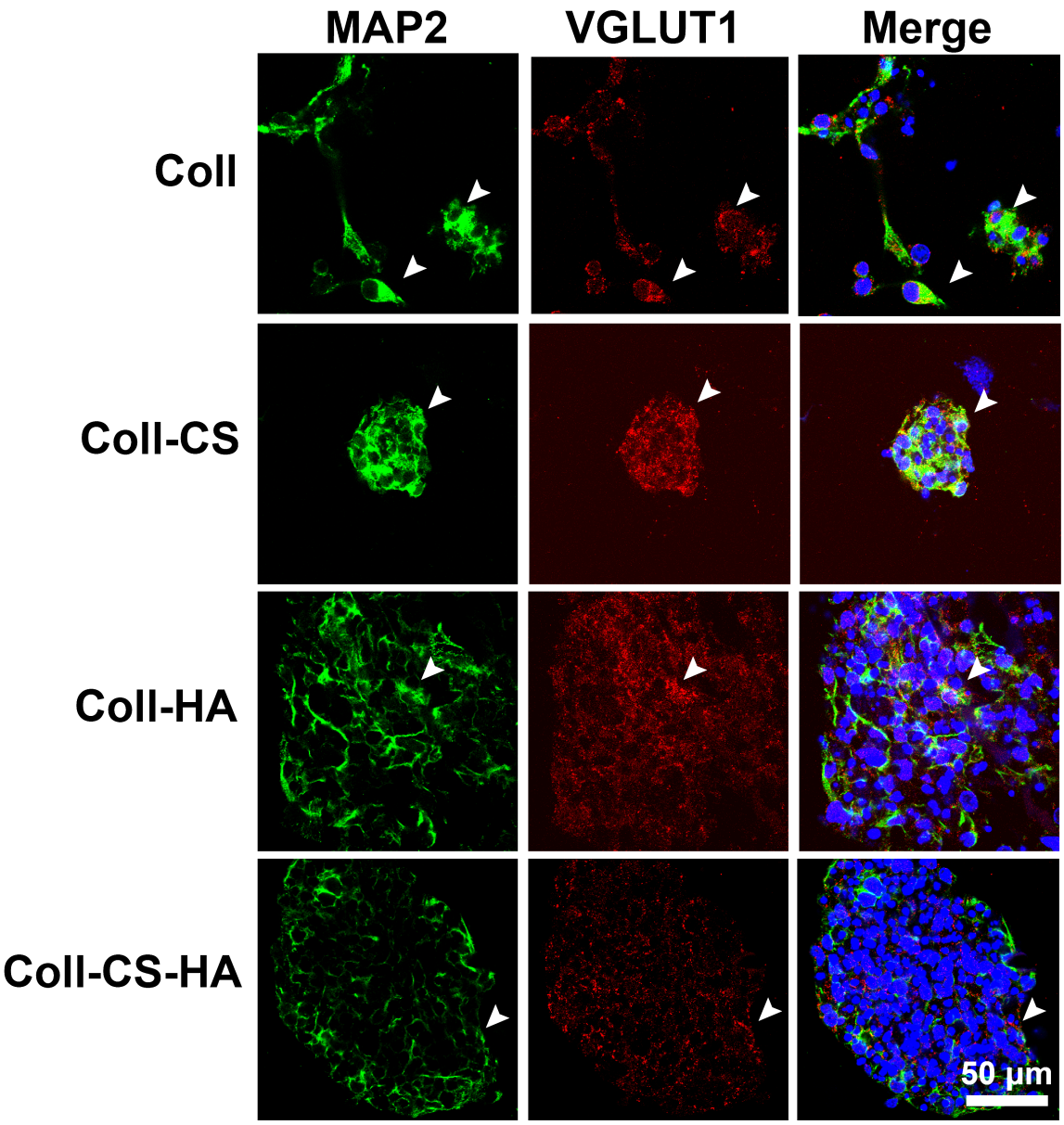


Figure 4.23 – MAP2 and VGLUT1 staining of 21-day NSC cultured in differentiation condition. Green: MAP2, red: VGLUT1, blue: DAPI. White arrowheads point at MAP2 and VGLUT1 co-localisation. Scale bar = 50 µm

Figure 4.23 above illustrates VGLUT1 expression of MAP2+ cells in a 21-day differentiation culture. VGLUT1 labels cells that were able to produce vascular glutamate transporters. It is also used to label glutamatergic neurons. Overall, the number of MAP2+/VGLUT1+ cells were low. There were even less VGLUT1+ cells in the 14-day differentiation study and the 14- and 21-day proliferation studies. It is worth noticing that the figure above is not a representative figure for VGLUT1/MAP2 co-labelling in the scaffolds. Figure 4.24 below illustrate that most MAP2+ cells expressed no VGLUT1. Notably, a faint VGLUT1 expression is shown in the Coll-HA image. However, the staining did not overlap with MAP2 and therefore should be regarded as a false positive.

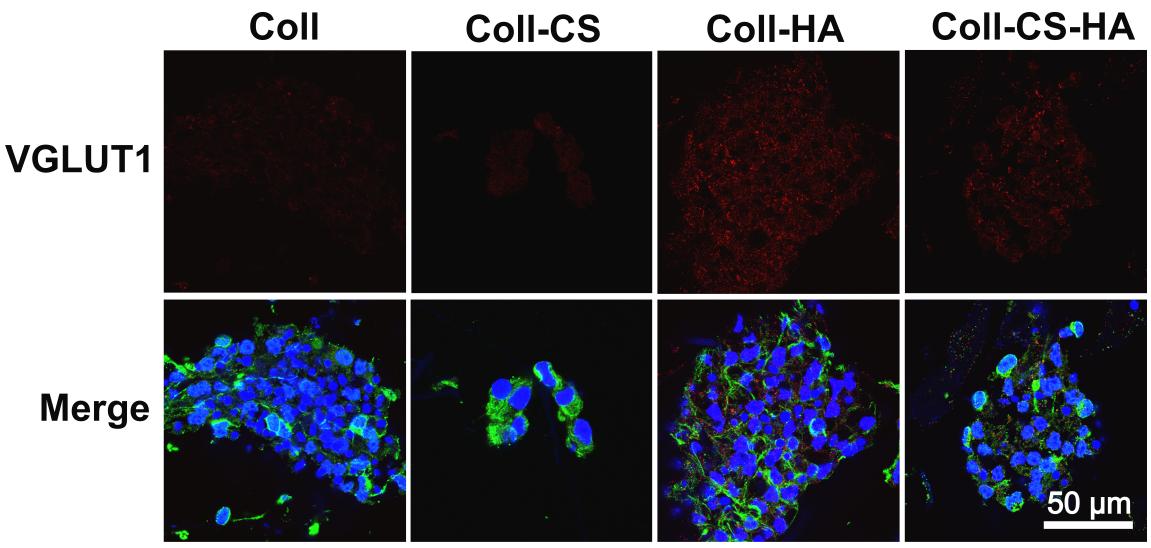


Figure 4.24 – Representative images of MAP2 and VGLUT1 staining of 21-day NSC cultured in differentiation condition. Green: MAP2, red: VGLUT1, blue: DAPI. Scale bar = 50 µm

4.3.11 Migration studies

4.3.11.1 Neuroblast spheroids

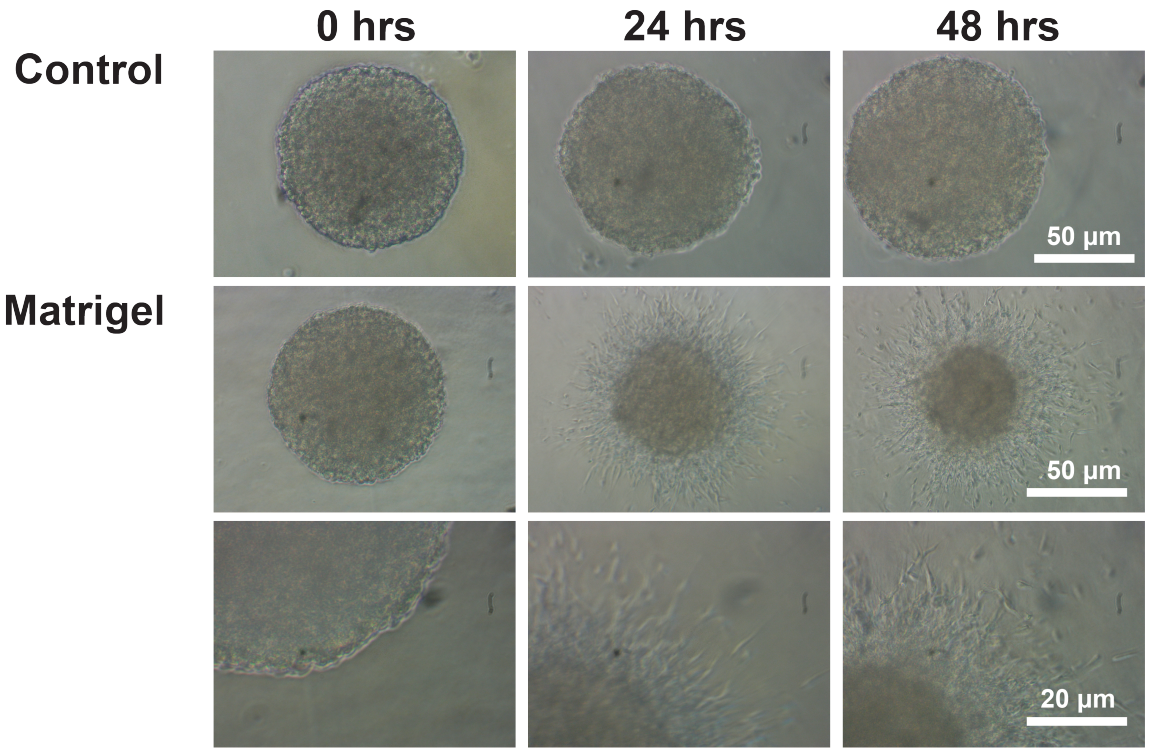


Figure 4.25 – Migration of neuroblasts from spheroids with matrigel and without matrigel (control group) at 0, 24 and 48 hours.

Figure 4.25 above illustrates the migration capability of spheroids in a matrigel. At 0, 24 and 48 hours after placing into media or matrigel, spheroids were observed under a light microscope. At 0 hour, spheroids appeared to have a defined edge in both conditions. In the control condition, spheroids remained spherical throughout the experiment. In matrigel however, a significant amount of migration has been observed by 24 hours. Higher magnification images showed these individual cells had migrated outside the spheroids and exhibited a bi-polar morphology similar to that of a migratory neuroblast.

Cells at 24 hours tend to align outwards. Meanwhile, the size of spheroids had shrunk considerably, as cells have left the colony. By 48 hours, the shrinkage was more obvious, and cells were oriented in more random directions. This indicates that these cells have fully migrated out of the colony, and started to randomly migrate. The figure showed that the spheroids were a good tool to study the effects of the environment on the migration of neuroblasts.

4.3.11.2 Migrations on scaffolds

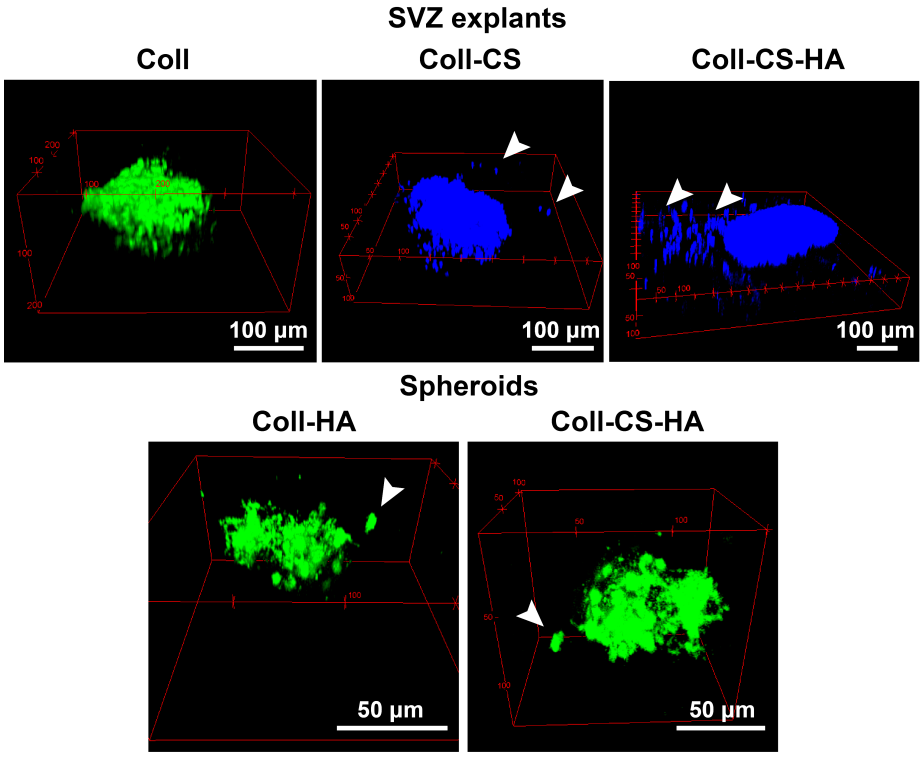


Figure 4.26 - Z-stack images reconstructed into 3D representations showing SVZ explants and neuroblast spheroids on scaffolds 48 hours after seeding. Arrowheads point at possible migrating cells. Green: GFP and blue: NucBlue

Figure 4.26 illustrates the migration of SVZ explants and neuroblast spheroids on scaffolds. The green labelling originated from GFP in Gad65-GFP mice. Adhesion of explants and spheroids proved to be more difficult than single cells, as many were washed away during fixing and IHC. GFP and NucBlue therefore, eliminated the need for immunocytochemistry and allowed better retaining of explants and spheroids. Having said that, we were only able to occasionally obtained images of explants or spheroids that remained on the scaffolds. Hence, although many experiments were carried out, only the above images were obtained successfully.

Migratory cells were occasionally observable on scaffolds, as shown by white arrowheads in figure 4.25. Explants on Coll-CS-HA here showed a large number of NucBlue+ cells around the explants, likely due to migrations. There were few horizontal migrations, suggesting poor attachment to the scaffolds. On Coll, there were limited cells found around the explant. The results however, were inclusive due to the lack of replicates.

4.4 Discussion

This chapter studies the biological responses of SVZ NSCs to Coll and Coll-GAG interlaced scaffolds. As a result, the interlaced scaffold proved to encourage higher NSC differentiation compared to Coll, as evidenced by a reduction in nestin expression and enhancement in GFAP and MAP2 expressions. *In vitro* studies are imperative in both the understanding the basic biological properties of our scaffolds, and future animal studies due to regulations on medical device development. Thus, this chapter provides a general analysis of *in vitro* cell behaviours of the scaffolds.

Our control in this study was Coll rather than neurospheres because we believe that a scaffold is essential in the tissue engineering therapy. To date, many researchers have attempted treatment of TBIs with 3D cultured cells from the SVZ. SVZ explants and neurosphere suspensions were among the most popular approaches. However, explant transplantations often lead to limited migration and cell survival [12-14] and neurosphere suspensions often lead to low survival rates [15]. Furthermore, most of these studies promoted glial differentiation rather than the desired neuronal differentiation.

In this study, we investigated NSCs differentiating into astrocytic and neuronal lineage. Oligodendrocytes were not studied into details because we believe that astrocytes and neurons are more crucial to consider in injury responses. Enhancing neuronal differentiation could potentially lead to functional recovery, and suppressing astrocytic differentiation would reduce glial scar formation by reducing CSPG production [16-18].

Similarly, most TBI studies also focused on neuronal and astrocytic responses. Hence, although oligodendrocytes are an important glial cell within the brain, we prioritised investigating astrocytic and neuronal differentiations.

Degeneration of the CNS after brain injuries includes both acute stages and chronic stages. During the acute stage, which lasts a few days after the injury, acute neuronal death takes place as severely damaged neurons undergo apoptosis and necrosis [19, 20]. It also triggers activation of astrocytes and microglia and other immune responses including macrophage and lymphocyte infiltrating into the injured brain lesions. In the chronic stage, which may last for a person's lifetime, continuous neurodegeneration may take place and lead to dementia and other neurodegenerative diseases [21]. While designing a tissue engineering therapy, therefore, it was imperative to consider how scaffolds would react and assist recovery in both stages. We designed *in vitro* cell studies aimed to investigate cellular responses over time. We have chosen a 21-day culture based on the hypothesis that our scaffolds would support mid to long term cell growth.

4.4.1 Cell seeding

In this chapter, addition of NSCs with media in one step into a 48 well plate was determined to be the best approach for cell seeding. This was due to a combination of reasons.

Firstly, cell culture on a 48 well plate allowed more conditions per experiment compared to a 24 or 12 well plate. It also allowed enough colonies to form per well. Compared to a

96 well plate, it was technically easier to conduct IHC on 48 well plates, as smaller scaffolds were readily aspirated during pipetting.

Also, in order to ensure that most of the cells would fall onto the scaffolds, scaffolds with the same diameter as the wells were used. This avoided cells growing on the walls of the plates, or in between the bottom of the wells and the scaffolds. In addition, upon fixing, scaffolds were removed from the culture plate and placed in a new plate. This further avoided any cells growing independently of the scaffolds to be imaged and analysed.

Although injecting cells into the scaffolds would allow more cells to be trapped in the scaffolds, this created a few problems. Firstly, injection could distort the pore structure, thereby creating larger pores than those originally designed. Secondly, accumulation of cells within one specific region would render diffusion of media and GFs more difficult. Hence, we decided that a large, thin scaffold seeded by a one-off addition of cells and media in a 48 well plate to be our seeding approach.

4.4.2 SVZ NSCs

Tertiary neurospheres were chosen based on the previous experience of our laboratory and literature. By the tertiary stage, most of the debris found in primary neurospheres and resulting from dissection, including tissue and unwanted cells, has been eliminated. Also, the SVZ cells still remained stem-like, evidenced by our nestin labelling at D0. At D7, the cells were able to express MAP2 and Dcx, which were indicative of mature and early neuronal differentiation. This result indicates that the cells dissociated from the SVZ were

indeed stem cells that could differentiate into the neuronal lineage. Furthermore, culture of NSCs on Coll showed their capability to express Dcx, MAP2, GFAP and Olig2, which resembles the natural cell population within the brain. Hence, we believe that NSCs from the SVZ were a reliable and consistent cell source to study cell behaviours on our scaffolds.

4.4.3 Colony size measurement

The measurement of total colony sizes on scaffolds revealed interesting results. It suggested that Coll-CS and Coll-HA enhanced the colony sizes in both proliferation condition and differentiation conditions. Interestingly, addition of both CS and HA in the proliferation condition did not lead to a compound effect. This was likely due to the physical constraint of the pore structure. As discussed in the previous chapter, addition of CS and HA led to formation of secondary pores and branches within the primary Coll network. These newly-form branches and walls could had impeded the growth of colonies after exceeding the size of the pores. While the outer cells met the walls of Coll-CS-HA, they reacted correspondingly to the surface receptors of the scaffolds. This could lead to earlier differentiation and thus reduced proliferation. This hypothesis is supported by a drastic reduction in the percent of nestin+ cells on Coll-CS-HA. After 4 days, colonies had grown into sizes that filled the wall structure of Coll-CS-HA, and started to differentiate, thereby losing nestin+ expression.

It is worth noting that the total colony size measured may be proportional to the total cell number on a scaffold, but not necessarily linked to proliferation. This was because many

other factors could contribute to a higher cell number, including cell attachment, diffusion, or technical issues including cell attachment onto the plates. Thus, this measurement only gives a rough understanding of approximately how many cells could be expected to obtain on different scaffolds.

Coll had the lowest colony size in the differentiation condition, but a considerably large colony size in the proliferation condition. This observation matches our hypothesis that Coll by itself may not be able to encourage proliferation. In the proliferation condition, cells have grown into considerably large colonies mainly because of the GFs. Even though the environment might not encourage proliferation, the free-floating GFs provided enough cues for NSCs to proliferate. In the differentiation condition, however, GFs were no longer present, and cells had to react based on its surrounding environment, where Coll did not support NSC proliferation. Therefore, the total colony size on Coll was much smaller than the Coll-GAGs in the differentiation condition.

3D culture often encounters problems on infiltration into scaffolds. Pore sizes and pore connectivity limit the diffusion of cells into the scaffolds. The pore size and side branches of Coll-CS-HA was suspected to inhibit cell diffusion. In such a scaffold, one should expect cells to stay at the edge and top or bottom surface. DAPI images however, showed the opposite, colonies on Coll-CS-HA showed a homogeneous distribution. Higher magnification images also indicated cells lying in different focal planes. Hence, this result suggests that the pore structure of Coll-CS-HA did not impede cell infiltrations.

Higher magnification images of the colonies showed that these colonies could react to the environment, as evidenced by DAPI+ cells branching outward from the centre of the

colonies. This could be due to either proliferation or migration. Due to the physical constraint of pore structure, proliferation of NSCs filled the open-pore structure and thus looked like branches. Also, migration of neuroblasts towards the environment may also lead to the formation of branch-like colony structure.

4.4.4 Morphologies of colonies and individual NSCs

Our results clearly showed that NSCs were able to form colonies in culture and on scaffolds. Upon removal of GFs, NSCs remained proliferative and formed large colonies. Compared to scaffold-free cultures, the colonies on scaffolds tended to be more randomly shaped. Also, low levels of Casp3 staining indicated healthy colonies on all scaffolds, suggesting that the NSCs were able to respond to the scaffolds, and the scaffolds provided proper environments for them to survive and proliferate.

Morphological studies of individual NSCs using IHC within a 3D culture proved to be more difficult than 2D, as neurites and axons often did not lie on the same focal plane of the cell bodies, leading to a variety of labelling issues. For example, axons were often absent in many cytoplasmic stainings due to their branches lying on a different focal plane and were thus not detected by individual optical sections taken with the confocal microscopy. In addition, the sizes of DAPI staining of cells was variable. Apart from some cell death, this was also likely due to cell nuclei residing in a 3D environment. Although z-stacks images could be taken to fully reflect their morphologies, manual 3D quantifications were technically very difficult. Hence, while interpreting and analysing

images, we need to consider that the IHC images shown in this thesis may not be exact representations of cell morphologies.

Significant shrinkage was regularly found in SEM imaging due to nucleating ice crystals often disrupt the cell structure while freezing the samples. In future, this can be avoided by successive treatment of glutaraldehyde, OsO_4, tannic acid and uranyl acetate solutions [7]. However, although SEM provided much better resolution and magnification that revealed more detailed cell-scaffold interactions, it was further limited by two factors. Firstly, it was difficult to distinguish cell types with SEM. Since IHC was based on fluorescence of antibodies, it was impossible to utilise the same approach to determine cell types under an SEM. Possible ways to distinguish cell types under an SEM could involve the use of gold nanoparticles. Reviewed by Kumar *et al*., adding gold nanoparticles to specific antigens had been previously used in cancer detection [22]. These nanoparticles are then detectable by backscattered electrons (BSE), which can reveal the cell types stained by the specific antigens.

The second drawback of using an SEM was its inability to image the centre of the scaffolds. Unlike a confocal microscope, which utilises a laser light source, SEM was designed to only scan the surface of a specimen. Hence, although an SEM was superior in imaging cell morphologies, its limitations restrict its use in cell culture. Therefore, the confocal microscopy was the primary imaging technique used for this chapter.

4.4.5 Nestin expression on scaffolds

Before scaffold seeding, nestin+ cells grown on 2D plastic exhibited mostly bi-polar morphologies. On scaffolds, they either remained spherical or developed branches. The difference in morphology, as mentioned before, was likely due to 2D representation of cells cultured in a 3D environment.

Compared with other scaffolds, Coll had more nestin+ cells on D4 and D7, indicating a higher degree of differentiation taken place on interlaced scaffolds. Addition of CS or HA dramatically decreased the percentage to around 10% at D7 compared to Coll of around 20%.

Although the cells were supplied with weekly addition of EGF and FGF, they gradually lost nestin expression. This is likely because in the culture medium, these GFs would be degraded over time. By the end of the week, the medium would have depleted GFs and thus allowing differentiation. In addition, the colony structure might have inhibited infiltration of GFs towards cells in the centre. During cell passaging, cells would normally be dissociated every 3-4 days, allowing cells in the centre of neurospheres to be in regular contact with GFs. On scaffolds however, NSCs in the centre of colonies had limited opportunities to be in contact with GFs, hence a higher differentiation. Alternatively, the physico-chemical characteristics of the scaffolds may have induced differentiation overcoming the anti-differentiation and pro-proliferative effects of the GFs.

The decline of nestin expression on Coll-CS and Coll-HA was modest from day 7 to day 21. During this period, addition of GFs led to continuous proliferation and thus growth in

cell numbers. The small decline of 3-5% in the 14-day period could be due to either a minimal differentiation or a continuous production of nestin+ cells by proliferation that offset the loss of nestin+ cells due to differentiation. Supporting the former possibility, we could relate the degree of differentiation to the bar charts illustrating GFAP and Dcx/MAP2 immunocytochemistry. No significant increase in cell numbers expressing these markers was observed in all stainings from day 7 to day 21. On the other hand, PHi3+/nestin+ co-labelling also showed a considerable amount of co-expression on Coll-CS and Coll-HA. Thus, we believe that both the reasons might have contributed to a small decline in nestin+ expression from day 7 to day 21.

On Coll-CS-HA scaffolds, no obvious nestin+ cells were found throughout the cultures after D4. It is reasonable to exclude cell death in this scenario, as Casp3 studies showed limited cell death on Coll-CS-HA on D7 under proliferation condition. Also, DAPI labelling and SEM showed round and relatively large nuclei, suggesting a healthy cell population. The lack of nestin+ expression may be due to no exposed Coll on the scaffold, hence encouraging most of the cells to differentiate. Another reason might be the pore size of Coll-CS-HA, which allowed cells to fill the pore and thus differentiate earlier as cells were in contact with GAGs, which were later proved to enhance astrocytic or neuronal differentiation. In our study, we cannot confirm this hypothesis by confocal microscopy, due to its inability to image the scaffolds themselves, or SEM, due to its inability to image the centre of the scaffolds. However, focused ion beam (FIB) microscopy that combines an SEM and ion beam sputtering may provide more details on the cell-scaffold interactions within the centre of the scaffolds in the future.

The lack of stem cells provides an advantage to Coll-CS-HA as an implant, since transplantation of undifferentiated cells could lead to tumour or teratoma growth due to the excessive growth of stem cells. To avoid this problem, it was suggested that the stem cells should be fully differentiated before any transplantation [23, 24]. According to our experiments, this is achievable in differentiation conditions. However, differentiation conditions did not lead to such large cell numbers. Thus, a Coll-CS-HA scaffold with a large starting cell number may be an option worth considering, as this option led to a faster cell differentiation.

Nestin and PHi3 co-labelling revealed a proliferating phenotype of NSCs and provided a possible explanation for a higher nestin+ expression on Coll. Co-expression of PHi3 and nestin indicated that the cells remained as stem cells and proliferating, which are classical stem cell behaviours. According to figure 4.13, Coll housed many PHi3+ cells at both time points. This provides a possible explanation to the increase of nestin+ cells on Coll. Proliferation and differentiation are often conflicting behaviours. Once a cell starts differentiating, it stops dividing. Hence, it can be implied that on Coll, NSCs tended to remain as stem cells rather than to differentiate, whereas on other Coll-GAGs, the opposite was favoured.

No quantification of PHi3 labelling was taken, as only n=1 was studied. We did not further label PHi3 because we prioritised our experiment on investigating neuronal differentiation, which we believe is of a higher concern for functional recovery after a TBI.

In addition, we also co-labelled nestin with MAP2 in the differentiation condition. As expected, very few cells expressed nestin on all scaffolds, including on Coll. This indicates

that the nestin+ cells found in Coll in proliferation condition remained undifferentiated mostly because of the GFs. This further suggests that Coll by itself did not encourage NSC differentiation as strongly as the Coll-GAGs.

4.4.6 Astrocytic differentiation

Although previously thought to only be supporting cells for neurons, astrocytes, along with other glial cells, have been found to regulate blood flow, synapse functions, blood brain barrier and homeostasis in the body [2].

After a brain injury, CS expression becomes significantly upregulated. Astrocytes secrete CS which forms part of the glial scar that inhibits neurite outgrowth, thereby hindering recovery. Several *in vivo* studies have confirmed this phenomenon, and the removal of CSPG by chondroitinase ABC (ChABC) has been proved to enhance axonal sprouting [17, 18]. Reviewed by Siebert *et al*., brevican, neurocan and phosphacan are all able to direct astrocytic formation in the ECM of CNS [25]. Additionally, *in vitro* culture of astrocytes also found an increased in CSPG production [26].

Although Coll-CS led to the highest percentage of GFAP+ cells of approximately 30-40% throughout the 21 days, the percentage on Coll-CS-HA remained unchanged. The HA is, therefore, likely the cause, since a similar discovery showing that high molecular weight HA inhibited astrocytic activation *in vivo* had been reported [27]. In addition, we have shown that HA encouraged neuronal differentiation. NSCs cued towards the neuronal lineage would hence exhibit no GFAP expression.

Physical reasons might have also contributed to the lack of GFAP+ expression on Coll-CS-HA. For example, NSCs attached onto Coll-CS-HA could have a smaller possibility of attaching to CS, since HA had masked the exposed CS. It is known that GFAP is also a stem cell marker. Coll-CS-HA had no cells with nestin expression after D7, thus, it may have been expected on this for it to support less GFAP expression.

There was no significant increase observed in GFAP+ labelling from day 4 to day 21 on all scaffolds. This suggests that astrocytic differentiation took place rapidly within the first 4 days. Comparing the decline in nestin from day 4 to day 7, it can be extrapolated that many of the nestin+ cells might have turned into astrocytic lineage.

Although both type 1 and type 2 astrocyte can be marked by GFAP, their morphologies are distinctly different [28, 29]. A culture from various parts of the brain showed that approximately 90% of GFAP+ cells exhibited type 1 morphology [30]. In addition, most of the astrocytes found in rats' white matter were type 1 [11]. In our culture, the percentage of type 2 astrocytes was even lower, indicating the culture condition exhibited at least a decent similarity to the white matter.

Activated astrocytes express higher level of GFAP, thus could be the reason of higher proportion of type 1 astrocytes [31]. In addition, early NSCs also express GFAP and are bipolar, thus could further explain a higher number of type 1 astrocytes across our culture.

Although different types of astrocytes are believed to have different functions, their exact differential functions, at this stage, have been poorly studied and understood [32]. Thus, we cannot conclude if our astrocyte population will be beneficial or detrimental. However,

it is well-known that astrocytes, upon a brain injury, become active and secrets CSPG and heparin sulfate proteoglycans (HSPG). Previous studies have discovered that the removal of CS *in vitro* led to a reduction of GFAP expression, indicating a correlation between CS and astrocytic differentiation [33]. Consistent with our results, CSPG was further reported to promote NPCs into GFAP+ cells *in vitro* by decreasing the phosphorylated states of Atk and Erk1/2, which transformed the differentiation of oligodendrocytes to astrocytes [34].

Possibly due to previous findings that CS inhibited neurite outgrowth, there are less reports of CS as a scaffold for TBI compared to Coll and HA. In this study, we provided another possible drawback for using CS, which is its ability to enhance astrocytic differentiation.

4.4.7 Neuronal differentiation

4.4.7.1 Dcx expression

In this study, we studied neurons at their different maturation levels: Dcx was used to label early, immature neuroblasts; and MAP2 was used to label mature neurons.

Dcx is often expressed by highly migratory neuroblasts. In the SVZ, NSCs leave the SVZ, differentiate into neuroblasts and enter the rostral migratory stream (RMS) before reaching the olfactory bulb (OB), where they differentiate into granule or periglomerular neurons. This phenomenon has been discovered in rodents, primates and neonatal humans [35]. Neuroblasts have been discovered to exhibit a highly migratory capability. After

brain injuries, proliferating neuroblasts have been discovered to migrate towards the injured sites [36]. In adult mammalian CNS, these cells could migrate 3-8 mm towards the OB [37].

In a neurosphere culture, we would expect that the Dcx level remain high at the beginning, and gradually decline as cells mature and start to express MAP2. However, such decline was not observed in 21 days of culture. This can be explained by a continuous differentiation of nestin+ cells to express Dcx. Unlike Dcx labelling, nestin showed a gradual decline throughout the culture. Approximately 50% of the nestin+ cells in Coll-GAGs scaffolds at D4 disappeared, accounting 10% of the total cell population. As these cells differentiated, many of them might have differentiated into neuroblasts and hence exhibited Dcx+ staining. Additionally, there are certain regions of the brain like the piriform cortex where Dcx+ cells that have remained immature are found even in adult brains. Similarly, an alternative explanation may be that our Dcx+ cells did not complete maturation.

Neuroblasts often have bipolar morphologies that assist their chain-like migration. The morphologies of Dcx+ cells found in our study resembled to those found in figure 4.1 and *in vivo* [35, 38].

4.4.7.2 MAP2 expression

MAP2+ quantification provided good evidence on the effect of GAGs on neuronal differentiation. The percentages of MAP2+ cells were remarkably higher on Coll-GAGs

scaffolds than that on Coll. Although no significant differences were found between Coll-CS, Coll-HA and Coll-CS-HA, theses scaffolds have all promoted higher MAP2 expression than Coll in both conditions.

Similar to previous studies, many of the MAP2+ cells found on the scaffolds were either monopolar or bipolar, indicating a relatively immature phenotype [39]. These cells generally overlapped with Dcx staining. However, morphological studies proved to be difficult due to the 3D shape of colonies and a crowded population. Multipolar MAP2+ cells residing in a dense MAP2+ rich colonies may be common, but difficult to differentiate as their branches and axons tend to overlap with adjacent MAP2+ cells.

Specific surface receptors of HA were found to regulate neuronal differentiation. In our study, the mechanism of an enhanced MAP2+ expression on Coll-HA scaffolds was potentially due to cluster of differentiation 44 (CD44), a commonly-found HA surface receptor that binds via its amino-terminal domain [40]. Previous studies discovered that the removal of CD44 in mouse brains had enhanced proliferation and delayed neuronal differentiation. More specifically, neuronal differentiation from Dcx+ to NeuN+, a more mature neuronal marker, was delayed. This is consistent with our finding that the Dcx+ population remained unchanged, but the MAP2 expression was elevated [41]. Although the expression of CD44 in the SVZ still lacks thorough study, it is known that HA remains at high level in the adult SVZ of rats, suggesting correlations between CD44 and SVZ NSC activities [42].

Although many have reported the biological functions of HA in neuronal differentiation, few have elucidated their mechanisms. However, possible mechanisms of HA on neuronal

differentiation can be referenced by their *in vivo* mechanisms. For example, the effect of HA-CD44 on neuronal differentiation may lie in the Wnt signalling pathway, an important cascade for driving neurogenesis and forming neuronal circuit in the nervous system. One previous research has discovered that CD44 is essential in activating Wnt-induced activation and nuclear translocation of β-catenin, as down- or upregulation of CD44 was directly related to a decrease or increase of Wnt/β-catenin signalling [43, 44].

The fact that both Coll-CS and Coll-HA enhanced MAP2+ expression to approximately the same percentage, while keeping Dcx+ expression almost unaffected, implies that the mechanism behind neuronal differentiation may have been similar, if not the same. Although not much has been studied between CS and Wnt signalling in the CNS, previous research has discovered that a reduction of C6S in articular cartilage by ChABC led to a reduction in chondrocytes' response to Wnt signalling [45]. Hence, it is possible that CS might have improved neuronal differentiation via a similar biological mechanism.

Furthermore, although CD44 is a common surface receptor for HA, it also binds readily to CS [46-48]. Thus, CS might enhance MAP2+ expression via CD44-Wnt signalling pathway.

However, the increase in MAP2+ expression on Coll-GAG scaffolds might be due to simpler reasons. It is widely agreed that CS and HA molecules can readily bind to GFs [49, 50], which could assist neuronal differentiation. A controlled-release system of bFGF for example, has been shown to increase the percentage of MAP2+ cell on a functional HA scaffold [16].

Combining the GFAP results, we believe that Coll-HA and Coll-CS-HA seem to be the two optimal scaffolds for tissue engineering for the brain. All three interlaced scaffolds had similar effects on neuronal differentiation, Coll-HA and Coll-CS-HA did not induced a higher astrocytic differentiation. Coll-HA had the advantage of a possibly higher cell number suggested by the total colony size measurement, while Coll-CS-HA showed much less nestin+ expression. Both could be extremely beneficial for an actual implant, and therefore should be considered in subsequent *in vivo* studies.

It is not reasonable to simply sum the quantification of nestin, MAP2 and GFAP to account for the percentages of different cell types in the scaffolds. This is partly because of potential dual expression. For example, GFAP can be expressed by both astrocytes and NSCs, hence we cannot conclude the percentage of a cell type by one staining. Also, GFAP is less capable to label quiescent astrocytes [2]. To better understand the quantification, two improvements can be made. Firstly, several antibodies could be used to stain one cell type, examples may include nestin and Sox2, GFAP and S100B, and MAP2 and NeuN. Observing the co-labelling will give a better understanding for the cell types. In addition, co-labelling one scaffold with different antibodies may help distinguish any overlaps. For example, nestin and GFAP co-staining may help to exclude any stem cells expressing GFAP. These studies can be carried out to further improve the accuracies of cell quantification. Recently, several single cell RNAseq studies have been published for the SVZ. Though difficult and expensive, this technique could also be used to elucidate the exact phenotype of NSC grown on engineered scaffolds.

4.4.7.3 VGLUT1 expression

Glutamatergic neurons express one of VGLUT1, VGLUT2 and VGLUT3. These expressions were widely used to distinguish glutamatergic neurons. In adult mammalian brains, VGLUT1 and VGLUT2 are most commonly expressed by glutamatergic neurons [51]. Therefore, the VGLUT1 antibody was utilised to characterise any glutamatergic neurons.

One previous study has successfully generated VGLUT1+ neurons from SVZ of rats [16]. In our study however, cells expressing both VGLUT1 and MAP2 were rare. Only a 21-day differentiation study showed scattered cells that expressed both antibodies. It is reasonable that other conditions produced less VGLUT1+ neurons, as the 21-day differentiation study was the most mature condition for cell differentiation.

Neurons within a mammalian CNS can be categorised by their neurotransmitter content: glutamatergic neurons and GABAergic neurons. Glutamatergic projections neurons are excitatory neurons that are able to send long axons. Within the SVZ, most cells reached the OB and differentiated into granule or periglomerular neurons were destined to become GABAergic neurons [52]. GABAergic neurons were not labelled in this study, as it is widely known that they are the main progeny cells for SVZ NSCs. Also, GABA acts as an inhibitory neurotransmitter in the brain. Future work to detect GABA and the rate-limiting enzyme of GABA synthesis, glutamic acid decarboxylase, may help define GABAergic differentiation of SVZ NSC grown in scaffolds. In healthy human, an imbalance of GABAergic and glutamatergic neurons leads to various diseases including autism [53]. After a severe TBI in humans and rodents, there is an immediate increase in

glutamate level in the brain [54]. The brain's natural response to injury suggests that glutamatergic neurons may play an important role in repair. Taking this idea forward, NSCs from the dentate gyrus (DG) of the hippocampus may be a more suitable cell source, as neurons differentiated from this region are glutamatergic [55].

Other potential cell sources may include human pluripotent stem cells (hPSCs). hPSCs were shown to be able to induce glutamatergic differentiation [56]. These cells may resemble better similarity to human physiology and lead to enhanced injury responses.

4.4.8 Migration

Compared to the NSCs from the DG, NSCs from the SVZ have the unique advantage of a superior migrating capability. Studies have shown NSCs from SVZ were able to migrate to injured sites caused by cerebral ischemia [57]. Migration of SVZ NSCs was evidenced as figure 4.25 and 4.26 illustrate that the neuroblasts from spheroids were able to migrate in matrigel and on scaffolds. However, a caveat to this study is that an ideal way to visualise migration in scaffolds still needs to be developed.

Unlike the spheroids in matrigel, light microscopy imaging for those on scaffolds was more difficult, as scaffolds were thick and opaque. Z-stack imaging on a confocal microscope was able to reveal more details. This however, posed technical challenges, since normal IHC involves multiple washing steps that had washed away many spheroids and explants in our previous experiments. Hence, auto-fluorescence cells from Gad65-GFP mice and NucBlue was used.

However, our experiments for migration studies still faced the same problem in retaining most of the spheroids and explants on the scaffolds. Despite many attempts on seeding, most of them were found to be absent while imaging.

Possible explanations for the absence may include water tension on the scaffolds and the location of spheroids and explants. After placement onto the scaffolds, some spheroids and explants would not even touch the scaffolds, suggested by limited vertical migrations of the SVZ explants. Before culturing, scaffolds undergo a series of washes in ethanol, PBS and media for sterilisation. At the end of the process, the scaffolds were soaked in media. The water tension at the surface may exclude the explants and spheroids touching the scaffolds. Hence, they could be easily washed away after the media was added.

In addition, explants and spheroids differed from individual NSCs as they were dramatically larger in size. Figure 4.26 showed that their diameter ranged from 50 to 100 μm, which were almost as large as the pores. Their sizes limited their ability to penetrate the scaffolds and thus would likely stay on the surface of scaffolds.

Due to the limitations on seeding explants and spheroids, only limited samples were obtained and imaged in migration studies. It was also difficult to conclude if migrations, if any, were due to the scaffolds or the media. The results were therefore inconclusive. On the other hand, this study provided cornerstone for future migration studies as it showed that it was possible to induce migration from the explants and spheroids on the scaffolds.

4.4.9 The optimal candidate scaffold for tissue engineering for the brain

In our study, we came to the conclusion that Coll-HA and Coll-CS-HA proved to be the two optimal scaffolds. As reviewed by Cave *et al*., there are a few major challenges for using SVZ NSCs for neuron replacement, including long term cell survival, suppression of glial differentiation, and efficient production of the desired neuron type [57]. From our results, we showed that Coll-HA and Coll-CS-HA both encouraged high MAP2+ expression, which would be beneficial for TBI recoveries. In addition, astrocytic differentiation was supressed, as evidenced by low GFAP+ expression on both scaffolds. Coll-CS-HA had the unique advantage of few nestin+ cells, suggesting potential benefits of avoiding tumour or teratoma growth. Coll-HA on the other hand, was able to promote a higher cell growth, as shown in the total area of colonies on a 7D proliferation culture.

Low differentiation on Coll was consistent with the prior literature [39]. Combined with an elevated level of nestin+ cells, we believe it is not optimal to use Coll by itself as a scaffold.

Coll-CS encouraged a higher GFAP+ expression, which may pose a challenge to the tissue engineering therapy. However, the cellular system on Coll-CS resembled better to the natural brains. The number of glial cells in the brain was thought to be approximately 10 times the number of neurons. More recent studies however, demonstrated that this ratio is actually closer to 1:1. In Coll-CS, the number of GFAP+ cells versus the number of MAP2+ cells was slightly over 1:1 in proliferation conditions [59, 60]. Although the number did not include other glial cells, Coll-CS could hold the potential to be a drug testing platform for brain diseases due to its advantages of 3D structure and simple

synthesis. Furthermore, most GFAP+ cells exhibited the morphology of type 1 astrocytes. Coll-CS can therefore be used as a potential cell selector that filters type 1 astrocytes, and be used for type 1 astrocytes-related research.

4.5 Conclusions

In this chapter, we compared the biological responses to Coll and three interlaced scaffolds: Coll-CS, Coll-HA and Coll-CS-HA. Cell differentiation, cell number, cell death, and migration studies were performed. Tripotent SVZ NSCs were found to grow in 3D colonies that showed high cell survival rates on all scaffolds. Colonies size measurement suggests that the interlaced scaffolds may promote a higher number of NSCs compared to Coll.

Nestin studies implied that more cells remained as stem cells on Coll, which might be due to a higher proliferation taken place on Coll. Coll-CS and Coll-HA both showed a significant decline in nestin+ expression to half of the expression on Coll. Coll-CS-HA showed no nestin+ cells after 4 days in the proliferation condition. This is a unique advantage of Coll-CS-HA as it could avoid tumour or teratoma growth after transplantation.

The interlaced scaffolds were equally capable of encouraging higher MAP2+ expression than Coll. For example, MAP2 expression increased by 50-100% in both the proliferation and differentiation conditions. Coll-CS also encouraged the highest GFAP+ expression across all scaffolds and time points, doubling the expression to around 40%. A high astrocytic differentiation may result in undesired injury responses, including glial scar formation.

Finally, migration studies utilising SVZ explants and neuroblast spheroids demonstrated possible migration along the scaffolds, suggesting scaffolds were able to direct migration of NSCs. However, the study has been limited by a low number of explants or spheroids remained on the scaffolds.

Overall, all scaffolds revealed excellent biocompatibility and were able to assist NSC growth. We believe that Coll-HA and Coll-CS-HA would be the most suitable candidates for a tissue engineering therapy for a TBI for future studies, due to their benefits of high MAP2+ expression yet low GFAP+ and nestin+ expression.

4.6 References

1. Chang EH, Adorjan I, Mundim MV, Sun B, Dizon MLV, Szele FG. Traumatic brain injury activation of the adult subventricular zone neurogenic niche. Frontiers in Neuroscience. 2016;10(332).

2. Sofroniew MV, Vinters HV. Astrocytes: biology and pathology. Acta Neuropathologica. 2010;119(1):7-35.

3. Fellers TJ, Davidson MW. Introduction to Confocal Microscopy: Olympus; [cited 2018 02/05].

4. Lim DA, Alvarez-Buylla A. The adult ventricular–subventricular zone (V-SVZ) and olfactory bulb (OB) neurogenesis. Cold Spring Harbor Perspectives in Biology. 2016;8(5):a018820.

5. Porter AG, Jänicke RU. Emerging roles of caspase-3 in apoptosis. Cell Death And Differentiation. 1999;6:99.

6. G. NB, J. R. Critical-point drying versus freeze drying for scanning electron microscopy: a quantitative and qualitative study on isolated hepatocytes. Journal of Microscopy. 1985;137(2):189-207.

7. Leo W, Roland S, Uwe G. The use of a simple method to avoid cell shrinkage during SEM preparation. Journal of Microscopy. 1981;121(2):185-9.

8. Sarnat HB, Flores-Sarnat L. Chapter 44 - Neuropathology of pediatric epilepsy. In: Dulac O, Lassonde M, Sarnat HB, editors. Handbook of Clinical Neurology. 111: Elsevier; 2013. p. 399-416.

9. Hendrickson ML, Rao AJ, Demerdash ONA, Kalil RE. Expression of nestin by neural cells in the adult rat and human brain. PLOS ONE. 2011;6(4):e18535.

10. Faiz M, Sachewsky N, Gasco S, Bang KWA, Morshead CM, Nagy A. Adult neural stem cells from the subventricular zone give rise to reactive astrocytes in the cortex after stroke. Cell Stem Cell. 2015;17:624–34.

11. Raff M, Abney E, Cohen J, Lindsay R, Noble M. Two types of astrocytes in cultures of developing rat white matter: differences in morphology, surface gangliosides, and growth characteristics. The Journal of Neuroscience. 1983;3(6):1289-300.

12. Lois C, Alvarez-Buylla A. Long-distance neuronal migration in the adult mammalian brain. Science. 1994;264(5162):1145-8.

13. Herrera DG, Garcia-Verdugo JM, Alvarez-Buylla A. Adult-derived neural precursors transplanted into multiple regions in the adult brain. Annals of Neurology. 1999;46(6):867-77.

14. Seidenfaden R, Desoeuvre A, Bosio A, Virard I, Cremer H. Glial conversion of SVZ-derived committed neuronal precursors after ectopic grafting into the adult brain. Molecular and Cellular Neuroscience. 2006;32(1):187-98.

15. Meissner KK, Kirkham DL, Doering LC. Transplants of neurosphere cell suspensions from aged mice are functional in the mouse model of Parkinson's. Brain Research. 2005;1057(1):105-12.

16. Duan H, Li X, Wang C, Hao P, Song W, Li M, *et al*. Functional hyaluronate collagen scaffolds induce NSCs differentiation into functional neurons in repairing the traumatic brain injury. Acta Biomaterialia. 2016;45:182-95.

17. Galtrey CM, Fawcett JW. The role of chondroitin sulfate proteoglycans in regeneration and plasticity in the central nervous system. Brain Research Reviews. 2007;54:1-18.

18. Dyck SM, Karimi-Abdolrezaee S. Chondroitin sulfate proteoglycans: Key modulators in the developing and pathologic central nervous system. Experimental Neurology. 2015;269:169-87.

19. Ramesh R. Cell Death Mechanisms Following Traumatic Brain Injury. Brain Pathology. 2004;14(2):215-22.

20. Rink A, Fung KM, Trojanowski JQ, Lee VM, Neugebauer E, McIntosh TK. Evidence of apoptotic cell death after experimental traumatic brain injury in the rat. The American Journal of Pathology. 1995;147(6):1575-83.

21. Ali Erturk, Mentz S, Stout EE, Hedehus M, Dominguez SL, Neumaier L, *et al*. Interfering with the chronic immune response rescues chronic degeneration after traumatic brain injury. The Journal of Neuroscience. 2016;36(38):9962–75.

22. Kumar P, Sharma A, Priyadarshini S E, Ambasta R. Notch signalling regulates cancer stem cells and tumour angiogenesis2012.

23. Nussbaum J, Elina Minami, Laflamme MA, Jitka A. I. Virag, Ware CB, Masino A, *et al*. Transplantation of undifferentiated murine embryonic stem cells in the heart: teratoma formation and immune response. The FASEB Journal. 2007;21(7):1345-57.

24. Murry CE, Keller G. Differentiation of embryonic stem cells to clinically relevant populations: lessons from embryonic development. Cell. 2008;132(4):661-80.

25. Siebert JR, Conta Steencken A, Osterhout DJ. Chondroitin sulfate proteoglycans in the nervous system: inhibitors to repair. BioMed Research International. 2014;2014:15.

26. Yu P, Wang H, Katagiri Y, Geller HM. An *in vitro* model of reactive astrogliosis and its effect on neuronal growth. in: milner r, editor. astrocytes: methods and protocols. Totowa, NJ: Humana Press; 2012. p. 327-40.

27. Zin ZK, Brian DM, Jennifer EV, Stephanie KS, Raymond JG, Christine ES. High molecular weight hyaluronic acid limits astrocyte activation and scar formation after spinal cord injury. Journal of Neural Engineering. 2011;8(4):046033.

28. Wolswijk G, Noble aM. Identification of an adult-specific glial progenitor cell. Development. 1989;105:387-400.

29. Montgome DL. Review - astrocytes: form, functions, and roles in disease Veterinary Pathology. 1994;31:145-67.

30. Kessaris N, Pringle N, Richardson WD. Specification of CNS glia from neural stem cells in the embryonic neuroepithelium. Philosophical Transactions of the Royal Society B. 2008;363:71-85.

31. Eng LF, Ghirnikar RS. GFAP and astrogliosis. Brain Pathology. 1994;4(3):229-37

32. Tabata H. Diverse subtypes of astrocytes and their development during corticogenesis. Frontiers in Neuroscience. 2015;9(114).

33. Gu W-L, Fu S-L, Wang Y-X, Li Y, Lü H-Z, Xu X-M, *et al*. Chondroitin sulfate proteoglycans regulate the growth, differentiation and migration of multipotent neural precursor cells through the integrin signaling pathway. BMC Neuroscience. 2009;10(1):128.

34. M. DS, Arsalan A, T. SK, H. PE, Chia-Lun W, Soheila KA. Chondroitin sulfate proteoglycans negatively modulate spinal cord neural precursor cells by signaling through LAR and RPTPσ and modulation of the Rho/ROCK pathway. STEM CELLS. 2015;33(8):2550-63.

35. Wang C, Liu F, Liu Y-Y, Zhao C-H, You Y, Wang L, *et al*. Identification and characterization of neuroblasts in the subventricular zone and rostral migratory stream of the adult human brain. Cell Research. 2011;21(11):1534-50.

36. Ramaswamy S, Goings GE, Soderstrom KE, Szele FG, Kozlowski DA. Cellular proliferation and migration following a controlled cortical impact in the mouse. Brain Research. 2005;2053:38-53.

37. Doetsch F, García-Verdugo JM, Alvarez-Buylla A. cellular composition and three-dimensional organization of the subventricular germinal zone in the adult mammalian brain. The Journal of Neuroscience. 1997;17(13):5046-61.

38. Zhang RL, Chopp M, Gregg SR, Toh Y, Roberts C, LeTourneau Y, *et al*. Patterns and dynamics of subventricular zone neuroblast migration in the ischemic striatum of the adult mouse. Journal of cerebral blood flow and metabolism : official journal of the International Society of Cerebral Blood Flow and Metabolism. 2009;29(7):1240-50.

39. Koutsopoulos S, Zhang S. Long-term three-dimensional neural tissue cultures in functionalized self-assembling peptide hydrogels, Matrigel and Collagen I. Acta Biomaterialia. 2013;9:5162-9.

40. Ponta H, Sherman L, Herrlich PA. CD44: From adhesion molecules to signalling regulators. Nature Reviews Molecular Cell Biology. 2003;4:33.

41. Su W, Foster SC, Xing R, Feistel K, Olsen RHJ, Acevedo SF, *et al*. CD44 transmembrane receptor and hyaluronan regulate adult hippocampal neural stem cell quiescence and differentiation. Journal of Biological Chemistry. 2017;292(11):4434-45.

42. Lindwall C, Olsson M, Osman AM, Kuhn HG, Curtis MA. Selective expression of hyaluronan and receptor for hyaluronan mediated motility (Rhamm) in the adult mouse subventricular zone and rostral migratory stream and in ischemic cortex. Brain Research. 2013;1503:62-77.

43. Schmitt M. The role of CD44 in Wnt/β-catenin signaling: Karlsruher Institut für Technologie 2014.

44. Schmitt M, Metzger M, Gradl D, Davidson G, Orian-Rousseau V. CD44 functions in Wnt signaling by regulating LRP6 localization and activation. Cell Death And Differentiation. 2014;22:677.

45. Shortkroff S, Yates KE. Alteration of matrix glycosaminoglycans diminishes articular chondrocytes' response to a canonical Wnt signal. Osteoarthritis and Cartilage. 2007;15(2):147-54.

46. Fujimoto T, Kawashima H, Tanaka T, Hirose M, Toyama-Sorimachi N, Matsuzawa Y, *et al*. CD44 binds a chondroitin sulfate proteoglycan, aggrecan. International immunology. 2001;13(3):359-66.

47. Hurt-Camejo E, Rosengren B, Sartipy P, Elfsberg K, Camejo G, Svensson L. CD44, a cell surface chondroitin sulfate proteoglycan, mediates binding of interferon-γ and some of its biological effects on human vascular smooth muscle cells. Journal of Biological Chemistry. 1999;274(27):18957-64.

48. Henke CA, Roongta U, Mickelson DJ, Knutson JR, McCarthy JB. CD44-related chondroitin sulfate proteoglycan, a cell surface receptor implicated with tumor cell invasion, mediates endothelial cell migration on fibrinogen and invasion into a fibrin matrix. The Journal of Clinical Investigation. 1996;97(11):2541-52.

49. Canning DR, Brelsford NR, Lovett NW. Chondroitin sulfate effects on neural stem cell differentiation. *In Vitro* Cellular & Developmental Biology - Animal. 2016;52(1):35-44.

50. Furuta M, Shiraishi T, Okamoto H, Mineta T, Tabuchi K, Shiwa M. Identification of pleiotrophin in conditioned medium secreted from neural stem cells by SELDI-TOF and SELDI-tandem mass spectrometry. Developmental Brain Research. 2004;152(2):189-97.

51. Wojcik SM, Rhee JS, Herzog E, Sigler A, Jahn R, Takamori S, *et al*. An essential role for vesicular glutamate transporter 1 (VGLUT1) in postnatal development and control of quantal size. Proceedings of the National Academy of Sciences of the United States of America. 2004;101(18):7158-63.

52. Betarbet R, Zigova T, Bakay RAE, Luskin MB. Dopaminergic and gabaergic interneurons of the olfactory bulb are derived from the neonatal subventricular zone. International Journal of Developmental Neuroscience. 1996;14(7):921-30.

53. El-Ansary A, Al-Ayadhi L. GABAergic/glutamatergic imbalance relative to excessive neuroinflammation in autism spectrum disorders. Journal of Neuroinflammation. 2014;11(1):189.

54. Guerriero RM, Giza CC, Rotenberg A. Glutamate and GABA imbalance following traumatic brain injury. Current neurology and neuroscience reports. 2015;15(5):27-.

55. Gonçalves JT, Schafer ST, Gage FH. Adult neurogenesis in the hippocampus: from stem cells to behavior. Cell. 2016;167(4):897-914.

56. Cao S-Y, Hu Y, Chen C, Yuan F, Xu M, Li Q, *et al*. Enhanced derivation of human pluripotent stem cell-derived cortical glutamatergic neurons by a small molecule. Scientific Reports. 2017;7(1):3282.

57. Yamashita T, Ninomiya M, Hernández Acosta P, García-Verdugo JM, Sunabori T, Sakaguchi M, *et al*. Subventricular zone-derived neuroblasts migrate and differentiate into mature neurons in the post-stroke adult striatum. The Journal of Neuroscience. 2006;26(24):6627-36.

58. Cave J, Wang M, Baker H. Adult subventricular zone neural stem cells as a potential source of dopaminergic replacement neurons. Frontiers in Neuroscience. 2014;8(16).

59. von Bartheld CS, Bahney J, Herculano-Houzel S. The search for true numbers of neurons and glial cells in the human brain: a review of 150 years of cell counting. The Journal of comparative neurology. 2016;524(18):3865-95.

60. Herculano-Houzel S. The glia/neuron ratio: How it varies uniformly across brain structures and species and what that means for brain physiology and evolution. Glia. 2014;62(9):1377-91.

Chapter 5 – Conclusions

5. Conclusions

This thesis aims at developing interlaced Coll-GAGs scaffolds for a potential treatment of TBI. Studies were divided into the materials science chapter, which included materials synthesis and characterisation, and the cell biology chapter, which included cellular responses to scaffolds.

The materials science chapter provided a comprehensive understanding of the physical properties and components of the scaffolds. Materials characterisations proved successful incorporations of HA and/or CS onto the Coll primary networks via physical entanglements and potentially chemical crosslinking. FTIR spectra indicated characteristic peaks of S-O-C on Coll-CS and Coll-CS-HA in both the spectra and the second derivatives spectra. Uronic acids moiety and carboxylic groups were also found to reflect HA in Coll-HA and Coll-CS-HA. The presence of CS was further validated by EDX, which discovered a drastic increase in sulfur content to 1.1at% and 0.7at% on Coll-CS and Coll-CS-HA respectively, while Coll only had a sulfur content of 0.1at%. In addition, alcian blue also indicated the presence of HA in the scaffolds by blue staining on Coll-HA scaffolds of different concentrations.

Physical characterisation showed that the interlaced scaffolds had similar properties to Coll. Compared to Coll, the interlaced scaffolds exhibited a similar local stiffness, which was an important consideration in scaffold design, as stiffness was shown to direct cell differentiation. Furthermore, degradation studies suggested that 80-90% of the scaffolds

remained stable after 28 days' incubation in physiological temperature and pH, indicating a decent structural integrity for implantation.

Subsequent cell biology studies investigated how SVZ NSCs from postnatal mouse brains would respond to the scaffolds in terms of cell differentiation, migration, survival and growth. Initial studies demonstrated the tripotent differentiation capabilities of SVZ NSCs and their stem cell phenotype. Coll and Coll-GAG scaffolds proved to demonstrate excellent biocompatibility, as evidenced by a low Casp3 labelling on 7 day proliferation and differentiation study.

As expected, differentiation of NSCs largely depended on the material components of the scaffolds. A larger percentage of cells were found to remain nestin+ on Coll compared to Coll-GAGs, indicating a more stem-like characteristics on Coll. MAP2 studies indicated an enhanced neuronal differentiation on all composite scaffolds by 50-100% in both the proliferation condition and differentiation condition, indicating potential therapeutic benefits. Interestingly, Coll-CS also showed a much higher GFAP+ expression of around 40% on all four time points. A high GFAP expression may be linked to a higher glial scar formation and therefore should be carefully studied in future.

As a result, we believe that Coll-HA and Coll-CS-HA are worth further studies for their therapeutic potential for TBI treatments. This is due to their capabilities of encouraging MAP2 differentiation, while keeping nestin and GFAP expression at low levels. Future studies involving *in vivo* transplantation of Coll-HA and Coll-CS-HA to mice may be considered.

Chapter 6 – Future work

6. Future work

The clinical development process for an implantable medical device, such as our scaffolds, includes *in vitro* cell studies, small and large animal testing, and subsequent human clinical trials. Our scaffolds are currently at the earliest stage of clinical development. Some studies that could be undertaken in future to help prepare the scaffolds for animal testing will be briefly described.

For materials science aspects, alterations of the ratio between Coll and GAGs were not extensively studied in this thesis due to time constraints. Future studies involving altering Coll and GAGs ratios may be undertaken to determine the optimal ratios that lead to better biological responses. In addition, future study should also synthesise a Coll-CS-HA scaffold that mimics the compressive modulus and pore structure similar to those of Coll-HA and observe if the results from this thesis also hold true. Scaffolds with similar sizes of TBI injuries (likely 1-2 mm in diameter) in animal models should be synthesised and characterised.

In vitro studies should attempt utilising hPSCs or other human neural cell lines to compare the production of glutamatergic neurons and other cell types. Next, a controlled TBI model on adult mice should be established for *in vivo* studies. Potential strategies for inducing a TBI include using a controlled-impact instrument (CCI), a Michele trephine biopsy, or simply pipettes. *In vivo* implantation studies may include comparing seeded versus unseeded scaffolds, long term cell survival, cell proliferation, cell differentiation,

migration of host cells into the scaffolds, growth of new tissue, and behavioural improvements.

These studies should provide a more in-depth understanding of the therapeutic potentials of our scaffolds and assist the clinical development process of our scaffolds in becoming a potential treatment for TBIs.